Towards optimal design of vehicles with low drag: Applications to sensitivity analysis and optimal control

by

Jan Pralits

April 2001
Technical Reports from
Royal Institute of Technology
Department of Mechanics
SE-100 44 Stockholm, Sweden

Typsatt i $\mathcal{AMS}$-LaTeX.

Akademisk avhandling som med tillstånd av Kungliga Tekniska Högskolan i Stockholm framlägges till offentlig granskning för avläggande av teknologie licentiatexamen onsdagen den 6:e juni 2001 kl 10.15 i sal E3, Huvudbyggnaden, Kungliga Tekniska Högskolan, Osquars Backe 14, Stockholm.

Kopiecenter, Stockholm 2001

Towards optimal design of vehicles with low drag: Applications to sensitivity analysis and optimal control

Jan Pralits 2001
Department of Mechanics, Royal Institute of Technology
SE-100 44 Stockholm, Sweden.

Abstract

The intention of the project is to develop a methodology for optimal design of vehicles with low drag, and the aim is to automatically incorporate a transition prediction method into the optimization process. The fundamental tool in this analysis are the Parabolized Stability Equations (PSE) which can predict the growth of disturbances in non-parallel boundary layers. The growth rate is used to calculate the N-factor in the so called e^N-method which can then be correlated in experimental data (e.g. wind tunnel or flight tests) to determine the value of N that corresponds to laminar-turbulent transition. An optimization procedure which results in changes of the geometry in turn causes changes in the external pressure distribution. The pressure distribution is obtained from inviscid equations e.g. the Euler equations which can then be used in the solution of the corresponding boundary layer equations (BLE). Finally, the stability analysis is done on the computed boundary layer. The chosen optimization procedure is gradient based and is formulated as an optimal control problem where the aim is to minimize an objective function balancing a measure of the state and the control. Here, the gradients are identified from so called adjoint equations. An outline is first presented, on how to solve the optimal design problem. However, derivations and results regarding modifications in the geometry are not presented in this thesis. The problem has instead been divided into a number of smaller parts which serve both as an interesting application by itself and provide knowledge which is useful for the optimal design problem. In the first application, the gradients (sensitivities) of the disturbance kinetic energy at a given position in the flow field due to unsteady forcing on the wall and within the boundary layer are derived. The gradients are identified from the adjoint of the PSE (APSE). Further, an application to optimal disturbance control is outlined where the unsteady disturbance velocity is used as control variable (blowing/suction) on the surface of a given geometry. In the second application, an optimal control problem is presented in which the wall normal velocity of the steady mean-flow is optimized to control disturbance growth in the whole flow domain. Here, the gradient of the objective function with respect to the control is derived from a coupling between the APSE and the adjoint of the boundary layer equations (ABLE). Related problems have also been solved regarding the gradient accuracy and the treatment of cases when different types of disturbances are present simultaneously.

Descriptors: Fluid mechanics, adjoint, optimal control, PSE, APSE, ABLE

Preface

This thesis considers the research approach taken towards optimal design of vehicles with low drag. The thesis is based on and contains the following papers on applications to sensitivity analysis and suction optimization for disturbance control.

Paper 1. Pralits, J. O., Airiau, C., Hanifi, A. & Henningson, D. S. 2001 Sensitivity analysis using adjoint parabolized stability equations for compressible flows. *to appear in Journal of Flow, Turbulence and Combustion.*

Paper 2. Pralits, J. O., Hanifi, A. & Henningson, D. S. 2001 Adjoint-based optimization of steady suction for disturbance control, Part 1. Incompressible flows. *submitted to Journal of Fluid Mechanics.*

Paper 3. Airiau C., Pralits, J. O., Bottaro, A. & Hanifi, A. 2001 Adjoint PSE and boundary layer equations for HLFC *Technical Report TR 10, ALTTA Deliverable No D 3.1.4-1.*

The papers are re-set in the present thesis format.

Division of work between authors

The theory in the first paper was done in cooperation between the Department of Mechanics at KTH, the Aeronautical Research Institute of Sweden (FFA) and Institut de Mécanique des Fluides de Toulouse (IMFT). The numerical code is based on the linear NOLOT-code which was developed by FFA and DLR. The numerical implementations needed for this work was performed by J.O. Pralits (JP) and A. Hanifi (AH).

The main part of the theory and the full numerical implementation in the second paper was done by JP and AH.

The third paper is based on a technical report from an ongoing European project (started in 1999) called Application of Hybrid Laminar Flow Technology on Transport Aircraft (ALTTA). The project is sponsored by the European Commission and the project coordinator is Daimler Chrysler Aerospace Airbus GmbH. One of the objectives of this project is to derive adjoint formulations to the non-local stability equations and demonstrate the application of sensitivity analysis to practical test cases. The technical report contains partially the theory from the first paper and an extension to compressible flows of the theory in the second paper. The latter was derived by AH, JP and Christophe Airiau at IMFT individually but some final details were provided by AH.

Contents

CHAPTER 1

Introduction

The final design of any vehicle shape is always a compromise in the intersection of feasibility imposed by various requirements. Aerodynamic properties are particularly important for the slender and smooth shapes needed for light, fast, and efficient vehicles. Especially in the initial phase of the design process, Computational Fluid Dynamic (CFD) analysis offers an efficient tool to rapidly explore the aerodynamic properties of numerous different possible shapes. The number of possible designs are large, and it is very unlikely that a truly optimal design can be found without assistance of automatic tools. It is therefore a growing interest in utilizing numerical optimization techniques to assist in the aerodynamic design process. Such methods need repeated computer simulations of the fluid flow, why the fact that the turnaround time for sophisticated numerical analysis keeps decreasing makes these techniques more and more feasible from an industrial perspective.

There are different ways in which automatic optimization can be incorporated in the design process. When the number of design variables are not too large, one may use *direct search methods*, for instance so-called genetic algorithms, to search the design space in order to reach some aerodynamic property given some predefined constrains. This method may be combined with an existing numerical code, which can more or less be regarded as a 'black box'. For large number of design variables, it is usually much more efficient to use gradient-based optimization algorithms. In this case, the CFD code needs to be augmented with routines to compute the gradients. An efficient way to compute the gradients is to use so called adjoint equations.

The development of efficient gradient-based algorithms cannot be done without the full knowledge of the CFD code, and thus can no longer be regarded as a black box. For a review of modern aerodynamic design methodology see e.g. Jameson (1997).

> *The general objective of this research is to link aerodynamic computational tools with optimization techniques to create a more automated flow design process in order to obtain vehicles with low aerodynamic drag.*

The research problem chosen here is the optimal design of vehicles with low aerodynamic drag. The need for correct prediction of drag resulting from surface friction as well as the need to improve the design to reduce vehicle drag is

one of the main industrial driver for improved prediction of laminar-turbulent transition. When one considers highly streamlined bodies, which is necessary if low drag is of interest, there is often a substantial laminar (low friction drag) portion of the vehicle. Thus a correct transition prediction becomes essential for a good estimate of the total drag. Today the most used method for transition prediction in industry is the so call e^N-method (see Arnal 1994), where the growth of disturbances in the boundary layers around the vehicle is empirically correlated with the onset of turbulent flow. However, today this method cannot be directly (theoretically) incorporated in the CFD analysis, and must therefore be used as an additional tool for each new design.

The aim here, is to integrate the transition prediction method in automatic way and thus substantially reduce the computational cost. The analysis is divided into three different steps with corresponding equations to solve. The first step is the calculation of the inviscid outer flow field which provides the pressure distribution for a given geometry. The given pressure distribution is then used to compute the corresponding viscous boundary layer. Finally, the stability analysis is performed on the boundary layer to provide the disturbance amplification for the e^N-method. The above mentioned steps are dependent of each other and as a result, all corresponding adjoint equations are needed to complete the optimal design procedure.

The problem described here should be seen as an example where optimal design methods can be applied to a system containing several sets of equations. The first expected result from the research problem is a design tool for shape optimization towards vehicles with low drag. However, these techniques are general and once the knowledge has been obtained, could be applied in other gradient based design applications where different scientific disciplines (sets of equations) are taken into account. An outcome of this research is therefore also a step towards an integration of different design areas such as flow design, structures, acoustics and materials for a more holistic design process.

CHAPTER 2

Solution strategy

The research problem described in the previous chapter is of great complexity as it involves several different systems of equations, questions regarding optimization procedures and limitations regarding both these issues. It is therefore of great importance at an initial stage to outline the full problem in order to localize those difficulties that appear during the solution procedure. In this chapter, our approach to solve the shape optimization problem is briefly described and then a summary of the works performed for each step towards our goal is given.

2.1. Shape optimization

The main idea behind this approach to perform shape optimization is to achieve low drag of highly streamlined bodies by maintaining the boundary layer laminar on as large part of the body as possible. This is equivalent of moving the point of transition, say X_1, as far downstream as possible. The fundamental tool in this analysis is the non-local stability analysis which is used to predict the growth of disturbances in non-parallel boundary layers. Here we use the Parabolized Stability Equations (PSE) (see Bertolotti *et al.* 1992). The growth can then be used to calculate the N-factor for a given disturbance, $N = \ln(A/A_n)$ where A_n and A are the disturbance amplitudes at the neutral (zero growth rate) and some downstream point respectively. These numerical results can then be correlated with experimental data in order to find the value of N which corresponds to the location of laminar-turbulent transition. Note here that this idea is based on the assumption that some receptivity process has already created a disturbance inside the boundary layer.

If the geometry is changed then this will cause a change in the external pressure distribution. The stability equations mentioned above are obtained from a linearization of the conservation equations around a given mean flow. This mean flow can be calculated using the boundary layer equations (BLE) given a prescribed pressure distribution which in turn can be computed from inviscid equations of motion e.g. the Euler equations.

The idea for the optimization procedure has been taken from optimal control theory which has been utilized in fluid mechanics problems for not more than a decade (see e.g. Joslin *et al.* 1995; Bewley & Moin 1997). Here, the objective is to minimize some measure of the state without using unlimited control (here constrained by specifications of the geometry). This can mathematically

be described by a minimization of an objective function which balances a measure of the state and a measure of the control (some measure of the geometry). The problem can be solved using the sensitivity information given by the gradient of the objective function with respect to the control in a gradient-based optimization routine. An efficient way to calculate the gradients is the adjoint approach which has shown to be successful in numerous applications where the number of constrains are low and the control-variable space is large (see e.g. Hall 1986; Hill 1995, 1997a,b; Andersson *et al.* 1999; Luchini 2000; Högberg & Berggren 2000; Berggren 1995).

The outline given above would work for the analysis of one given disturbance, however yielding a design which is optimal for just that disturbance. There is a potential risk that this new optimal design would trigger some other instability which might cause an even earlier transition than the original shape. To overcome this problem one has to look for the 'worst-case' disturbance at each iteration i.e. always consider the disturbance which will first cause transition to turbulence for each new design in the optimization process.

The full problem can now be seen as a min/max problem in which we have to find the shape that minimizes the disturbance energy at some downstream position X_1 given an initial disturbance at X_0, which has the largest energy at X_1. Here we measure the state as the disturbance kinetic energy at X_1, which in the case of incompressible flows is given as

$$E = \frac{1}{2}\int_0^\infty (u_1^2 + v_1^2 + w_1^2)\, dy, \tag{2.1}$$

where u_1, v_1 and w_1 are the streamwise, wall-normal and spanwise disturbance velocity components respectively at X_1 and y is the wall-normal coordinate. The shape optimization problem can now be written

$$\min_{\xi}\max_{q_0} J = \frac{1}{E_0}\int_0^\infty (u_1^2 + v_1^2 + w_1^2)\, dy + \frac{\epsilon}{2}\int_0^\infty q_0^2\, dy + \frac{\eta}{2}\int_\Gamma F(\xi)^2\, d\Gamma, \tag{2.2}$$

where J is the objective function, Γ is the surface of the geometry, $q_0 = (u_0, v_0, w_0, p_0)^T$ is the initial disturbance, p the disturbance pressure and ξ is a measure of the geometry. Here, ϵ and η are regularization parameters that are used to make sure that respective variable does not grow unbounded. $F(\xi)$ is a function describing the constrain on the geometry. Here, the gradients of J with respect to q_0 and ξ are identified from the so called adjoint equations.

The technique of identifying the gradients from adjoint equations is presented by considering the following problem. We wish to minimize the objective function

$$J(u_0) = \frac{1}{2}\int_0^\infty u(X_1, y)^2\, dy \tag{2.3}$$

which is a measure of the disturbance kinetic energy at a downstream position X_1 where the state variable u satisfies the state equation

$$\frac{\partial u}{\partial x} + gu = 0; \quad u(X_0, y) = u_0, \quad u(x, 0) = 0, \quad \lim_{y\to\infty} u(x, y) = 0 \tag{2.4}$$

which is integrated from $x = X_0$ to $x = X_1$. For a compact notation of the adjoint equations, we will use the *formal adjoint* L^* for the differential operator L defined by the relation

$$(p, Lq) = (L^*p, q) + \text{ boundary terms}, \tag{2.5}$$

where the inner product $(\cdot, \cdot)$ is defined as

$$(p, q) = \int_{X_0}^{X_1} \int_0^\infty p^H q \, dx \, dy \tag{2.6}$$

for $\mathbb{C}^n$-valued functions q and p. Here, the superscript * stands for adjoint quantities and ^{H} is the complex conjugate transpose. The derivation of the adjoint equations is done in the following steps: the first variation of equations (2.3) and (2.4) with respect to u_0 is derived. This is written as

$$\delta J(u_0) = \int_0^\infty \bar{u}(X_1, y)\delta u(X_1, y) \, dy, \tag{2.7}$$

$$\frac{\partial \delta u}{\partial x} + g\delta u = 0; \quad \delta u(X_0, y) = \delta u_0, \quad \delta u(x, 0) = 0, \quad \lim_{y\to\infty} \delta u(x, y) = 0 \tag{2.8}$$

where the super script $^-$ denotes complex conjugate. Then the left hand side of (2.5) is obtained by multiplying (2.8) with the co-state variable r according to the inner product given by (2.6). The right hand side of (2.5) is derived by removing the derivatives from δu using partial integration

$$(r, \frac{\partial \delta u}{\partial x} + g\delta u) = (-\frac{\partial r}{\partial x} + gr, \delta u) + \Big[\int_0^\infty \bar{r} \, \delta u \, dy\Big]_{X_0}^{X_1}. \tag{2.9}$$

We now demand that r satisfies the adjoint equation with initial and boundary conditions as

$$-\frac{\partial r}{\partial x} + gr = 0; \quad r(X_1, y) = u(X_1, y), \quad r(x, 0) = 0, \quad \lim_{y\to\infty} r(x, y) = 0. \tag{2.10}$$

Equation (2.10) is integrated from $x = X_1$ to $x = X_0$ and the initial condition is chosen such that the remaining boundary terms can be written

$$\int_0^\infty \bar{u}(X_1, y) \, \delta u(X_1, y) \, dy = \int_0^\infty \bar{r}(X_0, y) \, \delta u(X_0, y) \, dy. \tag{2.11}$$

Since the left hand side of (2.11) is equal to δJ, the gradient of J with respect to u_0 is identified as

$$\frac{\partial J}{\partial u_0} = \bar{r}(X_0, y) \quad \text{since} \quad \delta J(u_0) = \int_0^\infty \frac{\partial J}{\partial u_0} \delta u_0 \, dy \tag{2.12}$$

The right hand side of (2.5) can be derived using either a continuous or discrete approach. A continuous approach means that the adjoint equations are derived from the continuous state equation and then discretized. In the discrete approach, the adjoint equations are derived directly from the discretized state equation. The gradient which is later identified from the adjoint equations, should in the latter case have an accuracy close to machine precision. However, a gradient derived using the continuous approach will have an increased accuracy as the resolution of the computational domain is increased. This is well explained in Högberg & Berggren (2000). The adjoint equations used in this thesis have all been derived using a continuous approach. The accuracy of the numerically calculated gradients is discussed in papers 1 and 2.

A simple but often utilized gradient based optimization algorithm is the steepest descent. If we denote our control variable ζ and the iteration number of the optimization loop k, then this algorithm can be written as

$$\zeta^{k+1} = \zeta^k - \rho^k \frac{\partial J(\zeta^k)}{\partial \zeta} \tag{2.13}$$

where ρ^k is the 'step-length' determining how far one should go in the gradient direction in order to have maximum reduction of J at each iteration. As $k \to \infty$, J should approach some local minima. However, it has been shown in e.g. Bewley *et al.* (1999) that this algorithm does not necessarily reach a local minima, therefore other algorithms with higher order approximations has been used in the following papers.

The solution process of the shape optimization problem can now be described considering the chart given in figure 2.1. Here, the iteration number for the shape optimization loop is denoted with k and the corresponding number to find the optimal disturbance is denoted with j. Note here that the loop over j is a sub-optimization within the loop for k which is done for a given geometry with its corresponding mean flow.

In this chart, the gradients with respect to a measure of the geometry and the disturbance at X_0 are denoted $\nabla_\xi J$ and $\nabla_{q_0} J$, respectively. First, the homogeneous Euler equations and BLE are solved given an initial guess on the geometry. Then, a sub-optimization is done to find the optimal disturbance which involves a solution of the APSE to provide the gradient with respect to q_0. Thereafter, the adjoint equations, APSE, ABLE and AEuler are calculated given the solution from the previous equations. The gradient with respect to ξ is calculated and the geometry is updated. In the next loop, the Euler, BLE are solved with a new shape given by ξ^{k+1}. The sub-optimization is performed again providing a new optimal disturbance followed by the adjoint equations APSE, ABLE and AEuler. The optimization loop is continued until the variation of the objective function is less than a prescribed value.

One of the main difficulties in this procedure is the derivation of the adjoint equations. In the following section, the derivation of adjoint stability and

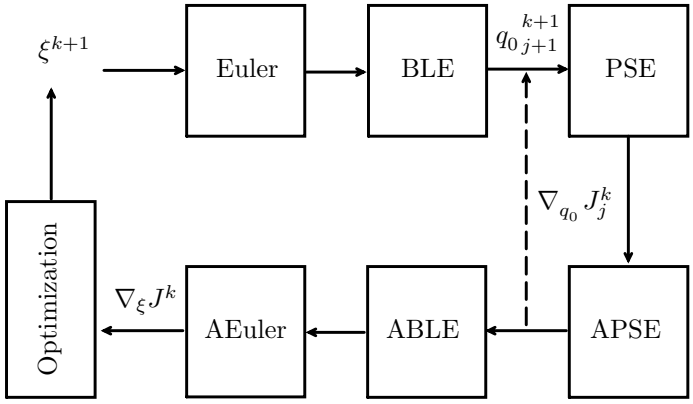

FIGURE 2.1. Chart of the shape optimization process

boundary layer equations and some of their applications are discussed. Changes in the geometry has not been considered yet and therefore the inviscid and their corresponding adjoint equations are not discussed in this thesis.

2.2. Application to sensitivity analysis and unsteady control

The first part of our shape optimization problem that has been analyzed is how to derive the adjoint of the PSE. This is described in detail in the first paper but an overview is given below. Here we consider a flat plate with the corresponding mean flow. Further, we assume that the receptivity has generated a disturbance which is then kept fixed at the initial streamwise point X_0. The adjoint equations are here used to express the sensitivity of an objective function measuring the terminal energy, see equation (2.1), to unsteady forcing on the wall and inside the boundary layer. One of the important issues here is the way the auxiliary condition of the PSE should be treated in order to obtain a consistent APSE. Another important aspect is the accuracy of the gradients derived from the adjoint equations. A comparison can be made by computing the gradients directly from the state equations. This is done by perturbing each degree of freedom at a time and then compute the corresponding gradient using a finite-difference approximation. If a second order finite-difference scheme is used then the state equations have to be solved $2N$-times to obtain the gradient, if N is the number of degrees of freedom. The gradient derived from the adjoint equations is computed more efficiently. Here, the state (PSE) and its adjoint (APSE) only have to be solved once. During the implementation of the adjoint equations, the finite-difference calculations also serve as a tool to check the implementation.

The gradients described above can be used to find the optimal unsteady blowing/suction for control of disturbance growth. Here, the aim is to optimize the wall-normal disturbance component on the wall v_{w} in order to minimize the disturbance kinetic energy at a downstream position X_1. The objective

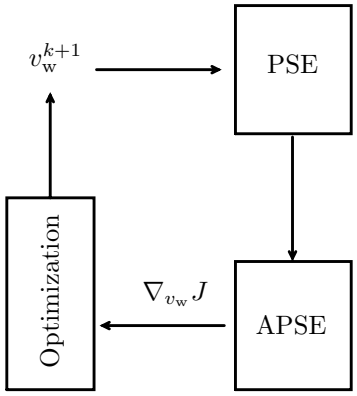

FIGURE 2.2. Chart of the optimization process for unsteady control

function can then be written

$$J(v_{\mathrm{w}}) = \int_0^\infty (u_1^2 + v_1^2 + w_1^2)\, dy + \frac{\epsilon}{2} \int_{X_0}^{X_1} v_{\mathrm{w}}^2\, dx. \tag{2.14}$$

The solution process of the optimal control problem due to unsteady blowing/suction on the wall can now be described considering the chart given in figure 2.2 where k is the iteration number of the optimization loop. Here we only consider the PSE and its adjoint, APSE, as the analysis is done for a given geometry and mean flow. An initial disturbance q_0 is superimposed to the mean flow at an initial position X_0 and the BLE, with homogeneous boundary conditions, followed by PSE are integrated from $x = X_0$ to $x = X_1$. The adjoint equations, APSE are then integrated from $x = X_1$ to $x = X_0$. The gradient is evaluated and the new boundary condition for the PSE is calculated using a chosen optimization algorithm. In the next loop, the PSE are solved with a new v_{w} followed by the APSE. The optimization loop is continued until the variation of the objective function is less than a prescribed value.

In paper 1, the full optimization loop is not done. Instead an analysis is presented on the derivation of the gradients (sensitivities) of equation (2.14), where $\epsilon = 0$, with respect to q_{w} and a forcing inside the boundary layer. Further, this is done for compressible flows expressed in curvilinear coordinates. The numerical implementation has been done in the linear NOLOT-code developed at FFA/DLR (see Hanifi *et al.* 1994; Hein *et al.* 1994).

2.3. Application to steady control

The second step is to derive the adjoint of the boundary layer equations, ABLE. Here, the idea is to use the wall-normal component of the steady mean flow on the wall V_{w} to control disturbance growth. This has an interesting application in itself but also serves as a tool to understand the coupling to the geometry through the pressure distribution. This can be understood by looking at the

streamwise momentum equation of the boundary layer equations on the wall

$$V_{\rm w}\frac{\partial U}{\partial y}+\frac{dP_e}{dx}=\frac{1}{Re}\frac{\partial^2 U}{\partial y^2} \qquad \text{on} \qquad y=0, \tag{2.15}$$

where U is the streamwise velocity, P_e the surface pressure and Re the Reynolds number. The effects of the application of suction on the wall when $dP_e/dx = 0$ is similar to those of applying a pressure gradient when $V_{\rm w} = 0$. We continue by assuming that the receptivity process has generated one or several disturbances which are kept fixed at the initial streamwise point X_0. Note here that accounting for more than one initial disturbance is an approach which can be considered to be more robust than the analysis for just one initial disturbance. However, this is not the same thing as to find the worst case initial disturbance at each iteration in the optimization loop, which was discussed in the previous section. A definition of robust control is found in Bewley & Moin (1997). The objective function now balances a measure of the total disturbance kinetic energy and the control energy due to the steady suction. This can be written

$$J(V_{\rm w})=\sum_{n=1}^{N}\int_{\Omega}({u_n}^2+{v_n}^2+{w_n}^2)\,d\Omega+\frac{\epsilon}{2}\int_{X_0}^{X_1}V_{\rm w}^2\,dx, \tag{2.16}$$

where Ω is the physical domain considered here and N is the number of disturbances present in the flow. The gradient of J with respect to $V_{\rm w}$ now express the sensitivity to modifications of the mean flow and is written as

$$\nabla_{V_{\rm w}}J=\epsilon V_{\rm w}+\sum_{k=1}^{N}(V_{\rm w}^*)_k \qquad \text{on} \qquad y=0, \tag{2.17}$$

where $V_{\rm w}^*$ is an adjoint quantity evaluated on the wall given by the ABLE. It is shown in paper 2 that the ABLE is forced in the whole computational domain by the solution of both the PSE and APSE. The evaluation of the gradient, (2.17), is done by a summation of $V_{\rm w}^*$, obtained by solving the ABLE for each disturbance. As the ABLE are linear equations, it is also possible to first sum the forcing terms obtained from the solution of the PSE and APSE for each disturbance and then compute the ABLE given the total forcing. The latter technique is more efficient as the BLE and ABLE are only solved once for each iteration in the optimization procedure.

The knowledge from section 2.2 can be used to derive the APSE, but the extension is the derivation of the ABLE. The adjoint equations are derived using the continuous approach which means that the gradient accuracy can be increased if the resolution of the computational domain is increased. However, it is known that the PSE become unstable as the step-size is decreased (see e.g. Andersson *et al.* 1998). In paper 2, a stabilizing procedure derived by Andersson *et al.* (1998) is used to stabilize the PSE which consequently affects the derivation of the adjoint equations. The stabilization procedure produces additional terms in both the APSE and the ABLE, however the gradient expression and boundary conditions are unchanged.

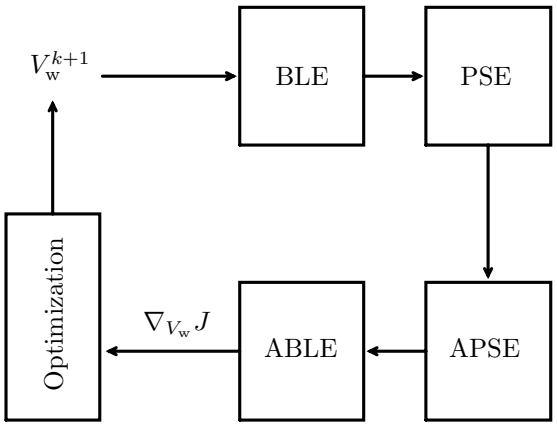

FIGURE 2.3. Chart of the optimization process for steady control

The optimization loop for control using steady suction on the wall can be described using the chart given in figure 2.3. N disturbances are superimposed to the mean flow at X_0. The homogeneous mean flow is obtained by integrating the BLE from $x = X_0$ to $x = X_1$. The forcing of the ABLE for each disturbance is obtained by first integrating the PSE from $x = X_0$ to $x = X_1$ and then integrating the APSE from $x = X_1$ to $x = X_0$. The total forcing is then computed by a summation of the forcing from each disturbance. Next, the ABLE is integrated from $x = X_1$ to $x = X_0$ given the total forcing. The gradient can now be evaluated and the new boundary condition for the BLE is calculated using an optimization algorithm. In the next loop, a new mean flow is computed using the BLE with a modified V_{w}. Again, the total forcing is computed by a summation of the solutions of the PSE and APSE, and then the ABLE are solved in order to compute then new gradient. The optimization loop is continued until the variation of the objective function is less than a prescribed value.

In paper 2, the optimal control problem presented in this section is derived in detail for quasi three-dimensional incompressible flows on a flat plate. Results are presented for optimal control of single and multiple disturbances in Blasius boundary layers, and single disturbances in three-dimensional boundary layers with adverse and favorable pressure gradients.

In paper 3, the theory in this section is extended for control of single disturbances in quasi three-dimensional compressible flows on an infinite swept wing. No results are shown on applications of optimal control in this paper.

CHAPTER 3

Conclusion and outlook

An outline has been given on using a gradient based shape optimization problem to obtain highly streamlined bodies with low drag. The idea is to decrease drag (increase the laminar portion) of the body by moving the point of laminar-turbulent transition downstream. The method incorporates an established transition prediction method which in turn can be correlated with experimental data. The optimization method is similar to optimal control theory in which the aim is to minimize an objective function balancing a measure of the state and control. Here, the state is measured as the disturbance kinetic energy at some downstream position and the control variables are the initial disturbances and some measure of the geometry. In order to have a more robust design, the idea here is to minimize the disturbance kinetic energy at a downstream position for a given disturbance which at the same time has the maximum kinetic energy over all possible disturbances at the same location. An adjoint approach has been chosen for the evaluation of the gradients.

The full shape optimization problem has so far been divided into three sub problems where some of the difficulties regarding adjoint equations, accuracy of the gradients and accounting for multiple disturbances have been analyzed. The results have provided knowledge and a good basis on which future work towards the goal of shape optimization can be based. Further, it has given numerical tools which can be used in sensitivity analysis, unsteady- and steady disturbance control in laminar boundary layers.

The next step will be to incorporate the inviscid equations of motion in order to account for the geometry modifications. Another interesting continuation of the present analysis is to incorporate the non-linear stability equations in both the unsteady and steady control problem. So far the adjoint equations have been derived using a continuous approach. This means that the adjoint equations have been derived from the continuous state-equations and then discretized. This has been shown to yield a good approximation of the gradients but further investigations should be done where the adjoint equations are derived directly from the discretized state-equations.

Acknowledgment

I want to express my gratitude for my supervisors Dan Henningson and Ardeshir Hanifi for their support and great knowledge that they have always shared generously with me. The major part of the computer software for both the boundary layer and stability analysis has been provided by Ardeshir Hanifi. This has given me a very good basis from which to start this work.

I want to thank Martin Berggren for many useful discussions which have provided more consistency in the mathematical formulations.

I also want to acknowledge Alessandro Bottaro and Christophe Airiau for the good cooperation which started in 1999, and the hospitality they showed me during my stay in Toulouse in October, 2000.

This work has been funded by the Swedish Foundation for Strategic Research (SSF) through the Integral Vehicle Structures (IVS)-program and partially by the Swedish Defence Research Agency (FOI).

Finally I want thank my colleagues at the department of mechanics for their friendship and Karimah for being the lovely person she is.

Bibliography

Andersson, P., Berggren, M. & Henningson, D. 1999 Optimal disturbances and bypass transition in boundary laye. *Phys. Fluids* .

Andersson, P., Henningson, D. S. & Hanifi, A. 1998 On a stabilization procedure for the parabolic stability equations. *J. Eng. Math.* **33**, 311–332.

Arnal, D. 1994 Boundary layer transition: Predictions based on linear theory. *Tech. Rep.* 193. AGARD.

Berggren, M. 1995 Optimal control of time evolution systems: Controllability investigations and numerical algorithms. PhD thesis, Rice University.

Bertolotti, F., Herbert, T. & Spalart, S. 1992 Linear and nonlinear stability of the blasius boundary layer. *J. Fluid Mech.* .

Bewley, T. & Moin, P. 1997 Optimal and robust approaches for linear and nonlinear regulation problems in fluid mechanics. *AIAA 97-1872* .

Bewley, T., Moin, P. & Temam, R. 1999 Dns-based predictive control of turbulence: an optimal benchmark for feedback algorithms. *submitted to J. Fluid Mech.* .

Hall, M. C. G. 1986 Application of adjoint sensitivity theory to an atmospheric general circulation model. *J. The Atmospheric Sci.* **43**, 2644–2651.

Hanifi, A., Henningson, D. S., Hein, S. & Bertolotti, F. P.and Simen, M. 1994 Linear non-local instability analysis - the linear nolot code. *FFA TN* **1994-54**.

Hein, S., Bertolotti, F. P., Simen, M., Hanifi, A. & Henningson, D. S. 1994 Linear non-local instability analysis - the linear nolot code. *DLR-IB* **223-94 A 43**.

Hill, D. C. 1995 Adjoint systems and their role in the receptivity problem for boundary layers. *J. Fluid Mech.* **292**, 183–204.

Hill, D. C. 1997a Receptivity in non-parallel boundary layers. In *ASME Fluids Engineering Division Summer Meeting, FEDSM '97*.

Hill, D. C. 1997b Inverse design for laminar three-dimensional boundary layers. *Bull. A. Phys. Soc.* **42**, 2120.

Högberg, M. & Berggren, M. 2000 Numerical approaches to optimal control of a model equation for shear flow instabilities. *to appear in J. Flow, Turbulence and Combustion* .

Jameson, A. 1997 Essential elements of computational algorithms for aerodynamic analysis and design. *Tech. Rep.* CR-97-206268, ICASE Report no. 97-68. NASA.

Joslin, R., Gunzburguer, M., Nicolaides, R., Erlebacher, F. & Husaini, M. 1995 A self-contained, automated methodology for optimal flow control validated for transition delay. *ICASE Report 95-96* .

Luchini, P. 2000 Reynolds-number-independent instability of the boundarylayer over a flat surface: optimal perturbations. *J. Fluid Mech.* **404**, 289–309.

1

Paper 1

Sensitivity Analysis Using Adjoint Parabolized Stability Equations for Compressible Flows

By Jan O. Pralits[1,3], Christophe Airiau[2], Ardeshir Hanifi[3] and Dan S. Henningson[1,3]

An input/output framework is used to analyze the sensitivity of two- and three dimensional disturbances in a compressible boundary layer for changes in wall- and momentum forcing. The sensitivity is defined as the gradient of the kinetic disturbance energy at a given downstream position with respect to the forcing. The gradients are derived using the parabolized stability equations (PSE) and their adjoint (APSE). The adjoint equations are derived in a consistent way for a quasi two-dimensional compressible flow in an orthogonal curvilinear coordinate system. The input/output framework provides a basis for optimal control studies. Analysis of two-dimensional boundary layers for Mach numbers between 0 and 1.2 show that wall- and momentum forcing close to branch I of the neutral stability curve give the maximum magnitude of the gradient. Forcing at the wall gives the largest magnitude using the wall normal velocity component. In case of incompressible flow, the two-dimensional disturbances are the most sensitive ones to wall inhomogeneity. For compressible flow, the three-dimensional disturbances are the most sensitive ones. Further, it is shown that momentum forcing is most effectively done in the vicinity of the critical layer.

1. Introduction

Transition from laminar to turbulent flow can be triggered by unstable disturbances inside the boundary layer. The growth of such1 disturbances are known to be sensitive to surface inhomogeneities, forcing inside the boundary layer and external acoustic perturbations, see *e.g.* Nishioka and Morkovin (1986), Saric (1993) and Corke, Bar-Sever and Morkovin (1986). The studies devoted to the birth of disturbances due to such forcing are called receptivity. The acoustic receptivity is explained by Goldstein (1983) as a wavelength conversion mechanism. The long wave length of an acoustic wave can be converted to a shorter wave length of an instability wave at the leading edge or where

[1]Department of Mechanics, KTH, SE-100 44 Stockholm, Sweden.
[2]Institut de Mécanique des Fluides de Toulouse, Allée du professeur Camille Soula, F-31 400 Toulouse, France.
[3]Swedish Defence Research Agency, FOI, Aeronautics Division, FFA, SE-172 90 Stockholm, Sweden.

a geometric inhomogeneity is present. Results of boundary layer receptivity are documented by Crouch (1992a, 1992b) and Choudhari and Street (1992) for two-dimensional disturbances in a Blasius boundary layer. Other references may be found in Goldstein (1989) and in Saric (1993).

A disturbance inside the boundary layer may encounter an unsteady wall inhomogeneity (forcing) which changes its growth. This problem can also be viewed as a receptivity to wall perturbations. If the perturbation is appropriate, it can be used to control the development of the disturbance. This is the wave cancellation concept proposed by Thomas (1983). Such study may be formulated as input/output problem where the input is some forcing on the wall or in the boundary layer, and the output is a measure of the disturbance in the domain. The sensitivity can be defined as the gradient of the output with respect to the input. A typical output measure is the disturbance energy at some downstream position or in the whole domain. Such a formulation can easily be extended to a control problem by using the gradient to update the input *i.e.* control variables in order to minimize the output. This analysis can be done with gradient based optimization techniques as shown in Gunzburger (2000) and Bewley, Temam and Ziane (2000).

Here we investigate the sensitivity of disturbances to unsteady wall conditions and source of momentum in a compressible boundary layer in framework of the non-local stability theory. This analysis is formulated as an input/output problem and provides information which is useful for the control of disturbances. The state equations are the so called Parabolized Stability Equations, PSE, and are written in an orthogonal curvilinear coordinates system. For a detailed presentation of PSE see *e.g.* Bertolotti, Herbert and Spalart (1992) and Simen (1992).

The main tool developed here is based on the adjoint equations. The approach of adjoint equations has been used for sensitivity studies in oceanography and atmospheric circulation models, *e.g.* Hall (1986). This approach has also appeared in receptivity studies. Tumin (1996) used it for confined flows. Hill (1995,1997) applied the adjoint approach for the local and nonlocal stability theories to study the receptivity of Tollmien-Schlichting waves in boundary layer flows. Receptivity of Görtler vortices was studied by Luchini and Bottaro (1998) using backward-in-time integration. The adjoint techniques has also been used for identifying the optimal disturbances in boundary layer flows, *e.g.* Andersson, Berggren and Henningson (1999) and Luchini (2000).

Sensitivity analysis may be performed by forward calculations. For each parameter that is changed (inhomogeneous wall boundary conditions, initial disturbance, momentum source) the forward problem has to be solved. The total time spent will be the product of the number of input parameters and the time spent for each calculation.

The advantage of the adjoint approach is that the sensitivity of a disturbance can be obtained by solving the state and adjoint equations once. This means that the adjoint method can provide an optimal distribution of suction

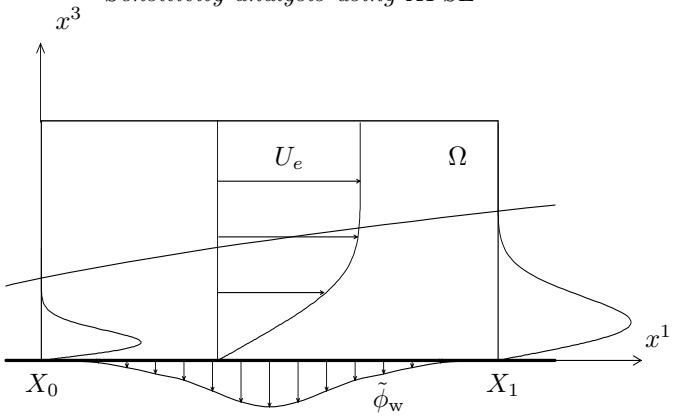

FIGURE 1. Computational domain

to suppress the growth of disturbances with a relatively low computational cost. Such a study was carried out by Cathalifaud and Luchini (2000) for optimal disturbances in a Blasius boundary layer.

The aim of the present work is to derive the adjoint of the parabolized stability equations for a compressible flow in a consistent way. The paper is organized as follows. In section 2 the problem is defined and section 3 gives the adjoint formulation and the gradient expressions. Validation and results of the sensitivity analysis are presented for a two-dimensional compressible boundary layer with two and three dimensional disturbances in section 4. The conclusions appear in section 5. Details of the derivation of nonlocal stability equations and their adjoint are given in the appendix.

2. Problem formulation

2.1. *Definition of the sensitivity*

The sensitivity of two- and three dimensional disturbances in a compressible boundary layer for changes in wall- and momentum forcing is investigated. This analysis is formulated as an input/output problem and will be discussed below considering the domain given in figure 1. Here, x^1, x^2 and x^3 are the streamwise, spanwise and wall normal coordinates, respectively, and U_e the free-stream velocity. The computational domain is defined such that $x^1 \in [X_0, X_1]$, $x^2 \in [Z_0, Z_1]$ and $x^3 \in [0, \infty[$. An initial disturbance is superimposed to the boundary layer base flow at an upstream position X_0.

In optimal control theory, sensitivity is defined as the derivative of the state variables (output) with respect to the control variables (input). It is related to the gradient of a functional J (called cost or objective functional) which includes both a measure of a state E and a measure of the control E_c. The measures are weighted together with a positive factor ϵ, so called the regularization parameter, as $J = E + \epsilon E_c$. The regularization parameter serves the purpose of limiting the size of the control. The optimal input can

then be obtained via an optimality condition using gradient based optimization techniques as *e.g.* steepest descent or conjugate gradient, see *e.g.* Bewley *et al.* (2000) and Gunzburger (2000).

Here, the input is defined as the inhomogeneities of velocity $\tilde{\mathbf{u}}_{\mathrm{w}}$ and temperature $\tilde{T}_{\mathrm{w}}$ on the wall $x^3 = 0$ and a source $\tilde{\mathcal{S}}$ in the boundary layer. The output is a function of disturbance variables, here written as the disturbance energy norm

$$E = \frac{1}{2}\int_{Z_0}^{Z_1}\int_{0}^{\infty} \tilde{\phi}_1^H \mathcal{M}\tilde{\phi}_1 h_2 h_3 \, dx^3 \, dx^2, \tag{1}$$

or alternatively

$$E = \frac{1}{2}\int_{X_0}^{X_1}\int_{Z_0}^{Z_1}\int_{0}^{+\infty} \tilde{\phi}^H \mathcal{M}\tilde{\phi} \, h_1 h_2 h_3 \, dx^1 \, dx^2 \, dx^3, \tag{2}$$

where $\tilde{\phi} = (\tilde{\rho}, \tilde{u}, \tilde{v}, \tilde{w}, \tilde{T})^{\mathrm{T}}$ with $\tilde{\rho}$ denoting the density perturbation, $\tilde{u}, \tilde{v}, \tilde{w}$ the streamwise, spanwise and normal velocity perturbations, respectively, and $\tilde{T}$ the temperature perturbation. The superscript ^{H} denotes the transpose complex conjugate, the subscript $_1$ refers to values at $x = X_1$ and h_i the scale factors of the coordinate system. The positive diagonal matrix $\mathcal{M}$ defines the measure of 'size' of disturbances. In this paper $\mathcal{M} = \mathrm{Diag}(0, 1, 1, 1, 0)$ such that disturbances are measured by the modulus of their velocity components. An example of another measure is given in Hanifi *et al.* (1994) where $\mathcal{M} = \mathrm{Diag}(T/\rho\gamma M^2, \rho, \rho, \rho, \rho/\gamma(\gamma-1)TM^2)$ with T being the mean temperature, ρ the mean density, γ the ratio of the specific heat coefficients and M the Mach number of the flow. We define the sensitivity as the gradient of E with respect to $\tilde{\mathbf{u}}_{\mathrm{w}}$, $\tilde{T}_{\mathrm{w}}$ and $\tilde{\mathcal{S}}$. Here we consider the case with no penalty, *i.e* $\epsilon = 0$, therefore can the output be written $J = E$.

In the present paper the amplitude of the control parameters are assumed to be so small that the nonlinear interaction with the mean flow can be neglected. However, the procedure presented here can be extended to account for the modification of the mean flow, see Pralits *et al.* (2000).

2.2. *State equations*

The governing equations are the non-local stability equations formulated using PSE technique for quasi-three dimensional viscous, compressible flow formulated in primitive variables and general, orthogonal curvilinear coordinates. Here, we consider a general case where the boundary layer is subjected to sources of mass, momenta and energy $\tilde{\mathcal{S}}$, and inhomogeneous boundary conditions on the wall $\tilde{\mathbf{u}}_{\mathrm{w}}$ and $\tilde{T}_{\mathrm{w}}$. The notation, the reference quantities, the assumptions and the derivation of the PSE are given in appendix Appendix A.

The equations in symbolic form are written as

$$\begin{aligned} \hat{\mathcal{L}}\,\hat{\phi} &= \hat{\mathcal{S}} && \text{in} && \Omega \\ \hat{\phi} &= \hat{\phi}_0 && \text{on} && x^1 = X_0 \\ \hat{\mathbf{u}} = \hat{\mathbf{u}}_{\mathrm{w}}(x^1), \quad \hat{T} &= \hat{T}_{\mathrm{w}}(x^1) && \text{on} && x^3 = 0 \\ \hat{\mathbf{u}} \to 0, \quad \hat{T} &\to 0 && \text{as} && x^3 \to \infty \\ \int_0^\infty \hat{\phi}^H \frac{\partial \hat{\phi}}{\partial x^1}\, h_2 h_3 dx^3 &= 0 && \forall && x^1 \end{aligned} \tag{3}$$

The disturbance $\tilde{\phi}$, the source $\tilde{\mathcal{S}}$ and the inhomogeneous boundary conditions have been divided into an amplitude function and a wave function

$$\tilde{\phi}(x^i, t) = \hat{\phi}(x^1, x^3)\Theta, \quad \tilde{\mathcal{S}}(x^i, t) = \hat{\mathcal{S}}(x^1, x^3)\Theta, \tag{4}$$

where

$$\Theta(x^1, x^2) = \exp\, i\,(\int_{X_0}^{x^1} \alpha(x')dx' + \beta x^2 - \omega t). \tag{5}$$

Here, α is the complex streamwise wavenumber, β the real spanwise wavenumber and ω the real angular frequency of the perturbations. The integral expression in equation (3), the so called auxiliary condition, is used to remove the ambiguity from the streamwise dependence that remains between the wave and the amplitude functions.

In accordance to the derivation of the nonlocal stability equations, the input parameters ($\hat{\mathbf{u}}_{\mathrm{w}}$, $\hat{T}_{\mathrm{w}}$ and $\hat{\mathcal{S}}$) are assumed to be weak functions of the streamwise coordinate, *i.e.* $\partial/\partial x^1 \sim \mathcal{O}(R^{-1})$. Note that $\tilde{\phi}_{\mathrm{w}}$ and $\tilde{S}$ have the same x^2, t and main x^1 dependence as the disturbances.

The system of equations (3), which is nonlinear in $(\alpha, \hat{\phi})$, is integrated in the downstream direction using a marching procedure, with the initial condition at $x^1 = X_0$ given by the local stability theory. At each streamwise position, the value of α is iterated such the auxiliary condition is satisfied.

3. Adjoint equations and gradients

The gradient of the output given by (1), is defined through the directional derivative as

$$\begin{aligned} \delta J = \quad \mathtt{Real} \Bigg\{ & \int_{X_0}^{X_1} \int_{Z_0}^{Z_1} \left(\nabla_{\tilde{\mathbf{u}}_{\mathrm{w}}} J^H \delta \tilde{\mathbf{u}}_{\mathrm{w}} + \nabla_{\tilde{T}_{\mathrm{w}}} J^H \delta \tilde{T}_{\mathrm{w}} \right) h_1 h_2 \; dx^2 \; dx^1 + \\ & \int_{X_0}^{X_1} \int_{Z_0}^{Z_1} \int_0^\infty \nabla_{\tilde{\mathcal{S}}} J^H \delta \tilde{\mathcal{S}} \; h_1 h_2 h_3 \; dx^3 \; dx^2 \; dx^1 \Bigg\}, \end{aligned} \tag{6}$$

where

$$\nabla_\xi J \; \delta\xi = \lim_{s \to 0} \frac{J(\xi + s\delta\xi) - J(\xi)}{s},$$

and $\delta\tilde{\mathbf{u}}_{\rm w}, \delta\tilde{T}_{\rm w}$ and $\delta\tilde{\mathcal{S}}$ are the variations of the input parameters. The gradient expressions, *i.e.* the sensitivities, are derived in appendix Appendix B, using a perturbation technique together with integration by parts in space. It yields

$$\begin{aligned}
\nabla_{\tilde{u}_{\rm w}} J &= \frac{\mu}{\bar{\Theta} R} D_3(u^*) && \text{on} \quad x^3 = 0 \\
\nabla_{\tilde{v}_{\rm w}} J &= \frac{\mu}{\bar{\Theta} R} D_3(v^*) && \text{on} \quad x^3 = 0 \\
\nabla_{\tilde{w}_{\rm w}} J &= \frac{\rho \rho^*}{\bar{\Theta}} && \text{on} \quad x^3 = 0 \\
\nabla_{\tilde{T}_{\rm w}} J &= -\frac{\kappa}{\bar{\Theta}\,{\rm Pr}\, R} D_3(T^*) && \text{on} \quad x^3 = 0 \\
\nabla_{\tilde{\mathcal{S}}} J &= \frac{\phi^*}{\bar{\Theta}} && \text{in} \quad \Omega
\end{aligned} \tag{7}$$

where the overbar denotes the complex conjugate, μ, κ, R and Pr are the dynamic viscosity, the heat conductivity, the Reynolds and Prandtl numbers, respectively, and

$$D_i = \frac{1}{h_i} \frac{\partial}{\partial x^i}.$$

The co-state variables $\phi^* = (\rho^*, u^*, v^*, w^*, T^*)$ and r^* satisfy the adjoint equations

$$\begin{aligned}
\hat{\mathcal{L}}^*\, \phi^* &= \mathcal{S}^* && \text{in} \quad \Omega \\
\mathbf{u}^* = 0, \quad T^* &= 0 && \text{on} \quad x^3 = 0 \\
\mathbf{u}^* \to 0, \quad T^* &\to 0 && \text{as} \quad x^3 \to \infty \\
\phi^* = \phi_1^*, \quad r^* &= r_1^* && \text{on} \quad x^1 = X_1 \\
\frac{\partial}{\partial x^1} \int_0^{+\infty} \phi^{*H} \frac{\partial \hat{\mathcal{L}}}{\partial \alpha}\, \hat{\phi}\, h_1 h_2 h_3\, dx^3 &= f^* && \forall \quad x^1
\end{aligned} \tag{8}$$

where

$$\mathcal{S}^* = -\left[\bar{r}^* D_1(\hat{\phi}) - D_1(r^* \hat{\phi}) - (m_{21} + m_{31}) r^* \hat{\phi}\right], \tag{9}$$

$$\begin{aligned}
f^* = i \int_0^{+\infty} \phi^{*H} \hat{\mathcal{S}}\, h_1 h_2 h_3\, dx^3 + i h_1 h_2 \Big[&-\frac{\kappa}{{\rm Pr}\, R} D_3(\bar{T}^*) \hat{T} \\
&+ (\rho \bar{\rho}^*) \hat{w} + \frac{\mu}{R} D_3(\bar{u}^*) \hat{u} + \frac{\mu}{R} D_3(\bar{v}^*) \hat{v} \Big] \Big|_{x^3 = 0}.
\end{aligned} \tag{10}$$

and

$$m_{ij} = \frac{1}{h_i h_j} \frac{\partial h_i}{\partial x^j}.$$

The co-state equations (8) are integrated in the upstream direction with the initial condition at $x^1 = X_1$ as :

$$\phi_1^* = |\Theta_1|^2 (\mathcal{D}^H)^{-1} (\mathcal{M} - c_1 \mathcal{I}) \hat{\phi}_1, \qquad r_1^* = |\Theta_1|^2\, c_1 \tag{11}$$

β		0	0.02	0.04
$M = 0,$	$\varphi =$	0°	22.3°	41.2°
$M = 0.7,$	$\varphi =$	0°	23.5°	42.5°
$M = 1.2,$	$\varphi =$	0°	25.9°	45.2°

TABLE 1. Spanwise wavenumber β with corresponding wave angle φ at $R = 160$ for different Mach numbers M. $F = 10^{-4}$

where c_1 is given in the appendix and $\mathcal{I}$ is the identity matrix. Equations (8) are solved iteratively to find r^* such that the integral expression is satisfied.

Now, the gradients of J can be obtained in following steps. First, the state variable ϕ is calculated by integrating equations (3) from $x^1 = X_0$ to X_1. Then the co-state equations (8) are integrated backward in the streamwise direction from $x^1 = X_1$ to X_0 to obtain the co-state variables ϕ^*. Finally, equations (7) give the gradients with respect to each control parameter.

It is worth mentioning that the expression for $\mathcal{S}^*$ depends on the choice of the auxiliary condition while the adjoint operator $\hat{\mathcal{L}}^*$ will remain unchanged for other choices of this condition. If the output is defined as in (2) the adjoint system will be

$$\begin{aligned} \hat{\mathcal{L}}^*\ \phi^* &= \mathcal{S}^* + \mathcal{M}^H \hat{\phi} |\Theta|^2 && \text{in} \quad \Omega \\ \mathbf{u}^* = T^* &= 0 && \text{on} \quad x^3 = 0 \\ \mathbf{u}^*,\ T^* &\to 0 && \text{as} \quad x^3 \to \infty \\ \phi^* = r^* &= 0 && \text{on} \quad x^1 = X_1 \end{aligned} \tag{12}$$

$$\frac{\partial}{\partial x^1} \int_0^{+\infty} \phi^{*H} \frac{\partial \hat{\mathcal{L}}}{\partial \alpha}\ \hat{\phi}\ h_1 h_2 h_3 dx^3 + |\Theta|^2 \int_0^{+\infty} \hat{\phi}^H \mathcal{M} \hat{\phi}\ h_1 h_2 h_3\ dx^3 = f^* \forall x^1$$

Note that in this case both ϕ^* and r^* are subjected to homogeneous initial conditions.

4. Results

The results presented here are obtained by numerically integrating the discretized state and co-state equations. The x^1-derivatives are approximated by a first-order accurate backward Euler scheme and the x^3-derivatives by a fourth-order accurate compact finite-difference scheme. For details the reader is referred to Hanifi *et al.* (1994).

The calculations are performed for two- and three dimensional disturbances in a two-dimensional compressible boundary layer on an adiabatic flat plate. The gradients express the sensitivity of disturbances to small unsteady inhomgeneities in the steady boundary layer flow. The stagnation temperature is 300 K and the Prandtl number is held constant to Pr = 0.72. The dynamic viscosity is calculated using Sutherland law and the coefficient of the specific

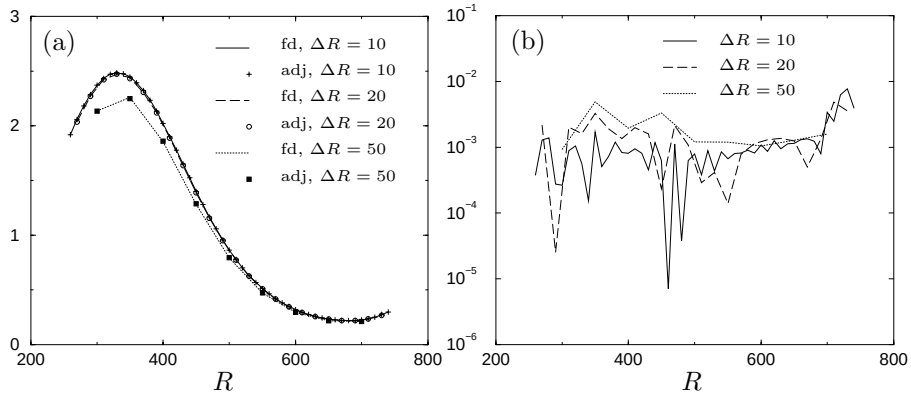

FIGURE 2. Comparison between adjoint (adj) and central difference (fd) calculations for different ΔR. Mach number $M = 0.7$, $\beta = 0$. a) lines denote $||(\partial J/\partial \tilde{w}_r, \partial J/\partial \tilde{w}_i)/\Delta_n||$ and symbols $|\nabla_{\tilde{w}_\mathrm{w}} J_n|$. b) relative error.

heat c_p is assumed to be constant. The ratio of the coefficients of second and dynamic viscosity is given by the Stoke's hypothesis, *i.e.* $\lambda/\mu = -2/3$. In all figures the reduced frequency, defined as $F = 2\pi f^\star \nu_e^\star / U_e^{\star 2}$, is equal to 10^{-4}. Here $f^\star$ is the dimensional physical frequency and the subscript $_e$ refers to values at the edge of the boundary layer. The output is measured at $R = \sqrt{U_e^\star x^{1\star}/\nu_e^\star} = 760$. The calculations have been performed for three values of spanwise wavenumbers β at different Mach numbers. Values of the wave angle φ given at $x^1 = X_0$ for the cases studied here are given in table 1. In all calculations, the metric coefficients $h_1 = h_2 = h_3 = 1$.

4.1. *Accuracy of the gradient, validation*

In order to verify the correctness of the gradient, we compare the adjoint based gradients to those obtained using the finite-difference approach. In the latter, the derivative of the output variable with respect to each input parameter is approximated by a second-order accurate central finite-difference scheme.

To compare the gradients given by the adjoint and finite-difference approaches let us consider the example of a wall normal velocity perturbation $\delta\tilde{w}_\mathrm{w}$ at $x^3 = 0$. The variation of a functional J with respect to this wall perturbation is :

$$\delta J = \frac{\partial J}{\partial \tilde{w}_r}\delta\tilde{w}_r + \frac{\partial J}{\partial \tilde{w}_i}\delta\tilde{w}_i \tag{13}$$

The subscripts $_r$ and $_i$ denote the real and imaginary parts of a complex number. In the finite-difference approach, the derivatives of J are obtained by imposing the inhomogeneous boundary condition $\tilde{w}_\mathrm{w} = \pm\varepsilon$ at $x^1 = x_n^1$. Here, ε is a small number and index n refers to n-th streamwise position. Then,

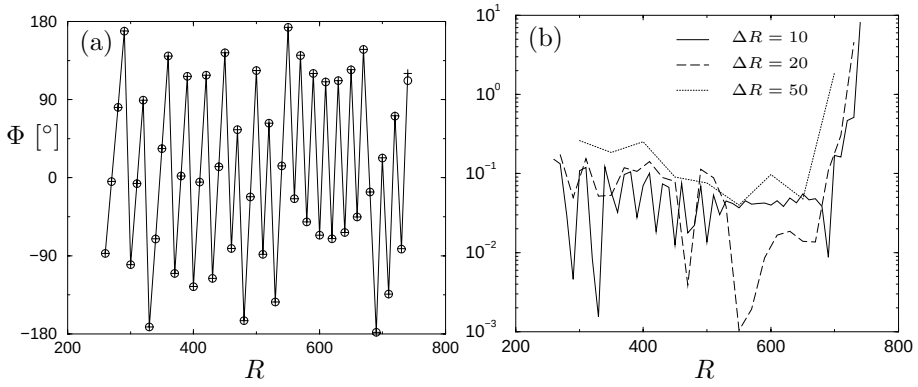

FIGURE 3. Comparison between adjoint and central difference calculations of the phase Φ in degrees for $M = 0.7$, $\beta = 0$. a) $\Delta R = 10$. + denotes central difference, and $\circ$ denotes adjoint calculations. b) absolute error in degrees.

the derivatives are calculated using a second-order accurate finite-difference scheme.

The expression for δJ in the adjoint approach, for a flat plate geometry, is in discretized form given as

$$\delta J = \int_{Z_0}^{Z_1} \sum_{n=2}^{N-1} \frac{1}{2} (\nabla_{\tilde{w}_\mathrm{w}} J_n^H \delta \tilde{w}_{\mathrm{w}_n} + c.c.) \Delta_n \, dx^2, \tag{14}$$

where $\Delta_n = (x_{n+1}^1 - x_{n-1}^1)/2$ and *c.c.* is the complex conjugate. In the following, the quantity $\nabla_{\tilde{w}_\mathrm{w}} J_n$ is compared to those of the finite-difference approach. The streamwise domain used here is $R \in [250, 750]$. In figure 2a the modulus $||(\partial J/\partial \tilde{w}_r, \partial J/\partial \tilde{w}_i)/\Delta_n||$, as a function of x_n^1, is compared to $|\nabla_{\tilde{w}_\mathrm{w}} J_n|$ for different resolution of the streamwise step ΔR. A good agreement is found between the approaches for a given ΔR, and both values converge as ΔR is decreased. The relative error given in figure 2b is below one percent for all cases and decreases slightly as ΔR is decreased.

The phase Φ of the gradients obtained by adjoint equations and central differences is compared in figure 3a for a given streamwise step, $\Delta R = 10$. The absolute error of the phase shown in figure 3b is less than 0.1 degrees except close to the outlet of the domain.

4.2. *Sensitivity to wall disturbances.*

In figures 4, 5 and 6 the modulus of the gradient for inhomogeneous wall boundary conditions are shown for three different Mach numbers M and spanwise wavenumbers β. As can be seen in there, the maximum value of the gradient is achieved if forcing is situated close to branch I of the neutral stability

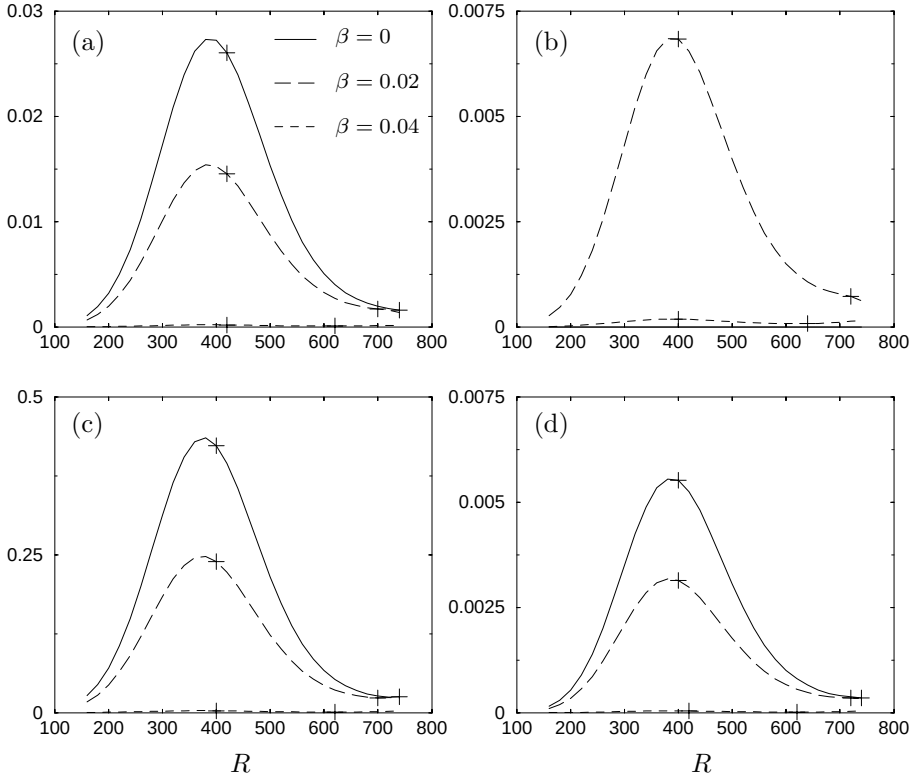

FIGURE 4. Modulus of the gradients due to 2D and 3D wall disturbances as a function of the Reynolds number for a Mach number $M = 0$. a) $|\nabla_{\tilde{u}_w} J|$, streamwise velocity component; b) $|\nabla_{\tilde{v}_w} J|$ spanwise velocity component; c) $|\nabla_{\tilde{w}_w} J|$ normal velocity component; d) $|\nabla_{\tilde{T}_w} J|$ temperature component.

curve. This is in agreement with receptivity studies of *e.g.* Hill (1995), Airiau, Walther and Bottaro (2001) and Airiau (2000). In Airiau *et al.* the wall gradients were interpreted as wall Green's functions. One should note that the distance between the maximum value of the gradient and Branch I of the neutral stability curve depends on the Mach number and the input parameter. Branch I and branch II are marked on each curve in the figures with + signs. For low Mach numbers, the two-dimensional waves, $\beta = 0$, give the largest value of the gradient for wall-disturbance components $\tilde{u}, \tilde{v}, \tilde{w}$ and $\tilde{T}$. This can be seen for $M = 0$ and $M = 0.7$ in figures 4 and 5, respectively. As is shown in figure 6, where $M = 1.2$, it is clear that for higher Mach numbers the two-dimensional waves do not have the largest gradient. This observation follows the fact that in compressible boundary layers the three-dimensional disturbances are the most unstable ones (see *e.g.* Mack 1984). The magnitude

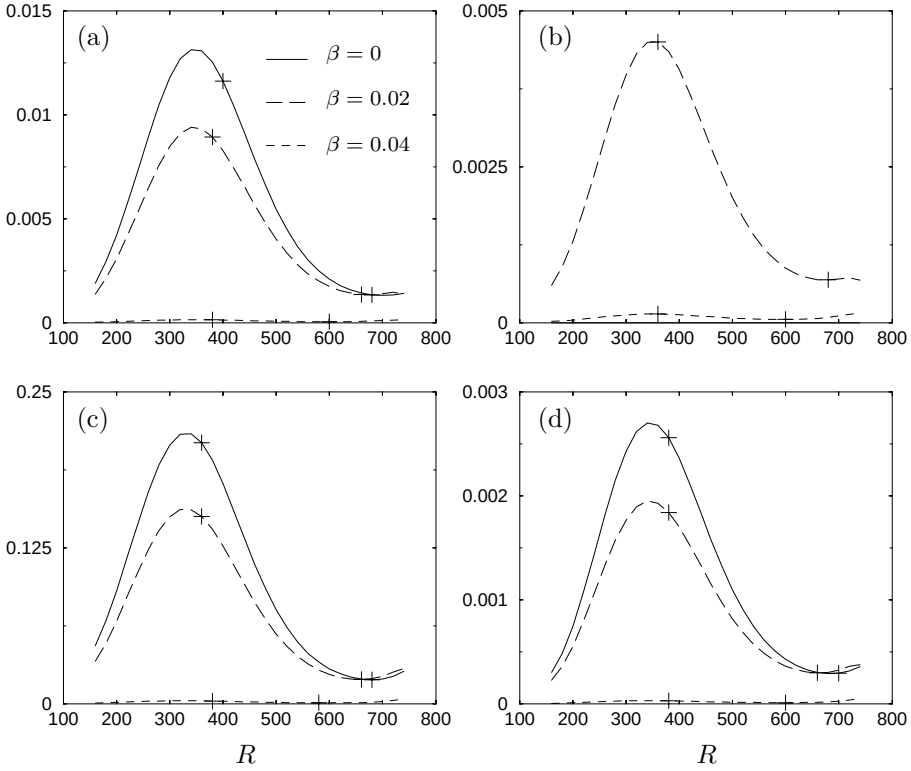

FIGURE 5. Modulus of the gradients due to 2D and 3D wall disturbances as a function of the Reynolds number for a Mach number $M = 0.7$. a) $|\nabla_{\tilde{u}_w} J|$, streamwise velocity component; b) $|\nabla_{\tilde{v}_w} J|$ spanwise velocity component; c) $|\nabla_{\tilde{w}_w} J|$ normal velocity component; d) $|\nabla_{\tilde{T}_w} J|$ temperature component.

of the gradient is quite different comparing $\tilde{u}, \tilde{v}, \tilde{w}$ and $\tilde{T}$ in figures 4, 5 and 6. It was noted that the normal velocity component gave the largest gradient for various spanwise wavenumber at Mach numbers between 0 and 1.2. The response to the wall normal velocity component was one order of magnitude larger than the streamwise and spanwise velocity components. In cases studied here, the normal component is about 15 times that of the streamwise component. This implies that blowing and suction at the wall is the most efficient mean of controlling the instability waves. However, as is shown in the figures, the maximum response to a wall disturbance decreases as the Mach number increases. This means that the efficiency of blowing and suction for control of disturbance growth decreases at higher Mach numbers.

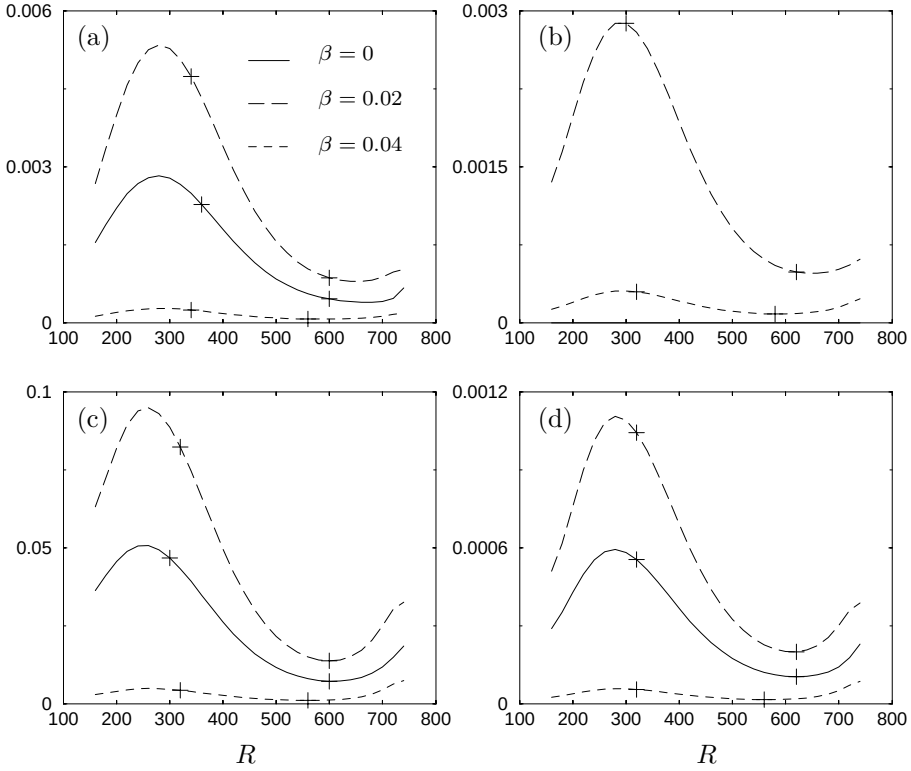

FIGURE 6. Modulus of the gradients due to 2D and 3D wall disturbances as a function of the Reynolds number for a Mach number $M = 1.2$. a) $|\nabla_{\tilde{u}_w} J|$, streamwise velocity component; b) $|\nabla_{\tilde{v}_w} J|$ spanwise velocity component; c) $|\nabla_{\tilde{w}_w} J|$ normal velocity component; d) $|\nabla_{\tilde{T}_w} J|$ temperature component.

4.3. *Sensitivity to momentum sources.*

In figure 7 the modulus of the gradients for the streamwise and normal momentum forcing are plotted. The Mach number and spanwise wavenumber are both zero in this case. However, the qualitative behavior does not change for higher Mach numbers up to 1.2, and spanwise wavenumbers of 0, 0.02 and 0.04 which were studied here. A first observation is that the gradient for the streamwise component of a source of momentum $|\nabla_{\tilde{S}_u} J|$ is about 10 times that of the normal component. Further, the maximum value of $|\nabla_{\tilde{S}_u} J|$ is located near branch I of the neutral stability curve. It was noted by *e.g.* Hill (1995) that forcing most effectively is done in the vicinity of the critical layer, *i.e.* where the streamwise velocity $U(x, y) = \omega/\texttt{Real}\{\alpha\}$. This was also found in our analysis. The location of the critical layer is marked with a line in figure 7a.

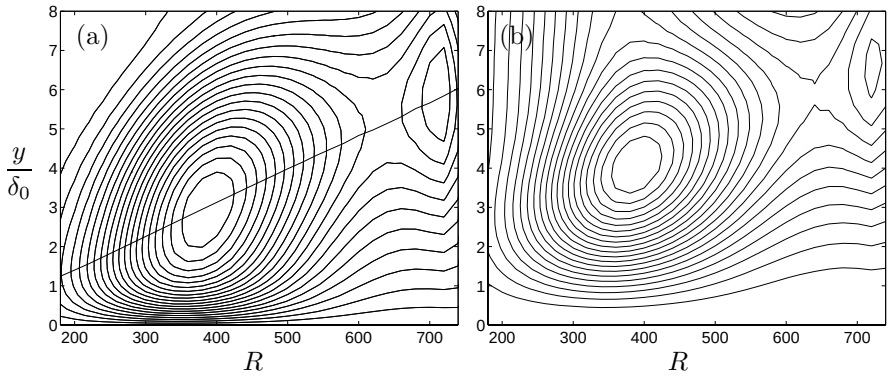

FIGURE 7. Contour plot of the gradients for momentum forcing. δ_0 denotes the boundary-layer thickness at streamwise position $x^1 = X_0$. $F = 10^{-4}$, $M = 0.7$, $\beta = 0$. The line in a) shows the position of the critical layer. a) $|\nabla_{\tilde{\mathcal{S}}_u} J|$, streamwise component with maximum = 1.8. Branch locations: I at $R \approx 400$, II at $R \approx 680$. b) $|\nabla_{\tilde{\mathcal{S}}_w} J|$, normal component with maximum = 0.16. Branch locations: I at $R \approx 360$, II at $R \approx 680$.

5. Conclusions

The Adjoint Parabolized Stability Equations (APSE) have been derived for quasi three-dimensional compressible flow using an input/output framework. The equations are given for an orthogonal curvilinear coordinate system. The adjoint field gives the sensitivity of disturbances to changes in boundary conditions and momentum forcing. These equations provide a basis for optimal control of disturbance growth using unsteady wall perturbation or unsteady momentum forcing.

In the present formulation, the sensitivity of the objective function (output) to all control parameters (input) is found by solving the state equations and their adjoint once. This will drastically reduce the computational costs in an optimal design procedure.

The accuracy of the gradients have been verified by comparing the gradients derived by the adjoint equations with a finite-difference approach. It was shown that as the streamwise resolution is increased the differences between these two methods decrease and the solution of the gradient converges.

Analysis of two-dimensional boundary layers shows that a given disturbance is most sensitive to wall- and momentum forcing close to branch I of the neutral stability curve. The streamwise distance between the maximum of sensitivity and Branch I depends on the input component. This was found to be true for $0 \leqslant M \leqslant 1.2$ studied here. We also found that the response to the

inhomogeneities of normal velocity at the wall is at least one order of magnitude larger than those of other the velocity components and temperature. This is in agreement with Hill (1995) for incompressible flow.

For incompressible flows, it has been shown that the two-dimensional disturbances are the most sensitive ones to wall inhomogeneity. However, for compressible flows, the three-dimensional disturbances are the most sensitive ones. Further, it has been observed that momentum forcing is most effectively done in the vicinity of the critical layer, which has earlier been shown by Hill for incompressible boundary layer.

The results shown here are obtained with an objective function solely defined by the terminal energy. If instead the disturbance energy over the entire domain is used then the peak of the gradient would probably move another streamwise position. Further, if the cost of the control energy is added to the objective function as $J = E + \epsilon E_c$ then the results will most certainly change. One point that has to be made clear when adding the control energy is that the goal is not just to find the gradient for the disturbance energy but also for the control energy used. In the simple case shown in this article it turns out that the gradient appear to be similar to well known stability results, however what will happen in the other cases described above is left for future investigations.

The second author wishes to thank the 'Conférence des Grandes Ecoles' and FFA for their financial support. This work was carried out during a three-months period at FFA where he appreciated the Swedish friendship. The authors also wish to thank Martin Berggren at FFA for valuable discussions.

Appendix A. The non-local stability equations

A.1. *Governing equations and assumptions*

A model of convectively unstable waves with curved or divergent wave-rays in a non-uniform flow is described here. The equations are derived from the equations of conservation of mass, momentum and energy and the equation of state governing the flow of a viscous, compressible, ideal gas expressed in primitive variables and curvilinear coordinates. The non-dimensional conservation equations in vector notation are given by

$$\rho\,[\frac{\partial \mathbf{u}}{\partial t} + (\mathbf{u}\cdot\nabla)\mathbf{u}] = -\nabla p + \frac{1}{R}\nabla[\lambda(\nabla\cdot\mathbf{u})] + \frac{1}{R}\nabla\cdot[\mu(\nabla\mathbf{u} + \nabla\mathbf{u}^T)], \tag{15}$$

$$\frac{\partial \rho}{\partial t} + \nabla\cdot(\rho\mathbf{u}) = 0, \tag{16}$$

$$\rho c_p[\frac{\partial T}{\partial t} + (\mathbf{u}\cdot\nabla)T] = \frac{1}{R\,\mathrm{Pr}}\nabla\cdot(\kappa\nabla T) + (\gamma-1)M^2[\frac{\partial p}{\partial t} + (\mathbf{u}\cdot\nabla)p + \frac{1}{R}\Phi], \tag{17}$$

$$\gamma M^2 p = \rho T, \tag{18}$$

with viscous dissipation given as

$$\Phi = \lambda(\nabla \cdot \mathbf{u})^2 + \frac{1}{2}\mu[\nabla\mathbf{u} + \nabla\mathbf{u}^T]^2.$$

Here t represents time, ρ, p, T stand for density, pressure and temperature, $\mathbf{u}$ is the velocity vector. The quantities λ, μ stand for the second and dynamic viscosity coefficient, γ is the ratio of specific heats, κ the heat conductivity, c_p the specific heat at constant pressure. All flow quantities are made non-dimensional by corresponding reference flow quantities at a fixed streamwise position $x_0^\star$, except the pressure which is referred to twice the corresponding dynamic pressure. The reference length scale is fixed and taken as

$$l_0^\star = \sqrt{\frac{\nu_0^\star x_0^\star}{U_0^\star}}.$$

The Mach number, M, Prandtl number, Pr and Reynolds number, R are defined as

$$M = \frac{U_0^\star}{\sqrt{\Re\gamma T_0^\star}}, \quad \mathrm{Pr} = \frac{\mu_0^\star c_{p0}^\star}{\kappa_0^\star}, \quad R = \frac{U_0^\star l_0^\star}{\nu_0^\star},$$

where $\Re$ is the specific heat constant and superscript * refers to dimensional quantities.

We decompose the flow and material quantities into a mean flow part Q and a disturbance $\tilde{q}$ as $Q_{tot}(x^i, t) = Q(x^i) + \tilde{q}(x^i, t)$ where x^1, x^2 and x^3 are the normal, spanwise and streamwise components respectively. Here $Q \in [U, V, W, p, T, \rho]$ and $\tilde{q} \in [\tilde{u}, \tilde{v}, \tilde{w}, \tilde{p}, \tilde{T}, \tilde{\rho}]$, where U, V, W are the streamwise, spanwise and normal components of the mean velocity vector, respectively. u, v, w are those of the perturbation velocity vector. The domain considered is defined as $x^1 \in [X_0, X_1]$, $x^2 \in [Z_0, Z_1]$ and $x^3 \in [0, \infty[$. To simplify the analysis the mean flow is considered to be independent of the spanwise coordinate x^2. Two assumptions are made to derive the non-local stability equations. The first is of WKB type where the disturbance $\tilde{q}$ is divided into an amplitude function and a wave function

$$\tilde{q}(x^i, t) = \hat{q}(x^1, x^3)\Theta, \quad \Theta = \exp\, i\,(\int_{X_0}^{x^1} \alpha(x')dx' + \beta x^2 - \omega t).$$

Here α is a complex wavenumber, β the real spanwise wavenumber and ω the real angular wave frequency. The second assumption is a scale separation $1/R$ between the weak variation in the x^1 direction and the strong variation in the x^3 direction analogous to the multiple scales method. We assume

$$\frac{\partial}{\partial x^1} \sim \mathcal{O}(R^{-1}), \quad V \sim \mathcal{O}(R^{-1})$$

Furthermore, it is assumed that the metrics are of order $\mathcal{O}(R^{-1})$.

A.2. *The linear non-local stability equations*

The non-local stability equations are derived using Parabolized Stability Equation approach (PSE). We consider a general case where the boundary layer is subjected to sources of mass, momenta and energy, $\tilde{\mathcal{S}}$, and inhomogeneous boundary conditions on the wall. The linearized disturbance equations are obtained by introducing the variable decomposition into the governing equations (15)-(18), subtracting the equations for the mean flow and removing the products of disturbances. We proceed with the derivation of the stability equations by introducing the scaling relations given in section A.1. Finally, collecting terms up to order $\mathcal{O}(R^{-1})$ gives a set of nearly parabolic partial differential equations. A note on the parabolic nature of PSE can be found in *e.g.* Li and Malik (1996), and Andersson, Henningson and Hanifi (1998). The equation can now be written

$$\hat{\mathcal{L}}\ \hat{\phi}(x^1, x^3) = \hat{\mathcal{S}}(x^1, x^3) \tag{19}$$

where the vector of the amplitude functions is $\hat{\phi} = (\hat{\rho}, \hat{u}, \hat{v}, \hat{w}, \hat{T})^{\mathrm{T}}$. The boundary conditions are

$$\begin{array}{l} \hat{\mathbf{u}}(x^1, 0) = \hat{\mathbf{u}}_{\mathrm{w}}(x^1), \quad \hat{T}(x^1, 0) = \hat{T}_{\mathrm{w}}(x^1), \\ \lim\limits_{x^3 \to \infty} \hat{\mathbf{u}} = 0 \quad \text{and} \quad \lim\limits_{x^3 \to \infty} \hat{T} = 0. \end{array} \tag{20}$$

The operator $\hat{\mathcal{L}}$ is defined as

$$\hat{\mathcal{L}} = \mathcal{A} + \mathcal{B}D_3 + \mathcal{C}D_{33} + \mathcal{D}D_1 \tag{21}$$

where

$$D_i = \frac{1}{h_i}\frac{\partial}{\partial x^i}, \qquad D_{ii} = \frac{1}{h_i^2}\frac{\partial^2}{(\partial x^i)^2}.$$

Here, h_i is the scale factor such that a length element is defined as $ds^2 = (h_1 dx^1)^2 + (h_2 dx^2)^2 + (h_3 dx^3)^2$. The coefficients of the 5×5 matrices $\mathcal{A}$, $\mathcal{B}$, $\mathcal{C}$ and $\mathcal{D}$ can be found in appendix Appendix C. Furthermore, as both the amplitude function and the wave function depend on the x^1 coordinate, this ambiguity is removed by specifying an auxiliary condition

$$\int_0^\infty \hat{\phi}^H \frac{\partial \hat{\phi}}{\partial x^1}\ h_2 h_3 dx^3 = 0, \tag{22}$$

where, superscript ^{H} denotes the transpose complex conjugate. This condition also guarantees that x^1-variation of the disturbance amplitude function remains small such that second streamwise derivatives are negligible.

Appendix B. Derivation of the gradient

The gradients are derived using the adjoint equations of the Parabolized Stability Equations. A discrete or a continuous formulation may be used. It was concluded by Högberg *et al.* (2000) that a continuous formulation is a good

enough approximation if control is performed on a problem with a dominating instability. This type of analysis can be done with the PSE therefore a continuous approach is used in this paper.

B.1. *Inner product*

For a compact notation of the adjoint equations, we will use the *formal adjoint* $\mathcal{L}^*$ of the differential operator $\mathcal{L}$ defined by the relation

$$(\mathcal{L}^*\Psi^*, \Phi) = (\Psi^*, \mathcal{L}\Phi) + \text{ boundary terms},$$

where the inner product $(\cdot,\cdot)$ is defined as

$$(\Phi, \Psi^*) = \int_{X_0}^{X_1}\int_{Z_0}^{Z_1}\int_0^{+\infty} \Phi^H\Psi^*\; h_1h_2h_3\; dx^3\; dx^2\; dx^1, \tag{23}$$

for $\mathbb{C}^n$-valued functions Φ and Ψ^*. Here, the superscript * stands for adjoint quantities.

B.2. *Derivation of adjoint equations*

At first, the equations (1), (19), (20) and (22) has to be differentiated with respect to the input variables $\hat{\mathbf{u}}_\mathrm{w}, \hat{T}_\mathrm{w}$,$\hat{\mathcal{S}}$ and the state variables α and ϕ

$$\begin{aligned}\delta J \;=\; \mathtt{Real}\Bigg\{ &\int_{Z_0}^{Z_1}\int_0^{\infty} |\Theta_1|^2\hat{\phi}_1^H\mathcal{M}\delta\hat{\phi}_1 h_2h_3\; dx^3\; dx^2 \;+\\ &\int_{Z_0}^{Z_1}\int_0^{\infty} |\Theta_1|^2\hat{\phi}_1^H\mathcal{M}\hat{\phi}_1\; i\int_{X_0}^{X_1}\delta\alpha dx'\; h_2h_3\; dx^3\; dx^2\Bigg\}\end{aligned} \tag{24}$$

$$\begin{aligned}
\hat{\mathcal{L}}\;\delta\hat{\phi} - \delta\hat{\mathcal{S}} + \frac{\partial\hat{\mathcal{L}}}{\partial\alpha}\delta\alpha\;\hat{\phi} &= 0 && \text{in} && \Omega\\
\delta\phi_0 &= 0 && \text{on} && x^1 = X_0\\
\delta\hat{\mathbf{u}}(x^1,0) &= \delta\hat{\mathbf{u}}_\mathrm{w}(x^1) && \text{on} && x^3 = 0\\
\delta\hat{\mathbf{u}} &\to 0 && \text{as} && x^3\to\infty\\
\delta\hat{T}(x^1,0) &= \delta\hat{T}_\mathrm{w}(x^1) && \text{on} && x^3 = 0\\
\delta\hat{T} &\to 0 && \text{as} && x^3\to\infty\\
\int_0^{\infty}(\delta\hat{\phi}^H\frac{\partial\hat{\phi}}{\partial x^1} + \hat{\phi}^H\frac{\partial\delta\hat{\phi}}{\partial x^1})\; h_2h_3dx^3 &= 0 && \forall && x^1
\end{aligned} \tag{25}$$

Note here that the variation of a disturbance ϕ results in the variation of both the amplitude function $\hat{\phi}$ and the streamwise wave-number α. A complex co-state vector $\phi^* = (\rho^*, u^*, v^*, w^*, T^*)^\mathrm{T}$ and complex function $r^*(x^1)$ are introduced. The adjoint equations are derived by taking the inner product of vector ϕ^* with the differentiated state equations, and r^* with the differentiated auxiliary condition according to the inner product (23). The complex conjugate of each term in the equation is added. Then, derivatives are removed from

the differentiated variables in equation (26) using integration by parts. After integrations, it yields (without complex conjugate for clarity)

$$
\begin{aligned}
&(\phi^*,\ \hat{\mathcal{L}}\ \delta\hat{\phi} - \delta\hat{\mathcal{S}} + \frac{\partial\hat{\mathcal{L}}}{\partial\alpha}\delta\alpha\ \hat{\phi}) + \\
&\int_{X_0}^{X_1}\int_{Z_0}^{Z_1}\bar{r}^*\int_0^{+\infty}[\delta\hat{\phi}^H D_1(\hat{\phi}) + \hat{\phi}^H D_1(\delta\hat{\phi})]\ h_1h_2h_3dx^3\ dx^2\ dx^1 = \\
&(\hat{\mathcal{L}}^*\phi^*, \delta\hat{\phi}) - (\phi^*, \delta\hat{\mathcal{S}}) - \\
&\int_{X_0}^{X_1}\int_{Z_0}^{Z_1}\int_0^{+\infty}\frac{\partial}{\partial x^1}(\phi^{*H}\frac{\partial\hat{\mathcal{L}}}{\partial\alpha}\ \hat{\phi}\ h_1h_2h_3)\int_{X_0}^{x^1}\delta\alpha dx'\ dx^3\ dx^2\ dx^1 + \\
&\int_{Z_0}^{Z_1}\int_0^{+\infty}\Big[\phi^{*H}\frac{\partial\hat{\mathcal{L}}}{\partial\alpha}\ \hat{\phi}\ h_1h_2h_3\int_{X_0}^{x^1}\delta\alpha dx'\Big]_{X_0}^{X_1}dx^3\ dx^2 + \\
&\int_{Z_0}^{Z_1}\int_0^{+\infty}\Big[\phi^{*H}\ \mathcal{D}\ \delta\hat{\phi}\ h_2h_3\Big]_{X_0}^{X_1}dx^3\ dx^2 + \\
&\int_{Z_0}^{Z_1}\int_{X_0}^{X_1}\Big[\Big\{\phi^{*H}\left(\mathcal{B}\ -\ (m_{13}+m_{23}-m_{33})\,\mathcal{C}\ -\ D_3(\mathcal{C})\right)\delta\hat{\phi}\ + \\
&\qquad -D_3(\phi^{*H})\,\mathcal{C}\ \delta\hat{\phi}\ +\ \phi^{*H}\,\mathcal{C}\ D_3(\delta\hat{\phi})\Big\}\ h_1h_2\ dx^2\ dx^1\Big]_0^{\infty} + \\
&\int_{X_0}^{X_1}\int_{Z_0}^{Z_1}\int_0^{+\infty}\Big(r^*D_1(\hat{\phi}^H) - D_1(\bar{r}^*\hat{\phi}^H) - \\
&\qquad (m_{21}+m_{31})\bar{r}^*\hat{\phi}^H\Big)\ \delta\hat{\phi}\ h_1h_2h_3dx^3\ dx^2\ dx^1 + \\
&\int_{Z_0}^{Z_1}\int_0^{+\infty}\Big[h_2h_3\bar{r}^*\hat{\phi}^H\delta\hat{\phi}\Big]_{X_0}^{X_1}dx^3\ dx^2 = 0
\end{aligned}
\tag{26}
$$

where

$$m_{ij} = \frac{1}{h_ih_j}\frac{\partial h_i}{\partial x^j}.$$

Terms of $\delta\alpha$ have also been integrated in equation (26) in order to identify from δJ the boundary terms at X_1. Collecting terms of $\delta\hat{\phi}$ leads to the adjoint equations

$$\hat{\mathcal{L}}^*\phi^* = -\Big[\bar{r}^*D_1(\hat{\phi}) - D_1(r^*\hat{\phi}) - (m_{21}+m_{31})\ r^*\hat{\phi}\Big] \tag{27}$$

In order to remove the terms of $\delta\hat{\phi}$ in the equation (26) as $x^3 \to \infty$, the following homogeneous boundary conditions are chosen

$$
\begin{array}{rclcrcl}
\mathbf{u}^*(x^1,0) & = & 0 & \text{and} & T^*(x^1,0) & = & 0, \\
\lim\limits_{x^3\to\infty}\mathbf{u}^* & = & 0 & \text{and} & \lim\limits_{x^3\to\infty}T^* & = & 0,
\end{array}
\tag{28}
$$

where $\mathbf{u}^* = (u^*, v^*, w^*)^{\mathrm{T}}$. Using the operator matrices of the forward problem, the adjoint operator $\hat{\mathcal{L}}^*$ can be identified

$$\hat{\mathcal{L}}^* \ =\ \tilde{\mathcal{A}}\ +\ \tilde{\mathcal{B}}\ D_3.\ +\ \tilde{\mathcal{C}}\ D_{33}.\ +\ \tilde{\mathcal{D}}\ D_1. \tag{29}$$

where $\tilde{\mathcal{A}}, \tilde{\mathcal{B}}, \tilde{\mathcal{C}}$ and $\tilde{\mathcal{D}}$ are

$$\begin{aligned}
\tilde{\mathcal{A}} &= \mathcal{A}^H - D_3(\mathcal{B}^H) - (m_{13}+m_{23})\,\mathcal{B}^H + D_{33}(\mathcal{C}^H) \\
&+ 2\,(m_{13}+m_{23}-m_{33})\,D_3(\mathcal{C}^H) \\
&- D_1(\mathcal{D}^H) - (m_{21}+m_{31})\,\mathcal{D}^H \\
\tilde{\mathcal{B}} &= -\mathcal{B}^H + 2\,D_3(\mathcal{C}^H) + 2\,(m_{13}+m_{23}-m_{33})\,\mathcal{C}^H \\
\tilde{\mathcal{C}} &= \mathcal{C}^H \\
\tilde{\mathcal{D}} &= -\mathcal{D}^H,
\end{aligned}$$

The system of equations (27) with corresponding boundary conditions (28) is parabolic in the streamwise direction and must be integrated upstream, from X_1 to X_0. The initial condition at X_1 is found by identifying δJ, equation (24), with the terms defined at X_1 in equation (26). Matching terms of $\delta\hat{\phi}$, and $\delta\alpha$ gives the following system of equations to solve for the initial condition for ϕ^* and r^*

$$\begin{aligned}
|\Theta_1|^2 \int_0^\infty \hat{\phi}_1^H \mathcal{M} \delta\hat{\phi}_1 h_2 h_3 \, dx^3 &= \int_0^{+\infty} (\phi^{*H}\,\mathcal{D} + \bar{r}^*\hat{\phi}^H)\,\delta\hat{\phi}\; h_2 h_3 dx^3 \Big|_{X_1} \\
i|\Theta_1|^2 \int_0^\infty \hat{\phi}_1^H \mathcal{M} \hat{\phi}_1 h_2 h_3 \, dx^3 &= \int_0^{+\infty} \phi^{*H} \frac{\partial\hat{\mathcal{L}}}{\partial\alpha}\,\hat{\phi}\; h_1 h_2 h_3 \, dx^3 \Big|_{X_1}
\end{aligned} \tag{30}$$

Solving the above equations gives the initial condition for the adjoint equations at X_1 as

$$\begin{aligned}
\phi_1^* &= |\Theta_1|^2 \mathcal{D}^+ (\mathcal{M} - c_1\mathcal{I})\hat{\phi}_1, \qquad r_1^* = |\Theta_1|^2\, c_1, \\
\bar{c}_1 &= \frac{\displaystyle\int_0^\infty (h_1 \hat{\phi}_1^H \mathcal{M}\; D^{+H} \frac{\partial\hat{\mathcal{L}}}{\partial\alpha}\hat{\phi}_1 - i\hat{\phi}_1^H \mathcal{M}\hat{\phi}_1)\; h_2 h_3 \, dx^3}{\displaystyle\int_0^\infty \hat{\phi}_1^H \mathcal{D}^{+H} \frac{\partial\hat{\mathcal{L}}}{\partial\alpha}\hat{\phi}_1\; h_1 h_2 h_3 \, dx^3},
\end{aligned} \tag{31}$$

where $\mathcal{D}^+ = (\mathcal{D}^H)^{-1}$. Since by definition $\delta\phi = 0$ at X_0, the remaining terms of equation (26) together with equation (24) can be written

$$\begin{aligned}
\delta J = \mathtt{Real}\Bigg\{ & \int_{X_0}^{X_1}\int_{Z_0}^{Z_1}\int_0^{+\infty} \phi^{*H}\delta\hat{\mathcal{S}}\; h_1 h_2 h_3 \, dx^3\, dx^2\, dx^1 + \\
& \int_{X_0}^{X_1}\int_{Z_0}^{Z_1}\int_0^{+\infty} \frac{\partial}{\partial x^1}(\phi^{*H}\frac{\partial\hat{\mathcal{L}}}{\partial\alpha}\;\hat{\phi}\; h_1 h_2 h_3) \int_{X_0}^{x^1} \delta\alpha dx'\, dx^3\, dx^2\, dx^1 + \\
& \int_{Z_0}^{Z_1}\int_{X_0}^{X_1} \Big\{ \phi^{*H}\Big[\mathcal{B} - (m_{13}+m_{23}-m_{33})\,\mathcal{C} - D_3(\mathcal{C})\Big]\,\delta\hat{\phi} + \\
& \qquad -D_3(\phi^{*H})\,\mathcal{C}\,\delta\hat{\phi} + \phi^{*H}\,\mathcal{C}\,D_3(\delta\hat{\phi})\Big\}\; h_1 h_2\, dx^2\, dx^1 \Big|_{x^3=0} \Bigg\}
\end{aligned} \tag{32}$$

The gradient should be identified from the variation of $\tilde{\phi}$ and of $\tilde{\mathcal{S}}$. However in equation (32) the variation of the momentum source and wall boundary

condition is expressed in terms of $\hat{\phi}$ and $\hat{\mathcal{S}}$. The total variation of $\tilde{\phi}$ and $\tilde{\mathcal{S}}$ is written

$$\delta\tilde{\phi} = \delta\hat{\phi}\ \Theta + \tilde{\phi}\ i\int_{X_0}^{x^1}\delta\alpha dx'\ , \qquad \delta\tilde{\mathcal{S}} = \delta\hat{\mathcal{S}}\ \Theta + \tilde{\mathcal{S}}\ i\int_{X_0}^{x^1}\delta\alpha dx' \tag{33}$$

From equation (33), $\delta\hat{\phi}$ and $\delta\hat{\mathcal{S}}$ are substituted into equation (32). The variation of the functional δJ with respect to the total variation of $\tilde{\phi}$ and $\tilde{\mathcal{S}}$ is now written

$$\begin{aligned}
\delta J = \mathtt{Real}\Bigg\{ & \int_{X_0}^{X_1}\int_{Z_0}^{Z_1}\int_0^{+\infty}\frac{1}{\Theta}\phi^{*H}\delta\tilde{\mathcal{S}}\ h_1h_2h_3\ dx^3\ dx^2\ dx^1 + \\
& \int_{X_0}^{X_1}\int_{Z_0}^{Z_1} h_1h_2\Big[-\frac{\kappa}{\Theta\,\mathrm{Pr}\,R}D_3(\bar{T}^*)\delta T + \frac{(\rho\bar{\rho}^*)}{\Theta}\delta\tilde{w} + \\
& \qquad \frac{\mu}{\Theta R}D_3(\bar{u}^*)\delta\tilde{u} + \frac{\mu}{\Theta R}D_3(\bar{v}^*)\delta\tilde{v}\Big]\ dx^2\ dx^1\Big|_{x^3=0} - \\
& \int_{X_0}^{X_1}\int_{Z_0}^{Z_1}\int_0^{+\infty}\frac{\partial}{\partial x^1}(\phi^{*H}\frac{\partial\hat{\mathcal{L}}}{\partial\alpha}\ \hat{\phi}\ h_1h_2h_3)\int_{X_0}^{x^1}\delta\alpha dx'\ dx^3\ dx^2\ dx^1 + \\
& \int_{X_0}^{X_1}\int_{Z_0}^{Z_1}\int_0^{+\infty}\phi^{*H}\hat{\mathcal{S}}\ h_1h_2h_3\ i\ \int_{X_0}^{x^1}\delta\alpha dx' dx^3\ dx^2\ dx^1 + \\
& \int_{X_0}^{X_1}\int_{Z_0}^{Z_1} h_1h_2\Big[-\frac{\kappa}{\mathrm{Pr}\,R}D_3(\bar{T}^*)\hat{T} + (\rho\bar{\rho}^*)\hat{w} + \frac{\mu}{R}D_3(\bar{u}^*)\hat{u} + \\
& \qquad \frac{\mu}{R}D_3(\bar{v}^*)\hat{v}\Big]\ i\ \int_{X_0}^{x^1}\delta\alpha dx'\ dx^2\ dx^1\Big|_{x^3=0}\Bigg\}
\end{aligned} \tag{34}$$

In equation (34) the expression for the wall boundary terms have been expanded to clarify the dependence between each state variable and the adjoint quantities. In the derivation of the adjoint equations the co-state variable $r^*(x)$ has been used in order to incorporate the auxiliary condition. However, equation (27) gives a system with five equations and six co-state variables. Therefore, an additional equation is needed to close the system. Collecting the terms of $\delta\alpha$ in equation (34) provides an additional equation which must be satisfied for each position in x^1

$$\begin{aligned}
& \int_0^{+\infty}\frac{\partial}{\partial x^1}(\phi^{*H}\frac{\partial\hat{\mathcal{L}}}{\partial\alpha}\ \hat{\phi}\ h_1h_2h_3)\ dx^3 = i\ \int_0^{+\infty}\phi^{*H}\hat{\mathcal{S}}\ h_1h_2h_3\ dx^3 + \\
& i\ h_1h_2\Big[-\frac{\kappa}{\mathrm{Pr}\,R}D_3(\bar{T}^*)\hat{T} + (\rho\bar{\rho}^*)\hat{w} + \frac{\mu}{R}D_3(\bar{u}^*)\hat{u} + \frac{\mu}{R}D_3(\bar{v}^*)\hat{v}\Big]\Big|_{x^3=0}
\end{aligned} \tag{35}$$

It is denoted 'adjoint auxiliary condition' and is solved with an iterative process for r^* in a similar manner that equation (22) is solved for the streamwise wavenumber α. The gradient of the functional ∇J, with respect to the momentum forcing and wall disturbances can now be identified from the remaining

terms of equation (34) as

$$\begin{aligned}
\nabla_{\tilde{u}_w} J &= \frac{\mu}{\bar{\Theta} R} D_3(u^*) && \text{on} \quad x^3 = 0 \\
\nabla_{\tilde{v}_w} J &= \frac{\mu}{\bar{\Theta} R} D_3(v^*) && \text{on} \quad x^3 = 0 \\
\nabla_{\tilde{w}_w} J &= \frac{\rho \rho^*}{\bar{\Theta}} && \text{on} \quad x^3 = 0 \\
\nabla_{\tilde{T}_w} J &= -\frac{\kappa}{\bar{\Theta} \Pr R} D_3(T^*) && \text{on} \quad x^3 = 0 \\
\nabla_{\tilde{\mathcal{S}}} J &= \frac{\phi^*}{\bar{\Theta}} && \text{in} \quad \Omega
\end{aligned} \tag{36}$$

Appendix C. Operator matrices

The non-zero components of matrices $\mathcal{A}, \mathcal{B}, \mathcal{C}$ and $\mathcal{D}$ in equation (21) are

$$\begin{aligned}
a(1,1) &= U(m_{31} + m_{21}) + D_3(W) + D_1(U) + i\xi \\
a(1,2) &= \rho(i\alpha_0 + m_{31} + m_{21}) + D_1(\rho) \\
a(1,3) &= i\beta_0 \rho \\
a(1,4) &= \rho(m_{13} + m_{23}) + D_3(\rho) \\
a(2,1) &= \frac{1}{\gamma M^2}(D_1(T) + i\alpha_0 T) + D_1(U)U + D_3(U)W - m_{21} V^2 \\
a(2,2) &= \rho(D_1(U) + i\xi) + \frac{\mu}{R}(\alpha_0^2 l_2 + \beta_0^2) \\
a(2,3) &= -2\rho m_{21} V + \frac{\mu}{R}\alpha_0 \beta_0 l_1 \\
a(2,4) &= \rho(m_{13} U + D_3(U)) - \frac{i\alpha_0}{R}\frac{d\mu}{dT} D_3(T) \\
a(2,5) &= \frac{1}{\gamma M^2}(D_1(\rho) + i\rho\alpha_0) + \frac{1}{R}(-\frac{d\mu}{dT} D_{33}(U) - D_3(U)\frac{d^2\mu}{dT^2} D_3(T)) \\
a(3,1) &= U(m_{21} V + D_1(V)) + D_3(V)W + \frac{i\beta_0}{\gamma M^2} T \\
a(3,2) &= \rho(m_{21} V + D_1(V)) + \frac{\mu}{R}\alpha_0 \beta_0 l_1 \\
a(3,3) &= \rho(m_{21} U + i\xi) + \frac{\mu}{R}(\beta_0^2 l_2 + \alpha_0^2) \\
a(3,4) &= \rho(m_{23} V + D_3(V)) - \frac{i\beta_0}{R}\frac{d\mu}{dT} D_3(T) \\
a(3,5) &= \frac{i\beta_0}{\gamma M^2}\rho + \frac{1}{R}(-\frac{d\mu}{dT} D_{33}(V) - D_3(V)\frac{d^2\mu}{dT^2} D_3(T)) \\
a(4,1) &= \frac{1}{\gamma M^2} D_3(T) - m_{13} U^2 - m_{23} V^2 + \frac{i\mu}{R}\frac{l_2}{\rho}(\beta_0 D_3(V) + \alpha_0 D_3(U))
\end{aligned}$$

$$
\begin{aligned}
a(4,2) &= -2\rho m_{13}U - \frac{i\alpha_0}{R}l_0\frac{d\mu}{dT}D_3(T) + \frac{D_3(\rho)}{\rho}\frac{i\alpha_0}{R}\mu l_2 \\
a(4,3) &= -2\rho m_{23}V - \frac{i\beta_0}{R}l_0\frac{d\mu}{dT}D_3(T) + \frac{D_3(\rho)}{\rho}\frac{i\beta_0}{R}\mu l_2 \\
a(4,4) &= \rho(D_3(W) + m_{31}U + i\xi) + \frac{1}{R}\mu(\beta_0^2+\alpha_0^2) + \frac{D_{33}(\rho)}{\rho}\frac{\mu}{R}l_2 \\
a(4,5) &= \frac{1}{\gamma M^2}D_3(\rho) + \frac{1}{R}\frac{d\mu}{dT}i(-\beta_0 D_3(V) - D_3(U)\alpha_0) \\
a(5,1) &= \frac{(\gamma-1)}{\gamma}(UD_1(T) + WD_3(T) + iT\xi) + c_p(-WD_3(T) - UD_1(T)) \\
a(5,2) &= (\gamma-1)M^2 D_1(p) - \rho c_p D_1(T) \\
a(5,4) &= (\gamma-1)M^2\left[D_3(p) + \frac{2i\mu}{R}(\beta_0 D_3(V) + D_3(U)\alpha_0)\right] - \rho c_p D_3(T) \\
a(5,5) &= \rho\left\{\frac{dc_p}{dT}(-WD_3(T) - UD_1(T)) + i\left[\frac{(\gamma-1)}{\gamma} - c_p\right]\xi\right\} + \\
&\quad \frac{1}{R\,\mathrm{Pr}}\left[\frac{d\kappa}{dT}D_{33}(T) + \frac{d^2\kappa}{dT^2}(D_3(T))^2 + \kappa(-\beta_0^2-\alpha_0^2)\right] + \\
&\quad \frac{(\gamma-1)}{R}\frac{d\mu}{dT}M^2\left[(D_3(U))^2 + (D_3(V))^2\right] + \\
&\quad \frac{(\gamma-1)}{\gamma}(UD_1(\rho) + WD_3(\rho)) \\
b(1,1) &= W \\
b(1,4) &= \rho \\
b(2,2) &= \rho W - \frac{1}{R}\frac{d\mu}{dT}D_3(T) \\
b(2,4) &= -\frac{i\mu}{R}\alpha_0 l_1 \\
b(2,5) &= -\frac{1}{R}D_3(U)\frac{d\mu}{dT} \\
b(3,3) &= \rho W - \frac{1}{R}\frac{d\mu}{dT}D_3(T) \\
b(3,4) &= -\frac{i\mu}{R}\beta_0 l_1 \\
b(3,5) &= -\frac{1}{R}D_3(V)\frac{d\mu}{dT} \\
b(4,1) &= \frac{1}{\gamma M^2}T + \frac{i\mu}{R}\frac{l_2}{\rho}\xi \\
b(4,2) &= \frac{i\mu}{R}\alpha_0 \\
b(4,3) &= \frac{i\mu}{R}\beta_0
\end{aligned}
$$

$$
\begin{aligned}
b(4,4) &= \rho W + \frac{l_2}{R}(2\mu\frac{D_3(\rho)}{\rho} - \frac{d\mu}{dT}D_3(T)) \\
b(4,5) &= \frac{1}{\gamma M^2}\rho \\
b(5,1) &= \frac{(\gamma-1)}{\gamma}WT \\
b(5,2) &= 2(\gamma-1)M^2\frac{\mu}{R}D_3(U) \\
b(5,3) &= 2(\gamma-1)M^2\frac{\mu}{R}D_3(V) \\
b(5,5) &= \rho W\left[\frac{(\gamma-1)}{\gamma} - c_p\right] + \frac{2}{R\,\mathrm{Pr}}\frac{d\kappa}{dT}D_3(T) \\
c(2,2) &= -\frac{\mu}{R} \\
c(3,3) &= -\frac{\mu}{R} \\
c(5,5) &= \frac{\kappa}{R\,\mathrm{Pr}} \\
d(1,1) &= U \\
d(1,2) &= \rho \\
d(2,1) &= \frac{T}{\gamma M^2} \\
d(2,2) &= \rho U \\
d(2,5) &= \frac{\rho}{\gamma M^2} \\
d(3,3) &= \rho U \\
d(4,4) &= \rho U \\
d(5,1) &= \frac{(\gamma-1)}{\gamma}UT \\
d(5,5) &= \rho U\left[\frac{(\gamma-1)}{\gamma} - c_p\right]
\end{aligned}
$$

where

$$D_i = \frac{1}{h_i}\frac{\partial}{\partial x^i}, \quad D_{ij} = \frac{1}{h_i h_j}\frac{\partial^2}{\partial x^i \partial x^j}, \quad \alpha_0 = \frac{\alpha}{h_1}, \quad \beta_0 = \frac{\beta}{h_2}, \quad l_j = \frac{\lambda}{\mu} + j,$$

and

$$\xi = (\alpha_0 U + \beta_0 V - \omega).$$

References

Airiau, C. 2000. 'Non-parallel acoustic receptivity of a Blasius boundary layer using an adjoint approach.' *to appear in Flow, Turbulence and Combustion.*

Airiau, C., Walther, S., Bottaro, A. 1999. 'Non-parallel receptivity and the adjoint PSE.' to appear in *IUTAM Symposium on Laminar-Turbulent Transition (September 1999, Sedona, AZ), Fasel, H. and Saric, W., eds. Springer.*

Andersson, P., Berggren, M. and Henningson, D.S. 1999. 'Optimal disturbances and bypass transition in boundary layer.' *Phys. Fluids*, **11**, pp. 134–150.

Andersson, P., Henningson, D.S. and Hanifi, A. 1998. 'On a stabilization procedure for the parabolic stability equations.' *J. Eng. Math.*, **33**, pp. 311–332.

Bewley, T.R., Temam, R. and Ziane, M. 2000. 'A general framework for robust control in fluid mechanics.' *Physica D*, **138**, pp. 360–392.

Bertolotti, F.P., Herbert, Th. and Spalart, S.P. 1992. 'Linear and Nonlinear Stability of the Blasius Boundary Layer.' *J. Fluid Mech.*, **242**, pp. 441–474.

Cathalifaud, P. and Luchini, P. 2000. 'Algebraic growth in a boundary layer: optimal control by blowing and suction at the wall.' *Eur. J. Mech. B/Fluids*, **19**(4), pp. 469–490

Choudhari, M. and Street, C.L. 1992. 'A finite reynolds-number approach for the prediction of boundary-layer receptivity in localized regions.' *Phys. Fluids A*, **4**, pp. 2495–2514.

Corke, T.C., Bar-Sever, A. and Morkovin, M.V. 1986. 'Experiments on transition enhancement by distributed roughness.' *Phys. Fluids.* **29**, pp. 3199–3213.

Crouch, J.D. 1992a. 'Localized receptivity of boundary layers.' *Phys. Fluids A* **4**, pp. 1408–1414.

Crouch, J.D. 1992b. 'Non-localized receptivity of boundary layers.' *J. Fluid Mech.* **244**, pp. 567–581.

Goldstein, M.E. 1983. 'The evolution of Tollmien-Schlichting waves near the leading edge.' *J. Fluid Mech.* **127**, pp. 59–81.

Goldstein, M.E. and Hultgren, L.S. 1989. 'Boundary-layer receptivity to long-wave free-stream disturbances.' *Ann. Rev. Fluid Mech.*, **21**, pp. 137–166.

Gunzburger, M. 2000. 'Adjoint equation-based methods for control problems in incompressible, viscous flows.' *in press in Flow, Turbulence and Combustion.*

Hall, M. C. G. 1986. 'Application of Adjoint Sensitivity Theory to an Atmospheric General Circulation Model.' *J. The Atmospheric Sci.* **43**, pp. 2644–2651.

Hanifi, A., Henningson, D.s., Hein, S., Bertolotti, F.P. and Simen, M. 1994. 'Linear Non-local Instability Analysis - the linear NOLOT code.' *FFA TN* 1994-54, See also Hein et al. 1994.

Hanifi, A. and Schmid, P.J., Henningson, D.S. 1996. 'Transient growth in compressible boundary layer flow' *Phys. Fluids* **8**(3), pp. 826–837.

Hein, S., Bertolotti, F.P., Simen, M., Hanifi, A. and Henningson, D.S. 1994. 'Linear Non-local Instability Analysis - the linear NOLOT code.' *DLR-IB* 223-94 A 43.

Herbert, Th. 1994. 'Parabolized Stability Equations.' *AGARD Report* No. 793, pp. 4-1–4-34.

Hill, D. C. 1995. 'Adjoint Systems and their role in the Receptivity Problem for Boundary Layers.' *J. Fluid Mech.* **292**, pp. 183–204.

Hill, D. C. 1997. 'Receptivity in non-parallel boundary layers.' *ASME Fluids Engineering Division Summer Meeting, FEDSM '97, June 22-26, 1997.*

Högberg, M. and Berggren, M. 2000. 'Numerical approaches to optimal control

of a model equation for shear flow instabilities. , *Submitted to Journal of Flow, Turbulence and Combustion*.

Li, F. and Malik, M.R. 1996 'On the Nature of PSE Approximation.' *Theoretical and Computational Fluid Dynamics* No.**8**, pp. 253–273.

Luchini, P. and Bottaro, A. 1998 'Görtler vortices : a backward-in-time approach to the receptivity problem.' *J. Fluid Mech.*, **363**, pp. 1–23.

Luchini, P. 2000 'Reynolds-number-independent instability of the boundarylayer over a flat surface: optimal perturbations.' *J. Fluid Mech.*, **404**, pp. 289–309.

Mack, L.M. 1984 'Boundary-layer stability theory.' *AGARD Report* No. 709, pp. 3-1–3-81.

Nishioka, M. and Morkovin, M.V. 1986. 'Boundary-layer receptivity to unsteady pressure gradients : experiments and overview.' *J. Fluid Mech.* **171**, pp. 219–261.

Pralits, J.O., Hanifi, A. and Henningson, D.S. 2000. 'Adjoint-based suction optimization for 3D boundary layer flows' *FFA TN* 2000-58.

Saric, W.S. 1993. 'Physical description of boundary-layer transition : experimental evidence' *AGARD report* **793**, pp. 183–204.

Simen, M. 1992. 'Local and Nonlocal Stability Theory of Spatially Varying Flows.' *Instability, Transition and Turbulence*, Springer Verlag, pp. 181–201

Thomas, A. 1983. 'The control of boundary-layer transition using a wave superposition principle.' *J. Fluid Mech.* **137**, pp.233–250.

Tumin, A. 1996. 'Receptivity of Pipe Poiseuille Flow.' *J Fluid Mech.* **315**, pp. 119–137.

Paper 2

2

Adjoint-based optimization of steady suction for disturbance control. Part 1. Incompressible flows

By Jan O. Pralits[1,2], Ardeshir Hanifi[2] and Dan S. Henningson[1,2]

The optimal distribution of steady suction needed to control the growth of single or multiple disturbances in quasi three-dimensional incompressible boundary layers on a flat plate is investigated. The evolution of disturbances is analyzed in the framework of the Parabolic Stability Equations (PSE). A gradient based optimization procedure is used and the gradients are evaluated using the adjoint of the parabolized stability equations (APSE) and the adjoint of the boundary layer equations (ABLE). The accuracy of the gradient is increased by introducing a stabilization procedure for the PSE. Results show that a suction peak appears in the upstream part of the suction region for optimal control of Tollmien-Schlichting (T-S) waves, steady streamwise streaks in a two-dimensional boundary layer and oblique waves in a quasi three-dimensional boundary layer subject to an adverse pressure gradient. The mean flow modifications due to suction are shown to have a stabilizing effect similar to that of a favorable pressure gradient. It is also shown that the optimal suction distribution for the disturbance of interest reduce the growth rate of other perturbations. Results for control of a steady cross-flow mode in a three-dimensional boundary layer subject to a favorable pressure gradient show that not even large amounts of suction manages to completely stabilize the disturbance.

1. Introduction

Laminar-turbulent transition in boundary layers on aircrafts causes a rapid increase of the skin friction and consequently a larger drag. Therefore, delay of transition occurrence will reduce the fuel consumption which results in a lower operation cost and less pollution. Transition in the boundary layer on aircraft wings is usually caused by break down of small disturbances which grow as they propagate down stream. It is well known that growth of such disturbances can be suppressed or controlled by steady- or unsteady wall-suction. The latter

[1]Department of Mechanics, KTH, SE-100 44 Stockholm, Sweden,
[2]Swedish Defence Research Agency, FOI, Aeronautics Division, FFA, SE-172 90 Stockholm, Sweden

is sometimes referred to as the wave-cancellation concept and has been investigated both numerically and experimentally by numerous authors, see Joslin *et al.* (1995) for an overview of earlier work.

Steady suction implies that a modification of the steady mean flow is done. Here, the aim is to reduce the thickness of the boundary layer and to stabilize the mean velocity profile. The inviscid instability, which is related to the second wall-normal derivative of the streamwise velocity at the wall, is stabilized by suction. The same stabilizing effect is obtained by imposing a favorable pressure gradient given zero suction on the wall. The relation between suction, the pressure gradient and the viscous terms is well explained in e.g. Schlichting (1979). A suction profile which is equivalent of imposing a favorable pressure gradient given zero suction, is large in the upstream region and decreases rapidly downstream. In the case of an adverse pressure gradient present in the flow, the superposition of suction will reduce the curvature of the velocity profile at the wall, weakening the inflection in the profile which inhibits the inviscid instability.

Constant steady suction has been studied both experimentally and numerically by several authors. Iglisch (1949) investigated theoretically the initial length needed for the shape factor (displacement thickness/momentum thickness) to reach a constant value in the case of a flat plate. Here, the streamwise velocity profile becomes 'fuller' downstream as suction is applied finally reaching the so called 'asymptotic suction profile'. With the assumption of an asymptotic velocity profile present along the whole plate, the laminar boundary layer is stable if the constant suction velocity $V_{\rm w} = 1.4 \times 10^{-5}$. However, Ulrich (1944) showed that the critical Reynolds number, Re_{crit}, in fact decreases as one approaches the leading edge. Hence, an increasing amount of suction is required in this region. In Schlichting (1979) it was shown that a correction due to increased amount of suction close to the leading edge leads to a constant suction velocity $V_{\rm w} = 1.2 \times 10^{-4}$ in order to maintain a laminar flow along the whole plate. The increased suction velocity due to the correction of the initial length is an increased amount of suction energy. If a large amount of suction is applied then the power saved by the reduction in drag might well be lost by the power used for the suction device. Further, if a large amount of suction is used, resulting in a thinning of the boundary layer then this may lead to an increase of the shear stress at the wall. It is therefore of interest to investigate if a more optimal suction distribution can be obtained which meets the objective of reducing the disturbances present in the flow while using the least amount of suction energy.

In the last decade more interest has been focused on optimal control of fluid flows in which optimal control theory has been utilized in different manners. Here, the objective is to minimize some measure of the state with a prescribed amount of suction on the wall. This can mathematically be described by a minimization of an objective function which balances a measure of the state and a measure of the control. The problem can be solved using

the sensitivity information given by the gradient of the objective function with respect to the control in a gradient based optimization routine. An efficient way to calculate the gradients is the adjoint approach which has been shown successful in numerous applications as long as the number of constrains are low and the control-variable space is large. Adjoint equations has been used for sensitivity studies in oceanography and atmospheric circulation models, e.g. Hall (1986). Tumin (1996) used it for confined flows in receptivity studies. Hill (1995, 1997a) applied the adjoint approach to the local and nonlocal stability theories to study the receptivity of T-S waves in boundary layer flows. Receptivity of Görtler vortices was studied by Luchini & Bottaro (1998) using backward-in-time integration. The adjoint techniques has also been used to identify the optimal disturbances in boundary layer flows, e.g. Andersson *et al.* (1999). Joslin *et al.* (1995) showed an automated control approach in which they coupled the Navier-Stokes equations and their adjoint in order to have a time-dependent control (suction on the wall) to meet a certain objective.

Here the wall-normal velocity component of the steady mean flow on the wall is used as the control, which means that the suction will modify the mean flow to control disturbance growth rather than generating an out-of phase disturbance by time periodic suction. Another investigation was done by Balakumar & Hall (1999) who used a Lagrangian approach to find the optimal suction distribution for Blasius and swept Hiemenz flows. The objective was to move the transition point downstream given by the e^N-method. They found that for Blasius boundary layers the optimal suction distribution peaked upstream of the maximum growth rate and decreases to zero at the transition point.

In the present work we use an approach different from that in Balakumar & Hall (1999). The control problem is defined using optimal control theory in which a gradient-based technique is used to update the control during the optimization process. The aim is to minimize a given objective function balancing a measure of the total disturbance kinetic energy and the control energy. An adjoint-based technique is used to evaluate the gradients (sensitivities). Here, we couple the adjoint of the PSE with the adjoint of the boundary-layer equations in order to find the gradient of the disturbance growth due to modifications of the mean flow. Hill (1997b) used a similar approach in inverse design for laminar boundary layer. The optimization process is dependent on the accuracy of the gradient (search-direction) which can be increased if the streamwise resolution is increased. However, the PSE is known for its instability for small streamwise steps due to the remaining ellipticity which mainly comes from the gradient of the disturbance pressure. To overcome this problem we use the technique by Andersson *et al.* (1998) to stabilize the PSE. Due to the use of the adjoint approach this stabilization procedure will also affect the adjoint equations.

In this paper we present a method which involves solving a number of problems regarding the derivation of the gradient, adjoint equations and stabilization of the adjoint equations. For this reason, a large part of the paper

is dedicated to explaining the different steps in detail. The optimal control problem and the corresponding equations are presented in § 2. In § 3, a validation of the adjoint equations is done by analyzing the gradient accuracy. Here we also show results on optimal control of steady streamwise streaks and T-S waves in a two-dimensional boundary layer, and oblique waves and a steady cross-flow mode in a quasi three-dimensional boundary layer. The discussion and concluding remarks are given in § 4 and the complete derivation of the gradient and the coupling of the adjoint of the parabolized stability and boundary layer equations are shown in appendix Appendix B. The work shown here is an extension of an earlier work by Pralits *et al.* (2000).

2. Problem formulation

This section presents the optimal control problem for incompressible flows. For simplicity, we restrict our analysis to a plane geometry.

2.1. *State equations*

The flow field is given by the equations of conservation of mass and momentum for a viscous flow. The equations are written for a Cartesian coordinate system with streamwise, normal and spanwise coordinates denoted as x, y and z, respectively. The flow field is decomposed into a mean, Q, and a perturbation part, q, as

$$Q_{tot}(x,y,z,t) = Q(x,y) + q(x,y,z,t)$$

where $Q = (U,V,W,P)^T$ and $q = (u,v,w,p)^T$. The mean flow is taken to be a quasi three-dimensional boundary layer. The evolution of disturbances is analyzed in the framework of the nonlocal stability theory (see e.g. Bertolotti *et al.* 1992).

In the following sections the equations for the mean flow and disturbances, in non-dimensional form, are given. The velocity components are made non-dimensional by $U^\star_\infty$, and pressure by $\rho {U^\star}^2_\infty$. The reference length is taken as $l^\star_0 = (\nu^\star x^\star_0/U^\star_\infty)^{\frac{1}{2}}$, where superscript * denotes dimensional quantities, ν the kinematic viscosity and U_∞ the free stream velocity.

2.1.1. *Mean flow equations*

The non-dimensional boundary layer equations for a quasi three-dimensional incompressible flow on a flat plate with an external pressure gradient given as $dP_e/dx = -U_e dU_e/dx$ can be written

$$\frac{\partial U}{\partial x} + \frac{\partial V}{\partial y} = 0, \tag{1}$$

$$U\frac{\partial U}{\partial x} + V\frac{\partial U}{\partial y} - U_e\frac{dU_e}{dx} - \frac{1}{Re}\frac{\partial^2 U}{\partial y^2} = 0, \tag{2}$$

$$U\frac{\partial W}{\partial x} + V\frac{\partial W}{\partial y} - \frac{1}{Re}\frac{\partial^2 W}{\partial y^2} = 0, \tag{3}$$

with the boundary conditions

$$\begin{aligned} U = W = 0,\ V = V_{\rm w} \qquad & \text{on} \qquad y = 0, \\ (U, W) \to (U_e, W_e) \qquad & \text{as} \qquad y \to \infty, \end{aligned} \tag{4}$$

where index e denotes that the variable is evaluated at the boundary layer edge and $Re = l_0^\star U_\infty^\star/\nu^\star$ is the Reynolds number. Note that for the boundary layer approximations to be valid, the normal velocity at the wall should be of order $O(Re^{-1})$.

2.1.2. *Disturbance equations*

We assume the pertubations to be time and spanwise periodic disturbances as

$$q(x, y, z, t) = \hat{q}(x, y) \exp i\Big(\int_{X_0}^{x'} \alpha\, dx' + \beta z - \omega t\Big) + c.c., \tag{5}$$

where α is the complex streamwise wavenumber, β the real spanwise wavenumber and ω the real disturbance angular frequency. We assume a scale separation Re^{-1} between the weak variation in x-direction and the strong variation in the y-direction. It is also assumed that $\partial/\partial x \sim O(Re^{-1})$ and $V \sim O(Re^{-1})$. Introducing (5) and the assumptions above in the linearized governing equations and keeping terms up to order $O(Re^{-1})$, yield a set of nearly parabolic partial differential equations

$$A\hat{q} + B\frac{\partial \hat{q}}{\partial y} + C\frac{\partial^2 \hat{q}}{\partial y^2} + D\frac{\partial \hat{q}}{\partial x} = 0, \tag{6}$$

where the matrices A, B, C and D are given in appendix Appendix A. For a note on the parabolic nature of the PSE see Andersson *et al.* (1998). To remove the ambiguity of having x-dependence of both the amplitude function and wave function of (5) and to maintain a slow variation of the amplitude function, a so called 'auxiliary condition' is introduced

$$\int_0^\infty \hat{\mathbf{u}}^H \frac{\partial \hat{\mathbf{u}}}{\partial x}\, dy = 0, \tag{7}$$

where $\hat{\mathbf{u}} = (\hat{u}, \hat{v}, \hat{w})^T$ and superscript ^{H} denotes the complex conjugate transpose. The disturbances are subjected to the following boundary conditions

$$\begin{aligned} \hat{\mathbf{u}} = 0 \qquad & \text{on} \qquad y = 0 \\ \hat{\mathbf{u}} \to 0 \qquad & \text{as} \qquad y \to \infty. \end{aligned} \tag{8}$$

Equations (6) are integrated in downstream direction with the initial condition given by solution of the local stability theory at $x = X_0$.

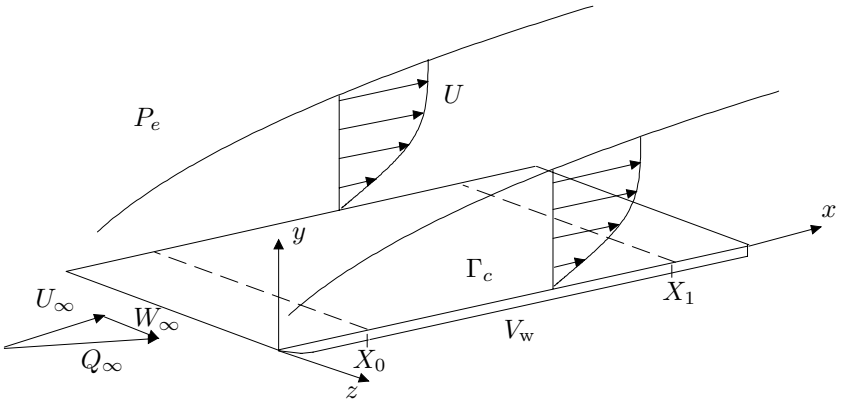

FIGURE 1. Computational domain: flat-plate boundary layer

2.2. *Optimal control of a single disturbance*

In this section, we define an optimal control problem where the mean normal velocity at the wall is optimized to reduce the growth of a single disturbance. The optimization problem is solved by minimizing an objective function balancing a measure of the state and the control using a gradient based method. We obtain the gradient of the objective function using an adjoint technique. The complete derivation of the equations can be seen in appendix Appendix B.

2.2.1. *Objective function*

We measure the size of a disturbance in domain Ω, defined such that $x \in [X_0, X_1]$, $y \in [0, \infty)$ and $z \in [Z_0, Z_1]$ (see figure 1), by its total kinetic energy defined as

$$E = \frac{1}{2}\int_{Z_0}^{Z_1}\int_{X_0}^{X_1}\int_{0}^{\infty} \mathbf{u}^T\mathbf{u}\, dy\, dx\, dz.$$

The objective function to be minimized is

$$J(V_\mathrm{w}) = \frac{1}{2}\int_{Z_0}^{Z_1}\int_{X_0}^{X_1}\int_{0}^{\infty} \mathbf{u}^T\mathbf{u}\, dy\, dx\, dz + \frac{\epsilon}{2}\int_{Z_0}^{Z_1}\int_{X_0}^{X_1} {V_\mathrm{w}}^2\, dx\, dz \qquad (9)$$

where ϵ, a positive number, is the regularization parameter and is used to insure that the size of the control parameter V_w does not grow unbounded. Now, the control problem can be defined mathematically as

$$\begin{aligned} &\text{find} \quad V_\mathrm{w}^{opt} \in L^2(\Gamma_c) \quad \text{such that} \\ &J(V_\mathrm{w}^{opt}) \leq J(V_\mathrm{w}) \;\forall\; V_\mathrm{w} \in L^2(\Gamma_c) \end{aligned} \qquad (10)$$

where V_w^{opt} is the optimal suction distribution on the wall.

2.2.2. *Adjoint equations and the gradient*

The gradient of the objective function (9) with respect to the control (input) variable is defined through the directional derivative as

$$\delta J = \int_{Z_0}^{Z_1} \int_{X_0}^{X_1} \nabla_{V_\mathrm{w}} J \; \delta V_\mathrm{w} \; dx \; dz, \tag{11}$$

where δV_w is the variation of the input parameter and

$$\nabla_\xi J \; \delta\xi = \lim_{s\to 0} \frac{J(\xi + s\delta\xi) - J(\xi)}{s}.$$

Here, we derive the gradient expression using the adjoint of the state equations. Details of the derivation is given in appendix Appendix B. This yields

$$\nabla_{V_\mathrm{w}} J = \epsilon V_\mathrm{w} + V_\mathrm{w}^* \qquad \text{on} \qquad y = 0. \tag{12}$$

The value of $V_\mathrm{w}^* = V^*(x, 0)$ in (12) is given by the solution of the adjoint of the PSE and boundary layer equations, hereafter referred to as APSE and ABLE, respectively. The APSE which is found as (42)–(46) in appendix Appendix B is here written

$$A^H q^* - B^H \frac{\partial q^*}{\partial y} + C^H \frac{\partial^2 q^*}{\partial y^2} - D^H \frac{\partial q^*}{\partial x} = f_{APSE}, \tag{13}$$

$$\frac{\partial}{\partial x} \int_0^\infty q^{*H} \frac{\partial A}{\partial \alpha} \hat{q} \; dy + i|\Theta|^2 \int_0^\infty |\hat{\mathbf{u}}|^2 \; dy = 0, \tag{14}$$

with boundary conditions

$$\begin{aligned} u^* = v^* = w^* = 0 \qquad &\text{on} \qquad y = 0, \\ u^*, v^*, w^* \to 0 \qquad &\text{as} \qquad y \to \infty. \end{aligned} \tag{15}$$

and initial conditions

$$q^* = r^* = 0 \qquad \text{on} \qquad x = X_1. \tag{16}$$

Here, $q^* = (p^*, u^*, v^*, w^*)$ and r^* are the co-state variables and f_{APSE} is the forcing due to the auxiliary condition of the PSE and the objective function. Equations (13)–(14) are integrated in the upstream direction starting at $x = X_1$. At each streamwise position, the value of the scalar r^* is iteratively found such that (14) is satisfied. The ABLE which are found as (47)–(48) in appendix Appendix B, are satisfied by the co-state variables $Q^* = (U^*, V^*, W^*)$. They are here written as

$$L_{BLE}^*(Q) Q^* = f_{ABLE}, \tag{17}$$

with boundary conditions

$$\begin{aligned} U^* = W^* = 0 \qquad &\text{on} \qquad y = 0, \\ U^*, V^*, W^* \to 0 \qquad &\text{as} \qquad y \to \infty, \end{aligned} \tag{18}$$

and initial conditions

$$U^* = V^* = W^* = 0 \qquad \text{on} \qquad x = X_1. \tag{19}$$

The forcing term in (17), f_{ABLE}, is a function of the solutions of both the PSE

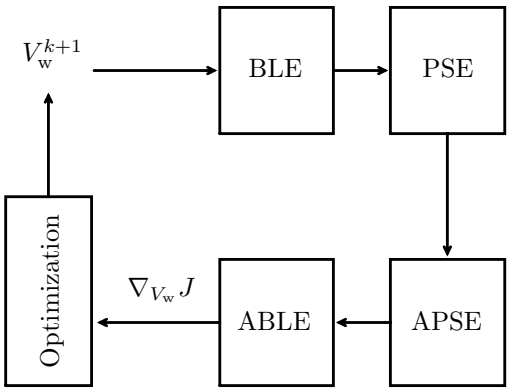

FIGURE 2. Chart of the solution process

and the APSE. Equations (17) are integrated in the upstream direction starting at $x = X_1$. The right hand of the these equations are given by the solution of the PSE and APSE. The optimization procedure can now be outlined following the steps below considering the chart given in figure 2 where k denotes the iteration number.

1. The BLE (1)–(3) are integrated from $x = X_0$ to $x = X_1$. If $k = 1$ then $V_{\rm w}^k = 0$ (initial guess on the suction distribution).
2. The PSE (6)–(7) are integrated from $x = X_0$ to $x = X_1$, then the APSE are integrated from $x = X_1$ to $x = X_0$ and f_{ABLE} is computed.
3. The ABLE (17) are integrated from $x = X_1$ to $x = X_0$ given the forcing, f_{ABLE}, from 2.
4. If $k < 2$ then goto 5, else evaluate the convergence criteria:
   If $J^{k+1} - J^k < err$ then convergence is reached else goto 5. Here err is a small real-valued parameter defining the convergence.
5. The gradient, (12), is evaluated and the new boundary condition for the BLE, $V_{\rm w}^{k+1}$, is calculated using an optimization routine (here we use a limited-memory quasi-Newton method). Update $k = k + 1$, goto 1.

The gradient of the objective function due to a variation of the free stream velocity can be derived in the same manner as for $V_{\rm w}$ and yields,

$$\nabla_{U_e} J = -U_e \int_0^\infty \frac{\partial U^*}{\partial x}\, dy. \tag{20}$$

This variation would be the result of a change in the geometry and consequently the pressure distribution. Effects due to geometry changes are not investigated here.

2.3. *Optimal control of multiple disturbances*

In this section we generalize the technique introduced above to find the optimal suction distribution of the steady mean flow that accounts for the growth of

more than one disturbance. This is necessary for cases where it is not possible to clearly state which disturbance gives the worst-case scenario. An example of this is the two-dimensional Blasius boundary layer where either T-S wave type instabilities or steady streamwise streaks could give the maximum growth. The analysis does not differ much from the one outlined in § 2.2 and is therefore done on a more compact form here.

The size of multiple disturbances in Ω, is now taken as the sum of the energy of a chosen number of disturbances. If we denote the total number of existing disturbances with N then the total kinetic energy is defined as

$$E = \sum_{k=1}^{N} \frac{1}{2} \int_{Z_0}^{Z_1} \int_{X_0}^{X_1} \int_{0}^{\infty} \mathbf{u}_k{}^T \mathbf{u}_k \, dy \, dx \, dz.$$

The objective function to be minimized is now

$$J(V_{\mathrm{w}}) = \sum_{k=1}^{N} \frac{1}{2} \int_{Z_0}^{Z_1} \int_{X_0}^{X_1} \int_{0}^{\infty} \mathbf{u}_k{}^T \mathbf{u}_k \, dy \, dx \, dz + \frac{\epsilon}{2} \int_{Z_0}^{Z_1} \int_{X_0}^{X_1} V_{\mathrm{w}}{}^2 \, dx \, dz. \quad (21)$$

The same procedure to find the gradient of J with respect to V_{w} given in appendix Appendix B for control of single disturbances is now used to account for several disturbances. As the control problem is derived using linear equations, the case of multiple disturbances does not introduce any further complications. Equation (11) is used to define the gradient which can now be written

$$\nabla_{V_{\mathrm{w}}} J = \epsilon V_{\mathrm{w}} + \sum_{k=1}^{N} (V_{\mathrm{w}}^*)_k \qquad \text{on} \qquad y = 0. \quad (22)$$

Equation (22) implies that each equation in the solution procedure given in figure 2 must be solved N times, i.e. for each disturbance, before evaluating the gradient. Instead, one can use the fact that the ABLE are linear equations and evaluate sum of the forcing terms $(f_{ABLE})_n$. Then the ABLE are solved once given the total forcing from all N disturbances. In this way computational time is saved for the optimization procedure.

The optimization procedure for control of N disturbances is similar to that given in § 2.2 and can be described using figure 2 for the case when the sum of the forcing terms are computed. The difference is that step 2 is performed N times for N disturbances and the ABLE in step 3 is evaluated with the total forcing term. In this case (22) is not used but instead the gradient expression (12) which was given for control of single disturbances.

2.4. *Adjoint of the stabilized PSE*

The success of finding the optimal distribution of suction is mainly depending on how accurate the gradient is calculated. The gradient presented here, (12), is derived using a so called continuous approach. This means that the adjoint of a state equation is derived from the continuous equation and then discretized. Another approach is to first discretize the state equation and then derive its

adjoint, the so called discrete approach. The latter yields a more accurate gradient in most cases but its derivation is more complicated. However, results of the continuous approach should converge to that of the discrete one as the grid resolution is refined, (see Högberg & Berggren 2000). It is a rather well know problem that the PSE equations become unstable as the grid in the streamwise direction is refined due to a remaining ellipticity in the equations, (see e.g. Andersson *et al.* 1998). This problem will therefore put a limit on the accuracy of the gradient unless some technique is used to overcome the instability problem and allow a smaller step-size in the streamwise direction. A stabilization procedure was presented by Andersson *et al.* (1998) in which they add terms proportional to the truncation error of the implicit scheme used in the streamwise direction. This procedure does however not only affect the PSE in this problem but also the derivation of the gradient and adjoint equations. Here, we present the outline on how the PSE, gradient and the adjoint equations are derived using the idea from Andersson et al. . The details of the derivation can be seen in appendix B.3. According to the stabilization procedure by Andersson et al. terms of order $O(Re^{-2})$ are introduced in (6). The stabilized PSE can be written

$$\begin{aligned} -D\frac{\partial \hat{q}}{\partial x} &= A\Big[\hat{q}+s\frac{\partial \hat{q}}{\partial x}\Big]+B\Big[\frac{\partial \hat{q}}{\partial y}+s\frac{\partial}{\partial x}\Big(\frac{\partial \hat{q}}{\partial y}\Big)\Big]+ \\ &\quad C\Big[\frac{\partial^2 \hat{q}}{\partial y^2}+s\frac{\partial}{\partial x}\Big(\frac{\partial^2 \hat{q}}{\partial y^2}\Big)\Big] \end{aligned} \tag{23}$$

where s is a positive real number. The gradient, (12) and the adjoint equations were derived in appendix Appendix B without the stabilization terms. Now, the derivation has to be done using (23) instead of (6) which yields the following adjoint equations

$$\begin{aligned} -D^H\frac{\partial q^*}{\partial x} &= -\Big[A^H q^*-s\tilde{A}^H\frac{\partial q^*}{\partial x}\Big]+B^H\Big[\frac{\partial q^*}{\partial y}-s\frac{\partial}{\partial x}\Big(\frac{\partial q^*}{\partial y}\Big)\Big]- \\ &\quad C^H\Big[\frac{\partial^2 q^*}{\partial y^2}-s\frac{\partial}{\partial x}\Big(\frac{\partial^2 q^*}{\partial y^2}\Big)\Big]+f_{APSE} \end{aligned} \tag{24}$$

$$\frac{\partial}{\partial x}\int_0^\infty q^{*H}\frac{\partial A}{\partial \alpha}\Big[\hat{q}+s\frac{\partial \hat{q}}{\partial x}\Big]\,dy+i|\Theta|^2\int_0^\infty |\hat{\mathbf{u}}|^2\,dy=0, \tag{25}$$

$$L^*_{BLE}(Q)Q^*=\tilde{f}_{ABLE}, \tag{26}$$

where f_{APSE} and f_{ABLE} denotes the forcing terms of the APSE and ABLE respectively and the accent $\tilde{}$ marks where additional terms due to the stabilization procedure appear. Note here, that there is no influence on the gradient expression or on the boundary conditions of the state and adjoint equations due to the stabilizing terms. The additional terms on the right hand side of (24) resembles the stabilizing terms in (23) apart from the sign difference on s. The APSE resembles the PSE and the new right hand side of (24) will indeed work as a stabilizing term allowing a smaller step-size in the streamwise direction.

3. Results

The results presented are obtained by numerically integrating the discretized state and co-state (adjoint) equations. The x-derivatives are approximated by a first- or second-order accurate backward Euler scheme. The y-derivatives of the PSE and APSE are approximated by Chebychev-polynomials and a second-order accurate finite-difference scheme for the BLE and ABLE. The L-BFGS-B package, which is based on the limited memory quasi-Newton method, is used in the optimization procedure (see Zhu *et al.* 1994; Byrd *et al.* 1995).

3.1. *Validation and accuracy of the gradient*

The convergence of the optimization procedure depends on the accuracy of the gradient expression. If its accuracy is low, problems will be encountered as the solution approaches the optimal value. Here, we check the accuracy of the gradient by a comparison of the adjoint based gradients (12) with those obtained from a finite-difference approach. The comparison is done considering a wall normal velocity perturbation $\delta V_{\rm w}$ at $y = 0$. The variation of the functional J with respect to this perturbation is

$$\delta J = \frac{\partial J}{\partial V_{\rm w}} \delta V_{\rm w}. \tag{27}$$

In the finite-difference approach $\partial J/\partial V_{\rm w}$ is obtained by using the inhomogeneous wall boundary-condition $V_{\rm w} = \pm\epsilon_{\rm w}$ at $x = x_n$. The index n refers to the n-th streamwise position and $\epsilon_{\rm w}$ is a small positive number. The derivative is then evaluated using a second-order accurate finite-difference scheme. The discretized expression for δJ in the adjoint approach is given by

$$\delta J = \int_{Z_0}^{Z_1} \Big(\sum_{n=2}^{N-1} \nabla_{V_{\rm w}} J_n \; \delta V_{{\rm w}_n} \Delta_n \Big) \, dz \tag{28}$$

where $\Delta_n = (x_{n+1} - x_{n-1})/2$. In figure 3(b), the relative error between $dJ/dV_{\rm w}$ and $\nabla_{V_{\rm w}} J_n \Delta_n$ is compared for different streamwise resolution ΔRe. The calculations are done for a streamwise range $Re = 250 - 760$ on a quasi three-dimensional boundary layer where $dP_e/dx = 0$ given a T-S wave as the initial disturbance at $x = X_0$. The inviscid flow at $Re = 250$ has an angle of 30^o, the non-dimensional spanwise wavenumber $\beta = 0$ and the reduced frequency $F = 2\pi f^\star \nu_e^\star / U_e^{\star 2} = 10^{-4}$. As can be seen in figure 3(b), the relative error decreases as the ΔRe is decreased. Here, $\Delta Re = 6$ is the minimum streamwise step size for which the PSE calculations are stable. The values for $\Delta Re = 2$ are computed using the stabilization terms, explained in § 2.4. In figure 3(a), the gradient obtained from the adjoint equations is compared with central-differences when $\Delta Re = 2$ in order to visualize the agreement.

3.2. *Convergence of the optimization problem*

The goal of the optimization procedure, explained mathematically by (10), is to minimize the objective function J. The problem is defined such that the

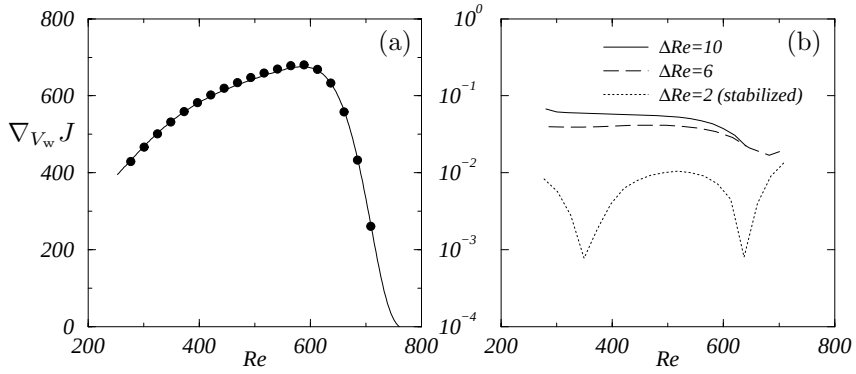

FIGURE 3. Comparison of the gradient from adjoint and central-difference calculations for different streamwise resolution ΔRe. (a) $\Delta Re = 2$, the continuous line is the gradient derived from adjoint equations, • marks central-difference calculations. (b) The relative error between adjoint and central-difference calculations of the gradient for different streamwise resolution ΔRe.

gradient of J with respect to the control variable V_w is used to update the control. A frequently used optimization algorithm is the steepest descent, here referred to as STD, to update the control. This algorithm can be written as

$$V_w^{k+1} = V_w^k - \rho^k \frac{\partial J(V_w^k)}{\partial V_w} \tag{29}$$

where k is the iteration number and ρ^k is the 'step length' determining how far one should go in the gradient direction in order to have maximum reduction of J at each iteration. As $k \to \infty$, J should approach some local minima. One might think that if a small enough constant step length is used then finally a local minima will be reached. However, as shown in e.g. Bewley *et al.* (1999) this is not always the case, not even if a more sophisticated line-search algorithm is used in order to find the best step length at each iteration. Here, we have used the Broydon-Fletcher-Goldfarb-Shanno (L-BFGS-B) method which is based on quadratic model rendered from a Taylor expansion of J around V_w. In this algorithm, an approximation of the Hessian matrix is used to reduce storage as the number of terms in the matrix scales with the square of the control-variables.

Some test-cases are computed for the STD with a constant step length of 10^{-6} and the L-BFGS-B algorithm to illustrate the efficiency of the latter algorithm and effects of different convergence criteria. One should note here that for each iteration of the L-BFGS-B algorithm, some sub-iterations are performed in order to find the best step length and gradient direction. The calculations are done for an oblique wave in a quasi three-dimensional boundary

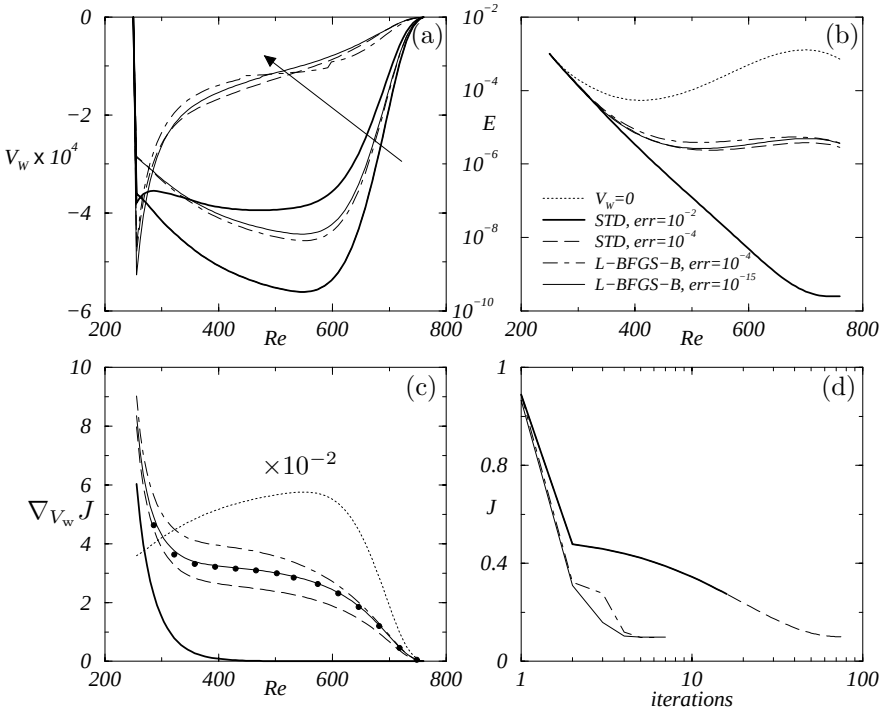

FIGURE 4. Comparison between the L-BFGS-B and steepest descent (STD) algorithm. Here $err = J^{k+1} - J^k$. (a) Suction distributions for the first and the last iteration, the arrow marks from right to left how the distribution is changed for each case. (b) The disturbance energy in a mean flow with zero and optimal suction. (c) The initial gradient $\times 10^{-2}$ and optimal gradients. • marks a finite difference calculation to be compared with L-BFGS-B for $err = 10^{-15}$. (d) The objective function as a function of the iteration step.

layer with a zero pressure-gradient for $Re = 250 - 760$. The inviscid flow at $Re = 250$ has an angle of 15^o, the non-dimensional spanwise wavenumber $\beta = -0.02$, the reduced frequency $F = 10^{-4}$ and $\epsilon = 10^3$. The results can be seen in figure 4. If the convergence criteria $err = J^{k+1} - J^k$ is large, here given for STD and $err = 10^{-2}$, then the reduction of the energy shown in figure 4(b) is extensive. However, the objective function has not reached its minimum which can be seen in figure 4(d). If instead the convergence criteria is lowered, here shown for both L-BFGS-B and STD with $err = 10^{-4}$, then the energy reduction is less but the objective function seems to be more converged. For this case the optimal suction distribution show a sharp peak upstream. As a

final case the L-BFGS-B is computed for $err = 10^{-15}$ which is close to machine precision.

It is important to remember that the objective function contains terms from both the disturbance kinetic energy E and the control energy E_c. Figures 4(b)-(c) might give an impression that the result of STD with $err = 10^{-2}$ give the optimal suction as both the energy and the gradient are small, but figure 4(a) shows that this solution does in fact use much larger control energy. During the optimization procedure it is also important to maintain the accuracy of the gradient as explained in § 3.1. In figure 4(c) the final gradient for $err = 10^{-15}$ is compared with a finite difference calculation (marked with •). Here we can see that as the solution has converged the gradient has maintained its accuracy. This means that the initial assumption of using the continuous instead of a discretized formulation manages well to predict the gradients also close to a minimum where the gradient directions are the most sensitive.

Here we take $err = 10^{-15}$ as a converged solution. The gradient accuracy has been continuously checked for the first and last iteration of the optimization process.

3.3. *Two-dimensional boundary layers*

In this section we investigate the disturbance control in a two-dimensional boundary layer with zero pressure gradient. The disturbances studied here are chosen to be a T-S wave and/or optimally growing steady streamwise streaks. The initial condition for the latter has been calculated using the theory given in Andersson *et al.* (1999). In § 3.3.1 the optimal suction distribution is calculated to control each of these disturbances individually. Here, we also investigate the effect of different domains along the streamwise axis for the control of T-S waves. In the Blasius boundary layer, it is not always clear which one of the above mentioned disturbances will give the largest amplification. In § 3.3.2 the theory given in § 2.3 is therefore used to give an example of a case where multiple perturbations are present.

The results in this section on control of T-S waves are produced for a disturbance with a frequency of $F = 10^{-4}$. It is shown that the optimal suction distribution obtained to control the chosen T-S wave has a stabilizing effect on T-S waves with other frequencies. A study has also been performed to control T-S waves with both higher and lower frequencies than the one shown here. However, the effect of the optimization process on the growth rate of these disturbances, the corresponding optimal suction profiles and mean flow modifications all show the same behavior. Thus this choice of frequency give the general behavior of the optimization process given a T-S wave instability in a two-dimensional boundary layer.

3.3.1. *Control of single disturbances*

The optimal distribution of suction to control steady streamwise streaks is calculated for a streamwise range $Re = 412 - 730$. The initial condition is

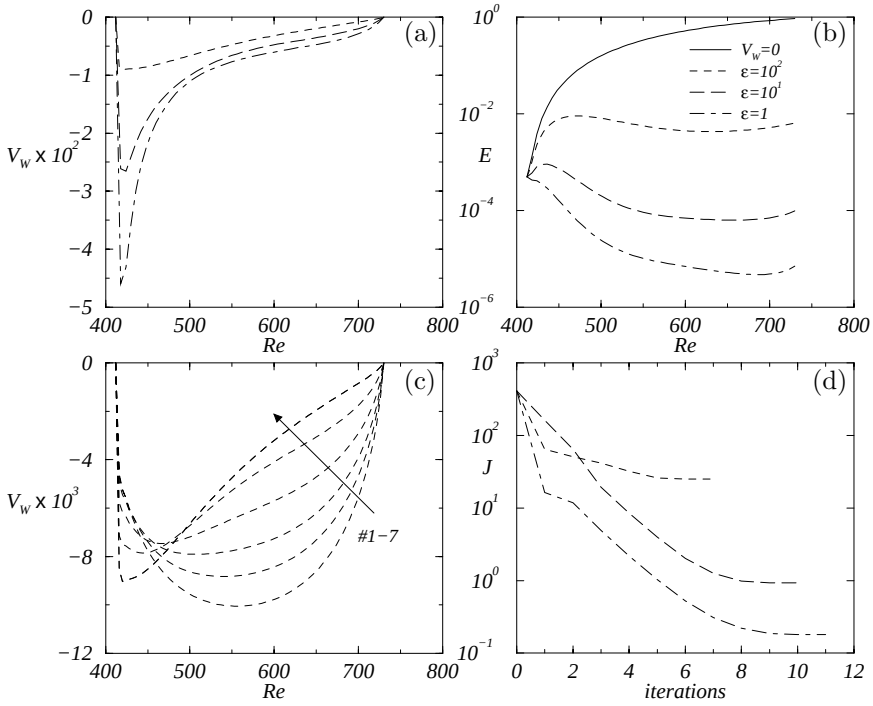

FIGURE 5. Disturbance control of optimally growing steady streamwise streaks in a two-dimensional boundary layer ($dP_e/dx = 0$). The non-dimensional spanwise wavenumber $\beta = 0.292$ at $Re = 412$. Results are shown for $\epsilon = 1, 10, 10^2$. (a) Optimal suction distributions. (b) The disturbance kinetic energy in a mean flow with zero and optimal suction distribution. (c) Suction profiles for the different steps in the optimization process, $\epsilon = 10^2$. (d) The objective function as a function of the iteration step.

computed using the optimization procedure given in Andersson *et al.* (1999) to provide the maximum energy at X_1. The non-dimensional spanwise wavenumber $\beta = 0.292$ and the frequency $\omega = 0$. Three test cases are analyzed for these parameters in which the regularization parameter ϵ was $1, 10$ and 10^2 and the control is applied at $Re = 418 - 724$. In figure 5(a) the optimal suction distributions for all cases are compared. A peak in the suction distribution is noticed upstream which becomes more pronounced as the regularization parameter is decreased. In figure 5(b) the disturbance kinetic energy of zero and optimal suction are compared. All three suction distributions result in a decrease of the disturbance kinetic energy. However, the main difference between the curves where control is applied is seen in the upstream region. The effect of the optimal suction distributions given in figure 5(a) is that the damping of

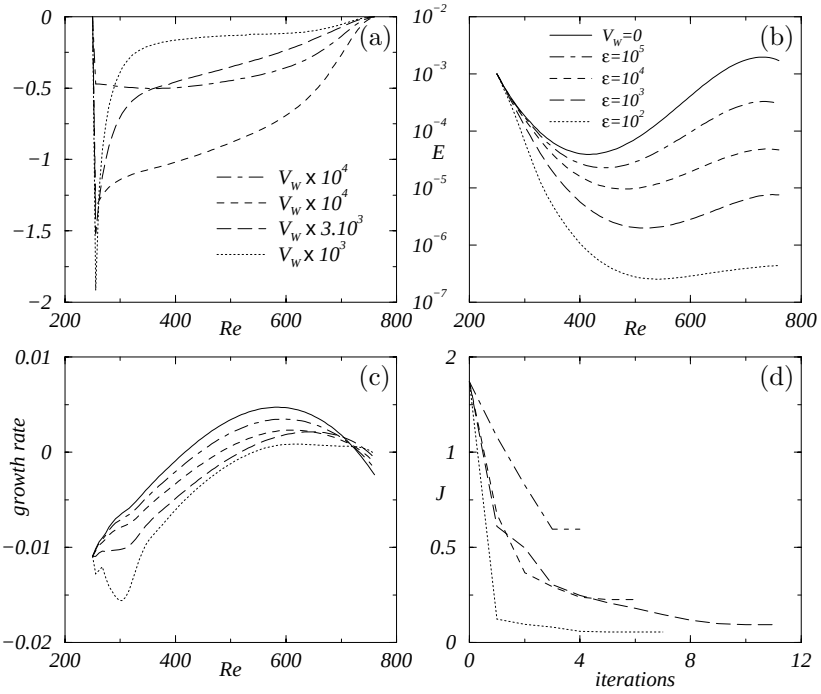

FIGURE 6. Disturbance control of a T-S wave with $F = 10^{-4}$ in a two-dimensional boundary layer ($dP_e/dx = 0$). Results are shown for $\epsilon = 10^2, 10^3, 10^4, 10^5$. (a) Optimal suction distributions (note the different scalings). (b) The disturbance kinetic energy in a mean flow with zero and optimal suction distribution. (c) The growth rate, -imag(α), in a mean flow with zero and optimal suction. (d) The objective function as a function of the iteration step.

the disturbance kinetic energy is increased in the upstream region as ϵ is decreased. Figure 5(c) illustrates the changes in the suction distribution during the optimization procedure. Here, $V_{\rm w}$ is plotted for each iteration in the optimization loop for the case with $\epsilon = 10^2$. The optimal distribution is found after 7 iterations. The difference between the sixth and seventh iteration can not be distinguished. In figure 5(d) the objective function is given as function of the iteration number for all cases to illustrate the convergence of the optimization procedure.

The optimal distribution of suction to control T-S wave instabilities is calculated for a streamwise range $Re = 250-760$. The first investigation is done by comparing different regularization parameters, here $\epsilon = 10^2, 10^3, 10^4, 10^5$ while control is applied at $Re = 256 - 754$. The results can be seen in figure 6. In figure 6(a) the optimal suction distributions from all cases are compared.

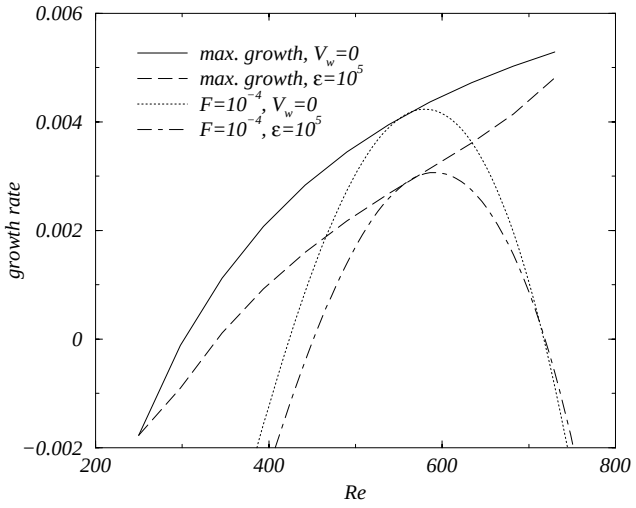

FIGURE 7. Maximum local growth rate compared with local growth rate of a T-S wave with $F = 10^{-4}$, for zero and optimal suction in a two-dimensional boundary layer ($dP_e/dx = 0$). The optimal suction is computed for control of a T-S wave with $F = 10^{-4}$ given that $\epsilon = 10^5$ for a streamwise range $Re = 250 - 760$. Calculations of maximum local growth rate are made with $\Delta F = 2.5 \times 10^{-6}$.

Here, it is noted that the optimal suction distribution tends to peak upstream as the penalty on the control is reduced. Further, this peak is upstream of the unstable region for all cases. In figure 6(b) the disturbance kinetic energy is compared for zero and optimal suction distribution. A reduction of disturbance kinetic energy can be observed as the penalty of the control is reduced. The growth rate for all cases can are given in figure 6(c). In all cases the growth rate is decreased as ϵ is decreased and the reduction is more pronounced in the upstream region. Finally, in figure 6(d) the objective function is plotted as a function of the iteration number to show the convergence of the optimization procedure.

A question that arises is if the suction distribution which is optimal for one chosen T-S wave will damp or amplify other instability waves in the chosen streamwise domain. This is analyzed by computing the maximum local growth rate, i.e. local growth rate over all possible frequencies, at a number of streamwise positions both with zero and the optimal suction distribution. The streamwise range and optimal suction distribution are taken from figure 6 with $\epsilon = 10^5$. The results are shown in figure 7 where the maximum local growth rate has been computed for $\Delta F = 2.5 \times 10^{-6}$ and $\Delta Re = 50$ as the reduced frequency and streamwise resolution respectively. Here, it is shown that the optimal suction distribution for one given frequency has a stabilizing effect on

all other frequencies in the given streamwise range. Further, the local growth rate for the T-S wave with $F = 10^{-4}$ has been plotted both with zero and optimal suction distribution. The result shows that the chosen disturbance corresponds to the maximum growth rate both with zero and optimal suction at a given streamwise position.

The effect of imposing suction at the wall is that the velocity profile of the mean flow becomes fuller which is known to stabilize the viscous instability waves. This effect is shown for the streamwise velocity component of the mean flow at three different streamwise positions in figure 8. There, the streamwise disturbance velocity component is also plotted. The optimal suction distribution is given by the case in figure 6 where $\epsilon = 10^2$. The first position $Re = 256$ is close to X_0, the second position $Re = 400$ is close to where the disturbance starts to grow and the last position $Re = 598$ is roughly half way into the the unstable region. In figure 8(a) the streamwise velocity profile has been plotted for the three positions, when zero and optimal suction is applied. In all three cases the mean flow profiles have become fuller (or thickened). It should be noted that even though the optimal suction distribution, see figure 6(a), shows a significant peak in the vicinity of $Re = 256$, the effect on the mean flow is not large. The amplitude of the streamwise disturbance velocity is shown in figure 8(b) for the cases of zero and optimal suction. The initial condition is the same for zero and optimal suction and the effect of suction at the upstream position on the disturbance velocity is small. The results at the most downstream position show a larger reduction of disturbance amplitude. Here, the results for the case of optimal suction at $Re = 400$ and 598 are magnified to make the shape visible. In all cases the disturbance shape is kept as the optimal suction distribution is applied but the magnitude is decreased.

Figure 9 illustrates the effects of changing the size and location of the control domain. Here, the same case as in figure 6 with $\epsilon = 10^3$ is used. Three different control regions are compared. In the first case, the control is applied to $Re = 412 - 554$ which is from the initial point of unstable region (branch I of the neutral stability curve) to roughly halfway into the unstable region. The second case, $Re = 412 - 718$ is the control domain extended over the whole unstable region and in the last case, $Re = 256 - 754$, the control is applied over the whole computational domain. The corresponding optimal suction velocity profiles can be seen in figure 9(a). Results for all cases show a suction peak in the upstream region of the control domain. In figure 9(b) the kinetic disturbance energy is shown for all cases. The first case shows a significant reduction of energy as the control is applied but continues to grow when the control is turned off. The second and last case show that approximately the same reduction of energy at the final streamwise position can be obtained either by acting only in the unstable region or in the whole domain. The growth rate is given in figure 9(c). In the first and second case, the growth rate follows the curve of zero suction until the control is turned on. A large reduction in growth rate can then be seen in the upstream region of the control domain. The first

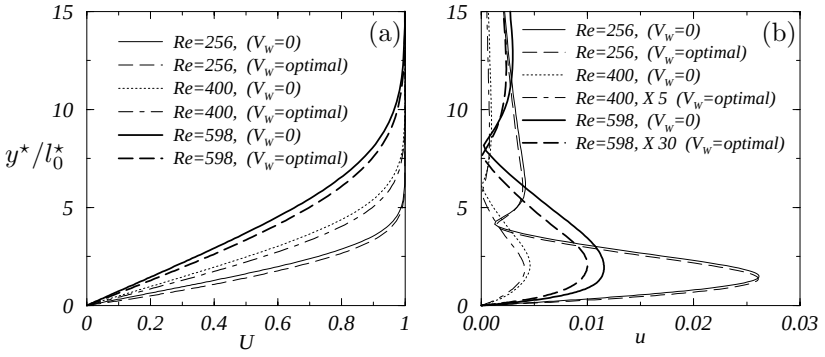

FIGURE 8. Modification of the two-dimensional mean flow ($dP_e/dx = 0$) and disturbance velocity due to optimal suction computed to control a T-S wave with $F = 10^{-4}$ when $\epsilon = 10^2$ in a streamwise range $Re = 250 - 760$. Results are presented for $Re = 256, 400, 598$. (a) Streamwise velocity of the mean flow subject to zero and optimal suction. (b) Absolute value of the streamwise disturbance velocity (note the different scalings).

case shows a significant increase as the control is turned off inside the unstable region. In figure 9(d) the objective function is plotted as a function of the iteration number to visualize the convergence of the optimization procedure.

3.3.2. *Control of multiple disturbances*

The theory in § 2.3 was introduced to account for more than one disturbance in the domain. This will produce an optimal suction profile that assures a minimum energy reduction for all disturbances accounted for. Here, we analyze two disturbances, a T-S wave and optimally growing streamwise steady streaks, with an initial energy such that they give the same maximum disturbance energy at the downstream position X_1. The domain is chosen so that X_0 and X_1 are at the first and second branch of the neutral stability curve for the T-S wave with $F = 10^{-4}$. The initial condition for the steady streaks is computed using the optimization technique given in Andersson *et al.* (1999) to provide the maximum growth at X_1 for the chosen domain. In all calculations $\epsilon = 10^3$ which means that the same weighting is given between the disturbance and control energy in all cases. The optimal suction profile was first computed for each of the disturbances individually. A comparison of the disturbance kinetic energy for zero and the corresponding optimal suction can be seen in figure 10(a). It is shown that the reduction of kinetic energy is more than two decades larger for the T-S wave as the optimal control is applied. Given the same ϵ, it is therefore possible to say that optimally growing streamwise streaks demand a stronger control than T-S waves. The corresponding suction

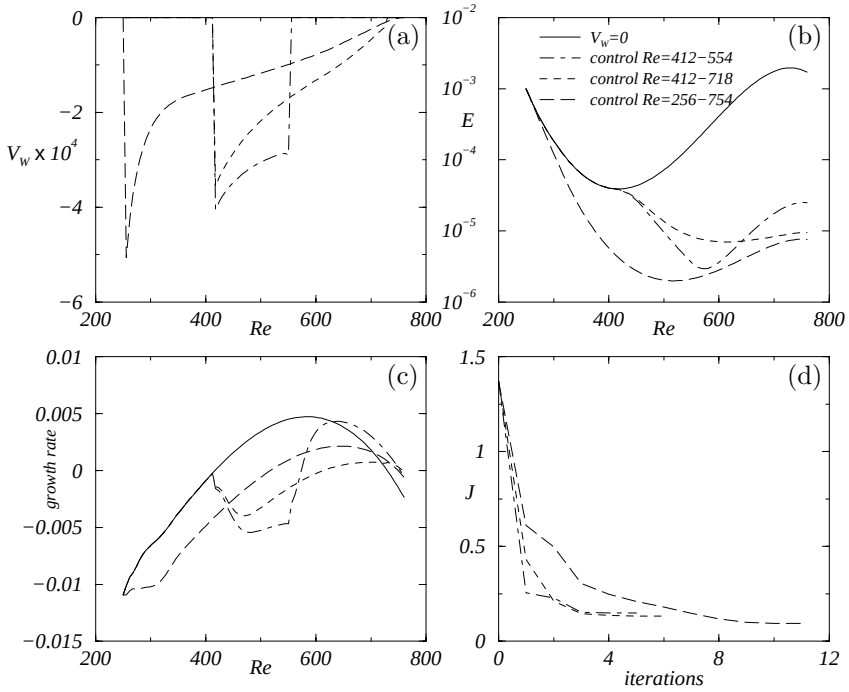

FIGURE 9. Disturbance control of a T-S wave with $F = 10^{-4}$ in a two-dimensional boundary layer ($dP_e/dx = 0$). Results are presented for different control domains given that $\epsilon = 10^3$. (a) Optimal suction distributions. (b) The disturbance kinetic energy in a mean flow with zero and optimal suction. (c) The growth rate, -imag(α), in a mean flow with zero and optimal suction. (d) The objective function as a function of the iteration step.

distributions can be seen in figure 10(c). It can be seen in this comparison that steady streaks has a stronger control when it is compared to T-S waves. This is however expected as the total disturbance kinetic energy of the streaks is larger than that of the T-S wave given that the energy is the same at X_1, see figure 10(a), and therefore should result in a larger control energy. Then, the optimal suction profile was calculated for the sum of both disturbances using (22) with $\epsilon = 10^3$. In figure 10(b), the disturbance kinetic energy is shown when the optimal control for the sum of both disturbances is applied to each disturbance individually and the sum of both disturbances. The corresponding optimal suction distribution can be seen in figure 10(c). Here, the total kinetic energy for the streaks is larger than for the T-S wave, and the control will act primarily on the streaks. Therefore, the optimal suction distribution for the sum of the disturbances is similar to that of the streaks. When the optimal

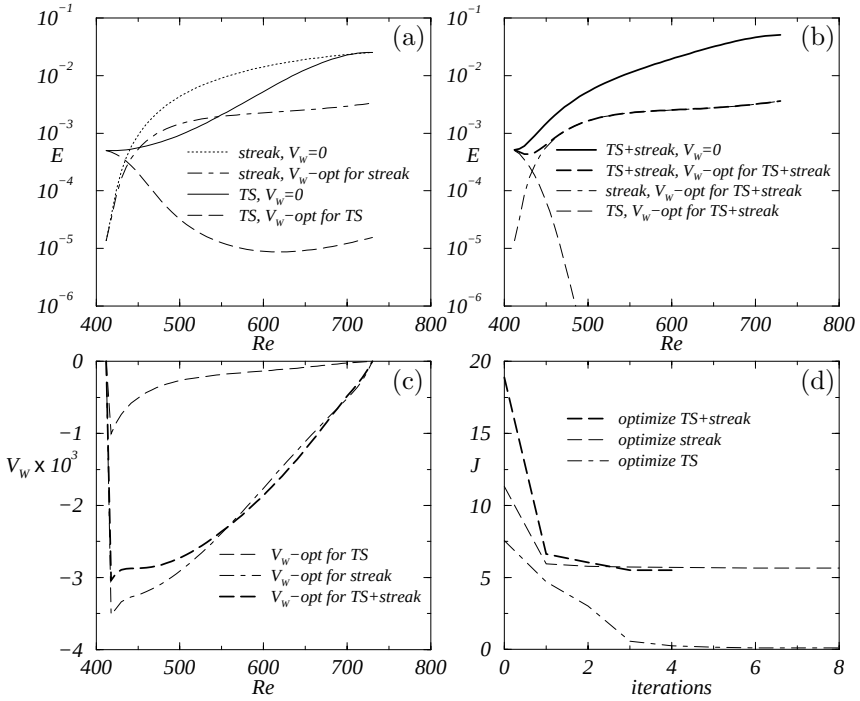

FIGURE 10. Control of two disturbances in a two-dimensional boundary layer ($dP_e/dx = 0$). The disturbances are a T-S wave ($F = 10^{-4}$) and optimally growing streamwise streaks ($\beta = 0.292$ at $Re = 412$) and $\epsilon = 10^3$. Disturbance kinetic energy in a mean flow with zero and optimal suction (a) the suction distribution is computed for each disturbance separately, (b) the suction distribution is computed to account for both disturbances (see § 2.3). (c) Optimal suction distributions. (d) The objective function as a function of the iteration step.

suction profile for the sum is used on the the T-S wave then the energy decreases further and drops to 10^{-11}, out of range in figure 10(b), at the downstream position X_1. This is 5 decades lower than the optimal suction profile for control of just the T-S wave gives. In figure 10(d) the objective function is given as function of the iteration number to show the convergence of the optimization process.

3.4. *Three-dimensional boundary layers*

Here, we study the control of three-dimensional disturbances in three-dimensional boundary layers subjected to a pressure gradient. In the first case, the flow

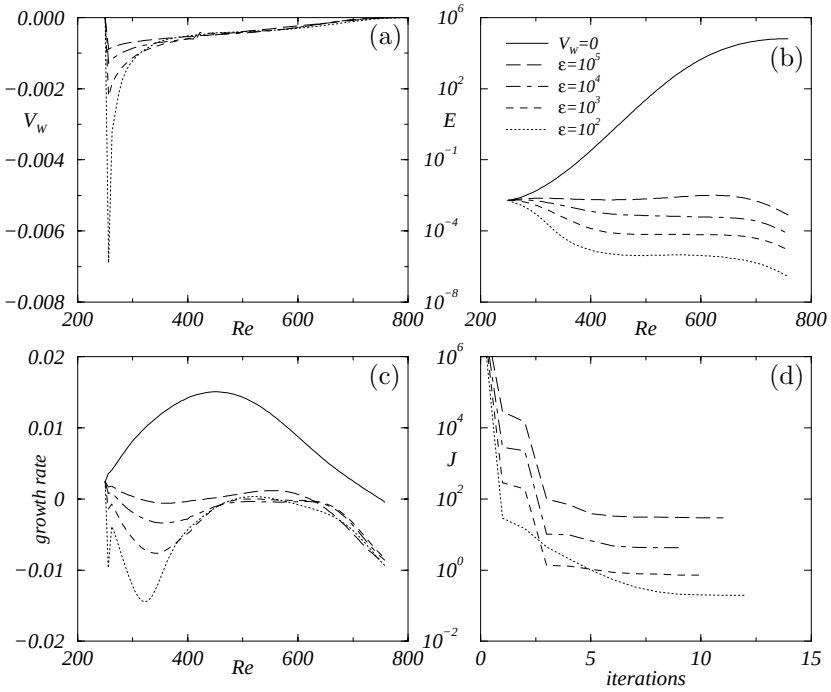

FIGURE 11. Control of an oblique wave in a three-dimensional boundary layer with an adverse pressure gradient ($U_e = (x/x_0)^{-0.05}$). The inviscid flow at $Re = 250$ has an angle of 45^o and the non-dimensional spanwise wavenumber $\beta = -0.02$. Results are shown for $\epsilon = 10^2, 10^3, 10^4, 10^5$. (a) Optimal suction distributions. (b) The disturbance energy in a mean flow with zero and optimal suction. (c) The growth rate, -imag(α), in a mean flow with zero and optimal suction. (d) The objective function as a function of the iteration step.

is subject to an adverse pressure gradient and the disturbance has been chosen such that it has the maximum local growth rate at some position in the computational domain. In the second case, control is presented for a steady cross-flow mode in a mean flow with a favorable pressure gradient.

3.4.1. *Control in a flow with an adverse pressure gradient*

The control of an oblique wave is analyzed in a quasi three-dimensional incompressible boundary layers with an adverse pressure gradient ($U_e = (x/x_0)^{-0.05}$). The streamwise range is $Re = 250{-}760$, the non-dimensional spanwise wavenumber $\beta = -0.02$ and the reduced frequency $F = 10^{-4}$. The inviscid flow at $Re = 250$ has an angle of 45^o and the control has been applied at $Re = 256{-}754$.

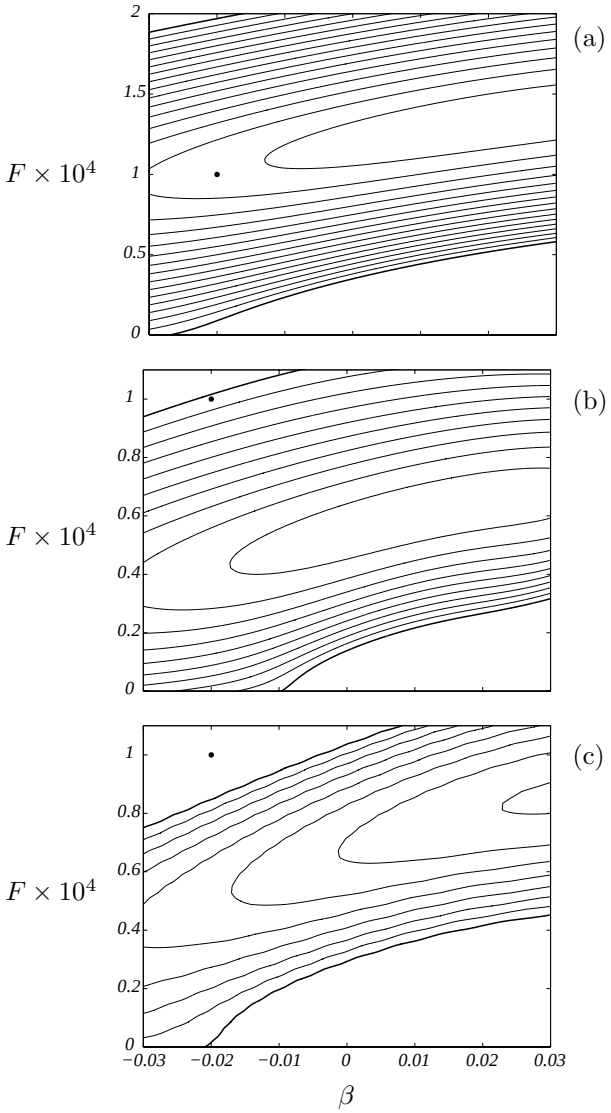

FIGURE 12. Contours of local growth rate at different streamwise positions in a flow with an adverse pressure gradient ($U_e = (x/x_0)^{-0.05}$). The inviscid flow at $Re = 250$ has an angle of 45^o. (a) At $Re = 418$ with zero suction. (b) At $Re = 676$ with zero suction. (c) At $Re = 676$ with an optimal suction distribution given by the case in figure 11 where $\epsilon = 10^2$. Here F, β and the local growth rate are scaled with reference values at X_0. The thick contours denote zero growth rate and the contour spacing is 0.0005. The • marks the disturbance initial condition used in figure 11.

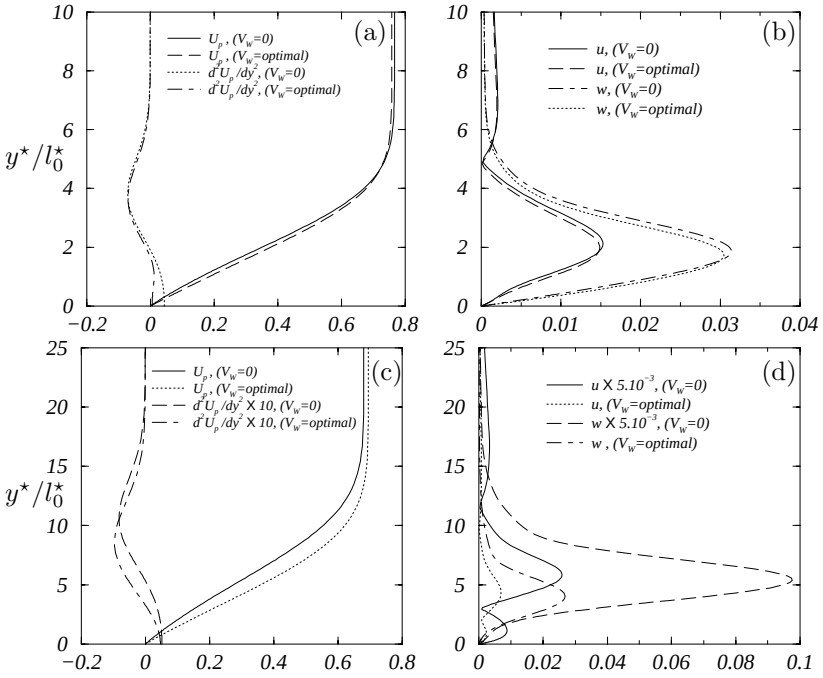

FIGURE 13. Modification of the three-dimensional mean flow with an adverse pressure gradient ($U_e = (x/x_0)^{-0.05}$) and disturbance velocity, due to optimal suction ($\epsilon = 10^5$). The inviscid flow at $Re = 250$ has an angle of 45^o and the control is computed for an oblique wave ($F = 10^{-4}, \beta = -0.02$ at $Re = 250$) between $Re = 250 - 760$. $U_p = (\alpha_r U + \beta W)/k$ and the absolute value of the streamwise and spanwise disturbance velocity are denoted u and w respectively. The streamwise positions are: $Re = 262$ in figures (a)-(b) and $Re = 694$ in figures (c)-(d)

In this case ϵ has been altered to compare the impact of different regularization parameters on the control energy used. The results comparing various ϵ can be seen in figure 11. In figure 11(a) the optimal suction distribution $V_{\rm w}$ is plotted. A suction peak appears at an upstream position of the control domain and is more pronounced as ϵ is decreased. Downstream of the suction peak the suction distribution is rather constant before it finally decreases to zero. The disturbance kinetic energy is compared in figure 11(b) for the case of zero and optimal suction distribution. A reduction of kinetic energy is observed in all cases starting in the upstream region of the control domain. Further, the reduction is increased as ϵ is decreased. In figure 11(c) the growth rate is compared for zero and optimal suction distribution. In figure 11(d) the objective

function is plotted for each iteration in the optimization loop to demonstrate the convergence of the optimization process.

In this analysis only one oblique wave has been considered. The effects on the growth rate on other oblique waves are investigated using the suction distribution from the analysis above with $\epsilon = 10^2$. This is done by computing the local growth rate in the $F - \beta$ plane at two different streamwise positions. Contours of the local growth rate can be seen in figure 12 where the thick contours mark zero growth rate and the $\bullet$ marks the oblique wave analyzed in figure 11. Note here that the reduced frequency F, the non-dimensional spanwise wavenumber β and the growth rate are scaled with the reference values taken at X_0. Figure 12(a) shows the local growth rate for oblique waves at $Re = 418$ with zero suction. Here it is shown that the disturbance analyzed in figure 11 is close to the maximum growth rate for all oblique waves at this streamwise position. No figure is shown for the case when optimal suction is applied as all waves are damped at this position. The result in figures 12(b)-(c) correspond to $Re = 676$ with the mean flow subjected to zero and optimal suction respectively. The optimal suction is shown to stabilize all oblique waves. However, the effect is less than in the upstream region.

It is also of interest to see how the inflection point due to the adverse pressure gradient is affected by the optimal suction. The suction distributions shown in figure 11(a) are similar except for the upstream region. Therefore, the case of figure 11 with $\epsilon = 10^5$ is chosen to see if the smallest amount of suction still affects the inflection point of the mean flow. The results for two different streamwise positions are seen in figure 13. Here the mean flow has been projected in the direction of $k = (\alpha^2 + \beta^2)^{\frac{1}{2}}$ and is given as $U_p = (\alpha U + \beta W)/k$. In figure 13(a) U_p and its corresponding second wall normal derivative are shown at $Re = 262$. The effect of the optimal suction is small but increases the velocity inside the boundary layer. The plot of the second wall normal derivative of U_p shows that the inflection point has almost disappeared. The effect on the disturbance velocities due to the mean flow modification at $Re = 262$ is shown in figure 13(b). Here, the absolute value of the streamwise and spanwise disturbance velocities are plotted. Both components have kept their shape but the maximum values are decreased and moved towards the wall. The quantities in figures 13(a)-(b) are plotted at $Re = 694$ in figures 13(c)-(d) respectively. At this streamwise position all suction distributions shown in figure 11(a) are similar and therefore are the mean flow modifications at this position similar for all cases shown in figure 11. The mean flow component shown in figure 13(c) have become fuller. However, the inflection point of the streamwise component does still exist but has moved towards the wall. The maximum value of the disturbance velocities shown in figure 13(d) have moved closer to the wall and decreased by a factor of 10^3. Further, it is noted that the disturbance shape has been kept also here.

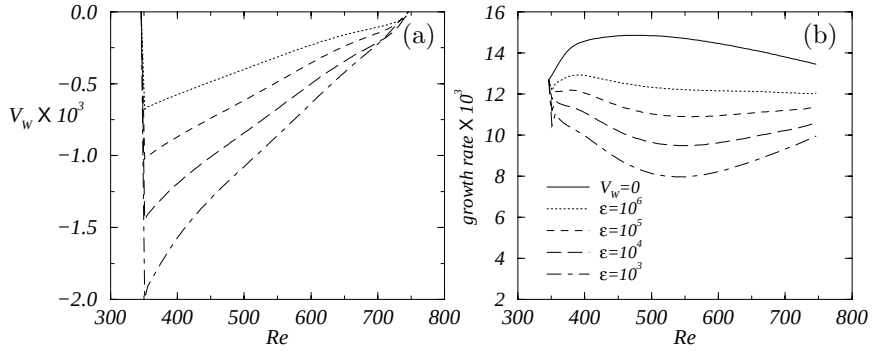

FIGURE 14. Control of a stationary cross-flow mode in a three-dimensional boundary layer with a favorable pressure gradient ($U_e = (x/x_0)^{0.34207}$). The inviscid flow at $Re = 346$ has an angle of 55.26^o and the non-dimensional spanwise wavenumber $\beta = -0.256$. Results are presented for $\epsilon = 10^3, 10^4, 10^5, 10^6$. (a) Optimal suction distributions. (b) Growth rate -imag(α).

3.4.2. *Control in a flow with a favorable pressure gradient*

The control of a steady cross-flow mode is analyzed in a quasi three-dimensional incompressible boundary layers with a favorable pressure gradient taken from Högberg & Henningson (1998) ($U_e = (x/x_0)^{0.34207}$). The streamwise range is $Re = 346 - 746$ and the inviscid flow at $Re = 346$ has an angle of 55.26^o. Here, the control has been applied at $Re = 351 - 741$. The initial condition of the disturbance is taken as the local solution at $Re = 346$ where the non-dimensional spanwise wavenumber is $\beta = -0.256$.

In figure 14 results are presented for the optimization with different values of the regularization parameter ϵ. Here, $\epsilon = 10^3$ gives a maximum suction velocity which is close to the maximum value for which the boundary layer equations are valid (see § 2.1.1). The optimal suction distributions due to the variation of ϵ are shown in figure 14(a). As ϵ is decreased the magnitude of the suction velocity is increased. The maximum of the suction velocity is found in the upstream region in all cases but does not appear as a pronounced peak as was shown in § 3.3 and § 3.4.1.

The corresponding growth rates for zero and optimal suction are presented in figure 14(b). The uncontrolled steady cross-flow mode studied here has a positive growth rate in the whole domain and it is shown here that the optimal suction manages to reduce the growth rate. However, not even the largest magnitude of steady optimal suction, i.e. the smallest ϵ, can stabilize the cross-flow mode. The largest reduction of growth rate is found at approximately the same streamwise position regardless of ϵ and it should be noted that this is far downstream of the point where suction has its maximum.

4. Discussion

A procedure to control disturbances in quasi three-dimensional incompressible boundary layers on a flat plate has been derived and analyzed. Here, control of disturbances is done by modifying the mean flow using the wall normal velocity component of the mean flow on the wall. The optimization procedure is gradient based and the aim is to minimize an objective function balancing a measure of the state and the control energy. The gradient is derived using adjoint equations and here it is shown how the coupling is done between the adjoint of the PSE (APSE) and the adjoint of the boundary layer equations (ABLE). The measure of the state is the disturbance kinetic energy in the whole domain and here it has been generalized to account for more than one disturbance.

To increase the streamwise resolution, a stabilization procedure has been derived which modifies both the APSE and the ABLE. The gradients derived using the adjoint equations has been validated with a finite-difference approach and it has been shown that the gradient accuracy is increased as the streamwise resolution is increased. A finite-difference check has also been continuously done on the final gradients in the optimization indicating that the continuous approach used for the derivation of the adjoint equations has been adequate.

Numerical results have been presented for disturbance control in both two and quasi three-dimensional incompressible boundary layers. The results shown on suction distributions have a similar shape for control of TS-wave instabilities and steady optimally growing streamwise streaks in two-dimensional boundary layers and oblique waves in quasi three-dimensional boundary layers. The suction profiles have a sharp peak close to the first point of the computational domain but become significantly smaller and rather constant further downstream. The only evident difference is seen in figure 6 for $\epsilon = 10^5$, i.e. when the regularization parameter of the control energy is large. In both two- and quasi three dimensional boundary layers it has been shown that the boundary layer velocity profiles have become fuller as the optimal suction distribution is applied. Both of these observations show that the stabilization obtained by the suction distribution is a modification of the mean flow similar to that of a flow with a favorable pressure gradient with zero suction. The relation between the suction velocity, pressure gradient and second wall normal derivative of the streamwise velocity on the wall is understood by looking at (2) for $y = 0$

$$V_{\mathrm{w}} \frac{\partial U}{\partial y} + \frac{dP_e}{dx} = \frac{1}{Re} \frac{\partial^2 U}{\partial y^2}. \tag{30}$$

In the case of a Blasius mean flow ($dP_e/dx = 0$), the right hand side of (30) give the favorable pressure gradient which corresponds to a certain suction velocity. However, in the case of an adverse pressure gradient ($dP_e/dx > 0$), the modification is dependent on the magnitude of the suction velocity as neither of the two terms on the left hand side of (30) is zero. Here, a favorable pressure gradient is only obtained if $V_{\mathrm{w}} \partial U/\partial y < dP_e/dx$. A stabilizing effect will still

occur if $V_w \partial U/\partial y > dP_e/dx$ but the location of the inflection point due to the adverse pressure gradient will be dependent of the magnitude of V_w.

As a result of the optimal suction distribution, the disturbance kinetic energy is decreased as the control energy is increased (here shown by decreasing ϵ). For control of T-S waves in two-dimensional boundary layers and oblique waves in quasi three-dimensional boundary layers, the growth rate has the largest decrease in the upstream domain when ϵ is decreased. This corresponds to where the optimal suction has its peak. In the case control is applied to the steady cross-flow mode studied here, the largest decrease in growth rate is positioned at the same streamwise location independent of ϵ. Further, this is far downstream of the point where the suction has its maximum. For T-S wave instabilities in the Blasius flow it has been shown that essentially the same energy reduction at the last streamwise point is achieved when the control is applied in the whole unstable region compared to control which starts upstream and ends downstream of the unstable region.

One of the assumptions made in this analysis is that the disturbances have homogeneous boundary conditions at the wall and therefore no coupling to the mean flow at the wall. This can be interpreted as uniform suction through a porous material. The validity of these boundary conditions should be analyzed if instead discrete holes are used.

In this analysis there is no constraint on the final solution of the optimal suction distribution other than a maximum value on V_w must be of order $O(Re^{-1})$ for the boundary layer equations to be valid and that $V_w = 0$ at X_0 and X_1. If solutions without sharp peaks are desired then additional terms can be added to the objective function in which a penalty is put on e.g. the streamwise derivative of the control variable. This procedure has been used in e.g. shape optimization problems where the goal has been to create not only an optimal geometry but also with a certain degree of smoothness. Such constrains are not investigated here as they are more connected to user applications and an extension of the optimal control theory rather than the methodology itself.

The first author wants to acknowledge the Swedish Foundation for Strategic Research (SSF) who has financed this work through the Integral Vehicle Structure (IVS)-program.

Appendix A. Matrices of the PSE

The matrices A, B, C and D in the PSE are given as

$$A = \begin{bmatrix} i\alpha & 0 & i\beta & 0 \\ \xi + \dfrac{\partial U}{\partial x} & \dfrac{\partial U}{\partial y} & 0 & i\alpha \\ 0 & \xi + \dfrac{\partial V}{\partial y} & 0 & 0 \\ \dfrac{\partial W}{\partial x} & \dfrac{\partial W}{\partial y} & \xi & i\beta \end{bmatrix}, \quad B = \begin{bmatrix} 0 & 1 & 0 & 0 \\ V & 0 & 0 & 0 \\ 0 & V & 0 & 1 \\ 0 & 0 & V & 0 \end{bmatrix},$$

$$C = \begin{bmatrix} 0 & 0 & 0 & 0 \\ -\dfrac{1}{Re} & 0 & 0 & 0 \\ 0 & -\dfrac{1}{Re} & 0 & 0 \\ 0 & 0 & -\dfrac{1}{Re} & 0 \end{bmatrix}, \quad D = \begin{bmatrix} 1 & 0 & 0 & 0 \\ U & 0 & 0 & 1 \\ 0 & U & 0 & 0 \\ 0 & 0 & U & 0 \end{bmatrix},$$

where

$$\xi = -i\omega + i\alpha U + i\beta W + \frac{1}{Re}(\alpha^2 + \beta^2).$$

Appendix B. Derivation of adjoint equations

The gradient of the objective function, J, with respect to the wall normal velocity component of the mean flow on the wall, $V_{\rm w}$, is derived using the APSE and the ABLE. The question is whether to use a 'discrete' or 'continuous' formulation. One of the conclusions in Högberg & Berggren (2000) was that a continuous formulation is a good enough approximation if control is performed on a problem with a dominating instability. Here, the analysis is done for dominating instabilities using the PSE why a continuous approach has been chosen for the derivation of the adjoint equations.

B.1. *Inner Product*

For a compact notation of the adjoint equations, we will use the *formal adjoint* L^* for the differential operator L defined by the relation

$$(\psi, L\phi) = (L^*\psi, \phi) + \text{ boundary terms}, \tag{31}$$

where the inner product $(\cdot,\cdot)$ is defined as

$$(\phi, \psi) = \int_{Z_0}^{Z_1}\int_{X_0}^{X_1}\int_0^{\infty} \phi^H \psi \; dy \; dx \; dz, \tag{32}$$

for $\mathbb{C}^n$-valued functions ϕ and ψ. Here, the superscript * denotes adjoint quantities and ψ is denoted the *co-state variable* which is chosen such that it satisfies the adjoint equations $L^*\psi = 0$.

B.2. *Derivation of the gradient*

The idea behind the derivation is to identify the gradient from the boundary terms in (31). There are earlier results on the derivation of the APSE (see Airiau 2000; Hill 1997a), however in this analysis, as in Pralits *et al.* (2001), the approach is somewhat different.

Here, we use a perturbation technique together with integration by parts in space. The APSE are derived directly from the PSE why also the auxiliary condition has to be taken into account. Further, there is no ansatz made on the co-state variables of the PSE such as (5). In this way a method has been introduced to derive the APSE which provides the corresponding adjoint auxiliary condition. The details of the derivation is given below. First, the objective function and the state equations are differentiated with respect to the control $V_{\rm w}$. Differentiating (9) and (6)–(7) yields

$$\delta J = \text{real}\Big\{\int_{Z_0}^{Z_1}\int_{X_0}^{X_1}\int_0^{\infty} \delta\mathbf{u}^H\mathbf{u} \; dy \; dx \; dz + \epsilon\int_{Z_0}^{Z_1}\int_{X_0}^{X_1} \delta V_{\rm w} V_{\rm w} \; dx \; dz\Big\}, \tag{33}$$

$$A\delta\hat{q} + B\frac{\partial\delta\hat{q}}{\partial y} + C\frac{\partial^2\delta\hat{q}}{\partial y^2} + D\frac{\partial\delta\hat{q}}{\partial x} + \Big(\frac{\partial A}{\partial Q}\delta Q + \frac{\partial A}{\partial\alpha}\delta\alpha + \frac{\partial B}{\partial Q}\delta Q + \frac{\partial D}{\partial Q}\delta Q\Big)\hat{q} = 0, \tag{34}$$

$$\int_0^\infty (\delta\hat{\mathbf{u}}^H \frac{\partial \hat{\mathbf{u}}}{\partial x} + \hat{\mathbf{u}}^H \frac{\partial \delta\hat{\mathbf{u}}}{\partial x})\, dy = 0. \tag{35}$$

The variations, δq, δQ are the variations of q, Q caused by the variation of V_{w}. Note also that the variation of q results in a variation of both the amplitude function $\hat{q}$ and the streamwise wave-number α as

$$\delta q = \delta\hat{q}\ \Theta + \hat{q}\ \Theta \int_{X_0}^{x'} \delta\alpha\ dx' \tag{36}$$

where

$$\Theta = \exp i(\int_{X_0}^{x'} \alpha\ dx' + \beta z - \omega t).$$

Proceed by differentiating (1)–(3). This is given on a compact form as

$$\frac{\partial L_{BLE}}{\partial Q}\delta Q Q + L_{BLE}\ \delta Q = 0. \tag{37}$$

Now, introduce the complex functions $q = (p^*, u^*, v^*, w^*)$ and r^*, the so called co-state variables, which are multiplied with (34)–(35) respectively according to (32). Then (37) are multiplied with the co-state variables $Q^* = (V^*, U^*, W^*)$ in the same manner. The corresponding left hand side of (31) can now be written

$$\begin{aligned}
&\int_{Z_0}^{Z_1}\int_{X_0}^{X_1}\int_0^\infty q^{*H}\Big(A\delta\hat{q} + B\frac{\partial\delta\hat{q}}{\partial y} + C\frac{\partial^2\delta\hat{q}}{\partial y^2} + D\frac{\partial\delta\hat{q}}{\partial x} + \frac{\partial A}{\partial Q}\delta Q\hat{q} + \frac{\partial A}{\partial\alpha}\delta\alpha\hat{q} + \\
&\qquad \frac{\partial B}{\partial Q}\delta Q\hat{q} + \frac{\partial D}{\partial Q}\delta Q\hat{q}\Big)\, dy\, dx\, dz + c.c. + \\
&\int_{Z_0}^{Z_1}\int_{X_0}^{X_1}\int_0^\infty \Big(\bar{r^*}\big(\delta\hat{\boldsymbol{u}}^H\frac{\partial\hat{\boldsymbol{u}}}{\partial x} + \hat{\boldsymbol{u}}^H\frac{\partial\delta\hat{\boldsymbol{u}}}{\partial x}\big) + r^*\big(\delta\hat{\boldsymbol{u}}^T\frac{\partial\bar{\hat{\boldsymbol{u}}}}{\partial x} + \hat{\boldsymbol{u}}^T\frac{\partial\delta\bar{\hat{\boldsymbol{u}}}}{\partial x}\big)\Big)\, dy\, dx\, dz + \\
&\int_{Z_0}^{Z_1}\int_{X_0}^{X_1}\int_0^\infty Q^{*T}\Big(\frac{\partial L_{BLE}}{\partial Q}\delta Q Q + L_{BLE}\delta Q\Big)\, dy\, dx\, dz
\end{aligned} \tag{38}$$

The right hand side of (31) is derived by removing the derivatives from the differentiated state equations using integration by parts in Ω. Note here that the co-state variable r^* has been introduced due to the additional equation, (7), of the PSE. Further, the complex conjugate has been added as the gradient by definition, (11), is a real-valued function.

Here, the complex conjugate is written out explicitly for the auxiliary condition. Note here that terms in (38) of $\delta\alpha$ now must be integrated in the x-direction in order to obtain the same integral form as in (36).

After collecting terms of $\delta\hat{\mathbf{u}}, \delta\hat{q}, \delta Q$ and $\int_{X_0}^{x'} \delta\alpha \; dx'$, the right hand side including boundary terms is written

$$
\begin{aligned}
&\int_{Z_0}^{Z_1}\int_{X_0}^{X_1}\int_0^{\infty}\Big(A^H q^* - B^H\frac{\partial q^*}{\partial y} + C^H\frac{\partial^2 q^*}{\partial y^2} - D^H\frac{\partial q^*}{\partial x}\Big)\delta\hat{q}\; dy\; dx\; dz + c.c. + \\
&\int_{Z_0}^{Z_1}\int_{X_0}^{X_1}\int_0^{\infty}\Big((r^* - \bar{r^*})\frac{\partial\bar{\hat{\mathbf{u}}}}{\partial x} + \frac{\partial\bar{r^*}}{\partial x}\bar{\hat{\mathbf{u}}}\Big)\delta\hat{\mathbf{u}}\; dy\; dx\; dz + c.c. + \\
&\int_{Z_0}^{Z_1}\int_{X_0}^{X_1}\int_0^{\infty}\Big(L^*_{BLE}(Q)Q^* - f_{ABLE}\Big)\delta Q\; dy\; dx\; dz - \\
&\int_{Z_0}^{Z_1}\int_{X_0}^{X_1}\int_0^{\infty}\frac{\partial}{\partial x}\Big(q^{*H}\frac{\partial A}{\partial\alpha}\hat{q}\Big)\int_{X_0}^{x'}\delta\alpha\; dx'\; dy\; dx\; dz + \\
&\int_{Z_0}^{Z_1}\int_{X_0}^{X_1}\int_0^{\infty}U_e\frac{\partial U^*}{\partial x}\delta U_e\; dy\; dx\; dz + \\
&\int_{Z_0}^{Z_1}\int_0^{\infty}\Big(\Big[q^{*H}D\delta\hat{q} + \bar{r^*}\hat{\mathbf{u}}^H\delta\hat{\mathbf{u}} + q^{*H}\frac{\partial A}{\partial\alpha}\hat{q}\int_{X_0}^{x'}\delta\alpha\; dx' + \bar{u}^*\hat{u}\delta U + \bar{w}^*\hat{u}\delta W \\
&+V^*\delta U + UU^*\delta U + U^*\delta P + W^*U\delta W - U^*U_e\delta U_e\Big]_{X_0}^{X_1}\Big)\; dy\; dz + \\
&\int_{Z_0}^{Z_1}\int_{X_0}^{X_1}\Big(\Big[q^{*H}B\delta\hat{q} + q^{*H}C\frac{\partial\delta\hat{q}}{\partial y} - \frac{\partial(q^{*H}C)}{\partial y}\delta\hat{q} + \bar{u}^*\hat{v}\delta U + \bar{v}^*\hat{v}\delta V \\
&+\bar{w}^*\hat{v}\delta W + V^*\delta V + VU^*\delta U + W^*V\delta W \\
&+\frac{1}{Re}(U_y^*\delta U + W_y^*\delta W - W^*\delta W_y - U^*\delta U_y)\Big]_0^{\infty}\Big)\; dx\; dz
\end{aligned}
\tag{39}
$$

Here, f_{ABLE} are the terms due the δQ in the PSE. In order to identify the objective function (33) in (39), we add and subtract the energy norm in (39). Using (36), this additional term can be written

$$
\int_{Z_0}^{Z_1}\int_{X_0}^{X_1}\int_0^{\infty}(\delta\mathbf{u}^H\mathbf{u} - \delta\hat{\mathbf{u}}^H\hat{\mathbf{u}}|\Theta|^2 - i|\hat{\mathbf{u}}|^2\int_{X_0}^{x'}\delta\alpha\; dx'|\Theta|^2)\; dy\; dx\; dz + c.c. \tag{40}
$$

Now impose the following boundary conditions on the state and co-state variables

$$
\begin{array}{lll}
\delta\hat{u} = \delta\hat{v} = \delta\hat{w} = 0 & \text{at} & y = 0 \\
\delta\hat{u}, \delta\hat{v}, \delta\hat{w}, \delta\hat{p} \to 0 & \text{as} & y \to \infty \\
\delta\hat{u} = \delta\hat{v} = \delta\hat{w} = \delta\hat{p} = 0 & \text{at} & x = X_0 \\
\delta\; U = \delta\; W = 0 & \text{at} & y = 0 \\
\delta\; U, \delta\; W \to 0 & \text{as} & y \to \infty \\
\delta U = \delta W = \delta U_e = 0 & \text{at} & x = X_0 \\
 & & \\
u^* = v^* = w^* = 0 & \text{at} & y = 0 \\
u^*, v^*, w^*, p^* \to 0 & \text{as} & y \to \infty \\
U^* = W^* = 0 & \text{at} & y = 0 \\
U^*, V^*, W^* \to 0 & \text{as} & y \to \infty
\end{array}
$$

Let q^* and r^* satisfy the equations given by $\delta\mathbf{u}, \delta\hat{q}$ and $\int_{X_0}^{x'} \delta\alpha \; dx'$. Further, let Q^* satisfy the equations given by δQ. This is written explicitly as

$$\bar{p}^* i\alpha - \frac{\partial \bar{p}^*}{\partial x} + \frac{\partial \bar{u}^*}{\partial y}V - \frac{\partial \bar{u}^*}{\partial x}U + \bar{w}^*\frac{\partial W}{\partial x} - \frac{1}{Re}\frac{\partial^2 \bar{u}^*}{\partial y^2} + \bar{u}^*\Big[-i\omega + i\alpha U + \frac{\partial U}{\partial x} + i\beta W + \frac{1}{Re}(\alpha^2+\beta^2)\Big] = -(r^* - \bar{r^*})\frac{\partial \bar{\hat{u}}}{\partial x} + \frac{\partial \bar{r^*}}{\partial x}\bar{\hat{u}} + \bar{\hat{u}}|\Theta|^2, \tag{41}$$

$$\frac{\partial \bar{p}^*}{\partial y} + \bar{u}^*\frac{\partial U}{\partial y} - \frac{\partial \bar{v}^*}{\partial y}V - \frac{\partial \bar{v}^*}{\partial x}U + \bar{w}^*\frac{\partial W}{\partial y} - \frac{1}{Re}\frac{\partial^2 \bar{v}^*}{\partial y^2} + \bar{v}^*\Big[-i\omega + i\alpha U + \frac{\partial V}{\partial y} + i\beta W + \frac{1}{Re}(\alpha^2+\beta^2)\Big] = -(r^* - \bar{r^*})\frac{\partial \bar{\hat{v}}}{\partial x} + \frac{\partial \bar{r^*}}{\partial x}\bar{\hat{v}} + \bar{\hat{v}}|\Theta|^2, \tag{42}$$

$$\bar{p}^* i\beta - \frac{\partial \bar{w}^*}{\partial y}V - \frac{\partial \bar{w}^*}{\partial x}U - \frac{1}{Re}\frac{\partial^2 \bar{w}^*}{\partial y^2} + \bar{w}^*\Big[-i\omega + i\alpha U + i\beta W + \frac{1}{Re}(\alpha^2+\beta^2)\Big] = -(r^* - \bar{r^*})\frac{\partial \bar{\hat{w}}}{\partial x} + \frac{\partial \bar{r^*}}{\partial x}\bar{\hat{w}} + \bar{\hat{w}}|\Theta|^2, \tag{43}$$

$$-\frac{\partial \bar{u}^*}{\partial x} + \bar{u}^* i\alpha - \frac{\partial \bar{v}^*}{\partial y} + \bar{w}^* i\beta = 0, \tag{44}$$

$$\frac{\partial}{\partial x}\int_0^\infty \Big(i(\bar{p}^*\hat{u} + \bar{u}^*\hat{p}) + (iU + \frac{2\alpha}{Re})(\bar{u}^*\hat{u} + \bar{v}^*\hat{v} + \bar{w}^*\hat{w})\Big)\, dy + i|\Theta|^2\int_0^\infty |\hat{\mathbf{u}}|^2 \, dy = 0, \tag{45}$$

$$\frac{\partial V^*}{\partial y} - \frac{\partial U}{\partial y}U^* - W^*\frac{\partial W}{\partial y} = \mathrm{real}\Big\{\bar{u}^*\frac{\partial \hat{u}}{\partial y} - \frac{\partial \bar{v}^*}{\partial y}\hat{v} + \bar{w}^*\frac{\partial \hat{w}}{\partial y}\Big\}, \tag{46}$$

$$\frac{\partial V^*}{\partial x} + U\frac{\partial U^*}{\partial x} + \frac{\partial V}{\partial y}U^* + V\frac{\partial U^*}{\partial y} - W^*\frac{\partial W}{\partial x} + \frac{1}{Re}\frac{\partial^2 U^*}{\partial y^2} = \mathrm{real}\Big\{i\alpha[\bar{u}^*\hat{u} + \bar{v}^*\hat{v} + \bar{w}^*\hat{w}] - \frac{\partial \bar{u}^*}{\partial x}\hat{u} - \frac{\partial \bar{u}^*}{\partial y}\hat{v} - \bar{u}^*\frac{\partial \hat{v}}{\partial y} + \bar{v}^*\frac{\partial \hat{v}}{\partial x} + \bar{w}^*\frac{\partial \hat{w}}{\partial x}\Big\} \tag{47}$$

$$\frac{\partial W^*}{\partial x}U + \frac{\partial W^*}{\partial y}V + \frac{1}{Re}\frac{\partial^2 W^*}{\partial y^2} = \mathrm{real}\Big\{i\beta[\bar{u}^*\hat{u} + \bar{v}^*\hat{v} + \bar{w}^*\hat{w}] - \frac{\partial \bar{w}^*}{\partial x}\hat{u} - \bar{w}^*\frac{\partial \hat{u}}{\partial x} - \frac{\partial \bar{w}^*}{\partial y}\hat{v} - \bar{w}^*\frac{\partial \hat{v}}{\partial y}\Big\}. \tag{48}$$

Equations (42)–(46) are the adjoint of the parabolized stability equation, APSE. The inhomogeneous right hand side of (42)–(44), here denoted f_{APSE}, comes from the auxiliary condition (7) and the objective function (9). Equation (46)

solves the additional unknown co-state variable r^* iteratively at each streamwise position. Equations (47)–(48) are the adjoint of the boundary layer equations, ABLE. The inhomogeneous right hand side, denoted f_{ABLE}, is calculated from the solution of the PSE and the APSE. However, only the real part is used as the left hand side consists of real-valued equations. The remaining boundary terms in (39) come from the boundary $x = X_1$ and the term of δV at $y = 0$. We impose the initial condition of both the ABLE and APSE to be zero at $x = X_1$. This does however not cause trivial solutions as both (42)–(46) and (47)–(48) have a non-zero right hand side in Ω. The remaining terms from (39) can now be written

$$\begin{aligned}\mathrm{real}\Big\{\delta J - \int_{Z_0}^{Z_1}\int_{X_0}^{X_1}\Big((\epsilon V_{\mathrm{w}} + V_{\mathrm{w}}^*)\delta V_{\mathrm{w}}\Big)\,dx\,dz \\ + \int_{Z_0}^{Z_1}\int_{X_0}^{X_1}\int_0^{\infty} U_e\frac{\partial U^*}{\partial x}\delta U_e\,dy\,dx\,dz\Big\} = 0.\end{aligned} \tag{49}$$

Index W, here denotes the value at $y = 0$. Equation (49) can now be rewritten as

$$\delta J = \int_{Z_0}^{Z_1}\int_{X_0}^{X_1}\Big((\epsilon V_{\mathrm{w}} + V_{\mathrm{w}}^*)\delta V_{\mathrm{w}}\Big)\,dx\,dz - \int_{Z_0}^{Z_1}\int_{X_0}^{X_1}\int_0^{\infty} U_e\frac{\partial U^*}{\partial x}\delta U_e\,dy\,dx\,dz. \tag{50}$$

If the first term on the right hand side of (50) is written, using (11) as

$$\delta J = \int_{Z_0}^{Z_1}\int_{X_0}^{X_1}\nabla_{V_{\mathrm{w}}} J\;\delta V_{\mathrm{w}}\,dx\,dz, \tag{51}$$

then the gradient of the objective function with respect to the wall normal velocity component of the mean flow at the wall can be identified as

$$\nabla_{V_{\mathrm{w}}} J = \epsilon V_{\mathrm{w}} + V_{\mathrm{w}}^* \quad \text{on} \quad y = 0. \tag{52}$$

The second term on the right hand side of (50) is the variation of the objective function due a variation of the free stream velocity. If a similar gradient definition as in (51) is used for U_e

$$\delta J = \int_{Z_0}^{Z_1}\int_{X_0}^{X_1}\int_0^{\infty}\nabla_{U_e} J\;\delta U_e\,dy\,dx\,dz, \tag{53}$$

then the gradient of the objective function with respect to the free stream velocity can be written

$$\nabla_{U_e} J = -U_e\int_0^{\infty}\frac{\partial U^*}{\partial x}\,dy. \tag{54}$$

The variation U_e would be the consequence of e.g. a change in the geometry and consequently the free stream pressure, and is therefore not considered in this paper.

B.3. *Derivation of the gradient including stabilization*

The derivation of the gradient including the stabilization terms does not differ much from the derivation done in appendix B.2. The same definition of the adjoint, (31), and inner product, (32), are used. The difference becomes clear if the stabilization terms are added to (39). This can be written

$$\begin{aligned}
&\int_{Z_0}^{Z_1}\int_{X_0}^{X_1}\int_0^{\infty} q^{*H}\Big(A\delta\hat{q}+B\frac{\partial\delta\hat{q}}{\partial y}+C\frac{\partial^2\delta\hat{q}}{\partial y^2}+D\frac{\partial\delta\hat{q}}{\partial x}+\frac{\partial A}{\partial Q}\delta Q\hat{q}+\frac{\partial A}{\partial\alpha}\delta\alpha\hat{q}+\\
&\qquad\frac{\partial B}{\partial Q}\delta Q\hat{q}+\frac{\partial D}{\partial Q}\delta Q\hat{q}\Big)\,dy\,dx\,dz+c.c.+\\
&s\int_{Z_0}^{Z_1}\int_{X_0}^{X_1}\int_0^{\infty} q^{*H}\Big(A\frac{\partial\delta\hat{q}}{\partial x}+B\frac{\partial}{\partial x}\Big(\frac{\partial\delta\hat{q}}{\partial y}\Big)+C\frac{\partial}{\partial x}\Big(\frac{\partial^2\delta\hat{q}}{\partial y^2}\Big)+\frac{\partial A}{\partial Q}\delta Q\frac{\partial\delta\hat{q}}{\partial x}+\\
&\qquad\frac{\partial A}{\partial\alpha}\delta\alpha\frac{\partial\delta\hat{q}}{\partial x}+\frac{\partial B}{\partial Q}\delta Q\frac{\partial\delta\hat{q}}{\partial x}\Big)\,dy\,dx\,dz+c.c.+\\
&\int_{Z_0}^{Z_1}\int_{X_0}^{X_1}\int_0^{\infty}\Big(\bar{r^*}\big(\delta\hat{\boldsymbol{u}}^H\frac{\partial\hat{\boldsymbol{u}}}{\partial x}+\hat{\boldsymbol{u}}^H\frac{\partial\delta\hat{\boldsymbol{u}}}{\partial x}\big)+r^*\big(\delta\hat{\boldsymbol{u}}^T\frac{\partial\bar{\hat{\boldsymbol{u}}}}{\partial x}+\hat{\boldsymbol{u}}^T\frac{\partial\delta\bar{\hat{\boldsymbol{u}}}}{\partial x}\big)\Big)\,dy\,dx\,dz+\\
&\int_{Z_0}^{Z_1}\int_{X_0}^{X_1}\int_0^{\infty} Q^{*T}\Big(\frac{\partial L_{BLE}}{\partial Q}\delta QQ+L_{BLE}\delta Q\Big)\,dy\,dx\,dz
\end{aligned}\tag{55}$$

The new terms only appear in the second integral expression in (55). However, this expression includes $\delta\hat{q},\delta\alpha$ and δQ why (42)–(46) and (47)–(48) will all have additional terms due to s. The full derivation of the gradient using (55) is not necessary due to the resemblance between (38) and (55). Instead, it suffices to evaluate the additional terms associated with the stabilization. This is done following the steps in appendix B.2 and yields

$$\begin{aligned}
&s\Big(\frac{\partial\bar{p}^*}{\partial x}i\alpha-\frac{\partial^2\bar{u}^*}{\partial x\partial y}V+\frac{\partial\bar{w}^*}{\partial x}\frac{\partial W}{\partial x}-\frac{\partial\bar{u}^*}{\partial x}\frac{\partial V}{\partial y}-\frac{1}{Re}\frac{\partial^3\bar{u}^*}{\partial x\partial y^2}+\\
&\qquad\frac{\partial\bar{u}^*}{\partial x}\Big[-i\omega+i\alpha U+\frac{\partial U}{\partial x}+i\beta W+\frac{1}{Re}(\alpha^2+\beta^2)\Big]\Big),
\end{aligned}\tag{56}$$

$$\begin{aligned}
&s\Big(-\frac{\partial^2\bar{p}^*}{\partial x\partial y}+\frac{\partial\bar{u}^*}{\partial x}\frac{\partial U}{\partial y}-\frac{\partial^2\bar{v}^*}{\partial x\partial y}V-\frac{\partial\bar{v}^*}{\partial x}\frac{\partial V}{\partial y}+\frac{\partial\bar{w}^*}{\partial x}\frac{\partial W}{\partial y}-\frac{1}{Re}\frac{\partial^3\bar{v}^*}{\partial x\partial y^2}+\\
&\qquad\frac{\partial\bar{v}^*}{\partial x}\Big[-i\omega+i\alpha U+\frac{\partial V}{\partial y}+i\beta W+\frac{1}{Re}(\alpha^2+\beta^2)\Big]\Big),
\end{aligned}\tag{57}$$

$$\begin{aligned}
&s\Big(\frac{\partial\bar{p}^*}{\partial x}i\beta-\frac{\partial^2\bar{w}^*}{\partial x\partial y}V-\frac{\partial\bar{w}^*}{\partial x}\frac{\partial V}{\partial y}-\frac{1}{Re}\frac{\partial^3\bar{w}^*}{\partial x\partial y^2}+\\
&\qquad\frac{\partial\bar{w}^*}{\partial x}\Big[-i\omega+i\alpha U+i\beta W+\frac{1}{Re}(\alpha^2+\beta^2)\Big]\Big),
\end{aligned}\tag{58}$$

$$s\Big(\frac{\partial\bar{u}^*}{\partial x}i\alpha-\frac{\partial^2\bar{v}^*}{\partial x\partial y}+\frac{\partial\bar{w}^*}{\partial x}i\beta\Big),\tag{59}$$

$$s\int_0^\infty \Big(\frac{\partial}{\partial x}\Big[i(\bar{p}^*\frac{\partial \hat{u}}{\partial x}+\bar{u}^*\frac{\partial \hat{p}}{\partial x})+(iU+\frac{2\alpha}{Re})(\bar{u}^*\frac{\partial \hat{u}}{\partial x}+\bar{v}^*\frac{\partial \hat{v}}{\partial x}+\bar{w}^*\frac{\partial \hat{w}}{\partial x})\Big]\Big)\,dy, \quad (60)$$

$$s\Big(\mathrm{real}\Big\{\bar{u}^*\frac{\partial^2 \hat{u}}{\partial x\partial y}-\frac{\partial \bar{v}^*}{\partial y}\frac{\partial \hat{v}}{\partial x}+\bar{w}^*\frac{\partial^2 \hat{w}}{\partial x\partial y}\Big\}\Big), \quad (61)$$

$$s\Big(\mathrm{real}\Big\{i\alpha[\bar{u}^*\frac{\partial \hat{u}}{\partial x}+\bar{v}^*\frac{\partial \hat{v}}{\partial x}+\bar{w}^*\frac{\partial \hat{w}}{\partial x}]-\frac{\partial}{\partial x}\Big(\bar{u}^*\frac{\partial \hat{u}}{\partial x}\Big)-\frac{\partial}{\partial y}\Big(\bar{u}^*\frac{\partial \hat{v}}{\partial x}\Big)\Big\}\Big), \quad (62)$$

$$s\Big(\mathrm{real}\Big\{i\beta[\bar{u}^*\frac{\partial \hat{u}}{\partial x}+\bar{v}^*\frac{\partial \hat{v}}{\partial x}+\bar{w}^*\frac{\partial \hat{w}}{\partial x}]-\frac{\partial}{\partial x}\Big(\bar{w}^*\frac{\partial \hat{u}}{\partial x}\Big)-\frac{\partial}{\partial y}\Big(\bar{w}^*\frac{\partial \hat{v}}{\partial x}\Big)\Big\}\Big). \quad (63)$$

Equations (56)–(59) are the additional terms in the (42)–(45) respectively. Equation (60) is the additional term in (46) and (61)–(63) are the additional terms in (47)–(48) respectively. It should be noted here that the boundary conditions do not change in any of the state or adjoint equations. Further, the gradient expression does not get any additional terms due to the stabilization parameter s.

References

Airiau, C. 2000 Non-parallel acoustic receptivity of a Blasius boundary layer using an adjoint approach. *to appear in J. Flow, Turbulence and Combustion* .

Andersson, P., Berggren, M. & Henningson, D. 1999 Optimal disturbances and bypass transition in boundary laye. *Phys. Fluids* .

Andersson, P., Henningson, D. S. & Hanifi, A. 1998 On a stabilization procedure for the parabolic stability equations. *J. Eng. Math.* **33**, 311–332.

Balakumar, P. & Hall, P. 1999 Optimum suction distribution for tranition prediction. *Theor. and Comp. Fluid Dyn.* **13**, 1–19.

Bertolotti, F., Herbert, T. & Spalart, S. 1992 Linear and nonlinear stability of the blasius boundary layer. *J. Fluid Mech.* .

Bewley, T., Moin, P. & Temam, R. 1999 Dns-based predictive control of turbulence: an optimal benchmark for feedback algorithms. *submitted to J. Fluid Mech.* .

Byrd, R., Lu, P., Nocedal, J. & Zhu, C. 1995 A limited memory algorithm for bound constrained optimization. *SIAM J. Scientific Computing 16* **5**, 1190–1208.

Hall, M. C. G. 1986 Application of adjoint sensitivity theory to an atmospheric general circulation model. *J. The Atmospheric Sci.* **43**, 2644–2651.

Hill, D. C. 1995 Adjoint systems and their role in the receptivity problem for boundary layers. *J. Fluid Mech.* **292**, 183–204.

Hill, D. C. 1997a Receptivity in non-parallel boundary layers. In *ASME Fluids Engineering Division Summer Meeting, FEDSM '97*.

Hill, D. C. 1997b Inverse design for laminar three-dimensional boundary layers. *Bull. A. Phys. Soc.* **42**, 2120.

Högberg, M. & Berggren, M. 2000 Numerical approaches to optimal control of a model equation for shear flow instabilities. *to appear in J. Flow, Turbulence and Combustion* .

Högberg, M. & Henningson, D. S. 1998 Secondary instability of cross-flow vortices in falkner-skan-cooke boundary layers. *J. Fluid Mech.* **368**, 339–357.

Iglisch, R. 1949 Exakte berechnung der laminaren reibungsschicht an der längsangeströmten ebenen platte mit homogener absaugung. *NACA RM* **1205**.

Joslin, R., Gunzburguer, M., Nicolaides, R., Erlebacher, F. & Husaini, M. 1995 A self-contained, automated methodology for optimal flow control validated for transition delay. *ICASE Report 95-96* .

Luchini, P. & Bottaro, A. 1998 Görtler vortices : a backward-in-time approach to the receptivity problem. *J. Fluid Mech.* **363**, 1–23.

Pralits, J. O., Airiau, C., Hanifi, A. & Henningson, D. S. 2001 Sensitivity analysis using adjoint parabolized stability equations for compressible flows. *to appear in J. Flow, Turbulence and Combustion* .

Pralits, J. O., Hanifi, A. & Henningson, D. S. 2000 Adjoint-based suction optimization for 3d boundary layer flows. *Tech. Rep.* FFA TN 2000-58. Swedish Defence Research Agency, FOI, Aeronautics Division, FFA, SE-172 90 Stockholm, Sweden.

Schlichting, H. 1943/44 Die beeinflussung der grenzschicht durch absaugung und ausblasen. *Jb. dt. Adad. d. Luftfahrtforschung* **90-108**.

Schlichting, H. 1979 *Boundary-Layer Theory*, 7th edn. Mc-GRAW HILL.

Schlichting, H. & Bussmann, K. 1943 Exakte lösungen für die laminare reibungsschicht mit absaugung und ausblasen. *Schriften dt. Adad. d. Luftfahrtforschung* **7 B, No. 2**.

Tumin, A. 1996 Receptivity of pipe poiseuille flow. *J. Fluid Mech.* **315**, 119–137.

Ulrich, A. 1944 Theoretishce untersuchungen über die widerstandsersparnis durch laminarhaltung mit absaugung. *Schriften dt. Adad. d. Luftfahrtforschung* **8 B, No. 2**.

Zhu, C., Byrd, R., Lu, P. & Nocedal, J. 1994 L-bfgs-b: Fortran subroutines for large scale bound constrained optimization. *Tech. Rep.* NAM-11. EECS Department, Northwestern University.

Paper 3

3

Adjoint PSE and boundary layer equations for Hybrid Laminar Flow Control (HLFC)

By Christophe Airiau[1], Jan Pralits[2,3], Alessandro Bottaro[1] and Ardeshir Hanifi[3]

1. Objectives

This report aims, first, at explaining how by the use of the adjoint approach one may gain insight on the sensitivity to unsteady or steady forcing, and how a control by a steady blowing and suction of a three dimensional compressible boundary layer can be effected. The second goal is to provide an agreed formulation of well-posed adjoint, non-local stability equations and adjoint boundary layer equations, whose numerical resolution will provide an answer to receptivity and control issues. The application of the adjoint approach to configurations of industrial concerns is the subject of ongoing work. In particular, the efficient placement of the suction systems and the evaluation of manufacturing tolerances in HLFC surfaces need to be analyzed carefully and used as input to the optimal control strategy described in the present report.

1.1. *Work performed*

A bibliography on receptivity investigations using the adjoint approach and on optimal control has been carried out. Then, the different ways of obtaining the adjoint, nonlocal stability equations have been studied; their implementations into the NOLOT code (see Hanifi *et al.* 1994; Hein *et al.* 1994) has first been examined and then performed.

[1]Institut de Mécanique des Fluides de Toulouse, Université Paul Sabatier, 118 route de Narbonne, F-31062 Toulouse Cedex , France.
[2]Department of Mechanics, KTH, SE-100 44 Stockholm, Sweden.
[3]The Swedish Defense Research Agency, FOI, Aeronautics Division, FFA, SE-172 90 Stockholm, Sweden.

2. Notations

General notations

$\bar{q}$, *c.c.*(q)	Complex conjugate of q
x^1, x	Streamwise coordinate
x^2	Spanwise coordinate
x^3, y	Normal to the wall coordinate
(U, V, W)	Boundary layer mean flow velocity components in the directions (x^1, x^2, x^3)
ρ, T	Boundary layer mean flow density and temperature
μ, ν	Boundary layer mean flow dynamic and kinematic viscosities
κ	Boundary layer mean flow heat conductivity
$\tilde{q}$	Total disturbance of q
$\hat{q}$	amplitude function of the disturbance $\tilde{q}$
$(\tilde{u}, \tilde{v}, \tilde{w})$	Total disturbance velocity components in the directions (x^1, x^2, x^3)
$\tilde{p}$	Total disturbance of the pressure
$\tilde{\rho}$	Total disturbance of the density
$\tilde{T}$	Total disturbance of the temperature

Superscript

$*$	Reference to the 'adjoint' of a quantity (co-state), in the dual space
^{T}	Transpose of a vector or a matrix
^{H}	Complex conjugate transpose of a vector or matrix

Subscript

w	Reference to a wall quantity $(x_3 = 0)$
e	Reference to quantity outside the boundary layer
∞	Reference to quantity when $y \to \infty$

3. The adjoints for sensitivity

3.1. *A brief review of previous work*

The receptivity is the crucial step in the laminar-to-turbulent transition process for any convectively unstable flow. It can be defined as the way a given flow responds to excitations within the flow domain and its importance in the definition of the transition process was brought to light in the late sixties by Mark Morkovin. It is customary to classify receptivity in two categories: natural and forced receptivity.

Natural receptivity phenomena are typically those involving the interaction of acoustic waves with surface inhomogeneities. Loosely speaking, the acoustic wave provides the appropriate frequency, whereas the wavelength is given by the surface inhomogeneity. In order for external, long wave acoustic disturbances to induce a Tollmien-Schlichting wave, a coupling must exist in the boundary layer with a rapid streamwise variation in the boundary layer; only in this way the external disturbance can transfer energy to the instability wave at the appropriate combination of wavelength and frequency. This mechanism of scale reduction can occur at the leading edge, we speak then of leading edge receptivity Goldstein (1983), and near regions where the boundary layer encounters a surface irregularity (a discontinuity in curvature, a hump, a roughness element, a region of blowing and/or suction, a heated strip, etc.) In this case we speak of localized receptivity, whereas if the wall is covered with irregularities the term non-localized receptivity is employed. A natural way of treating the rapid variation of the boundary layer produced by the surface inhomogeneity is that of employing the triple-deck theory Goldstein (1985); Goldstein & Hultgren (1987). Although this represents the most consistent and elegant way of handling the problem, the results are valid for such large values of the Reynolds number as to become impractical for applications. The conventional manner of treating the localized acoustic receptivity of a boundary layer relies on the search for a solution of an inhomogeneous Orr-Sommerfeld system (see Crouch 1992, 1995; Crouch & Spalart 1995) and Choudhari & Street (1992). A residue contour integration in the complex wavenumber plane is then called for, the solution of which provides the Tollmien-Schlichting wave amplitude at a desired location. For boundary layers the procedure requires an integration contour with a branch cut, because of the presence of a continuous spectrum. Recently, it has been shown that the same receptivity results can be obtained by employing the adjoint Orr-Sommerfeld equations, by virtue of the Green-Lagrange identity which defines adjoint operators (see Tumin & Fedorov 1984; Tumin 1996; Hill 1995). Even more recently, acoustic receptivity has been treated in a non-parallel approximation by the employment of the adjoint PSE (see Airiau 2000).

Forced receptivity is defined as the direct response of the flow to an unsteady forcing such as harmonic blowing/suction, or plate vibrations. The adjoint approach lends itself naturally to this type of studies, both in the local Hill (1995) and the non-local approximation Hill (1997*b*); Airiau *et al.* (2000);

Collis & Dobrinsky (2000); Dobrinsky & Collis (2000). The reason is that the adjoint variables represent directly the Green's functions which must be scalarly multiplied by whatever forcing to yield the downstream mode amplitude. A detailed description of why this is the case is given in Luchini & Bottaro (1998).

A particularly important case of inflow forcing is that which may lead the boundary layer to by-pass transition. It has been shown that some initial flow configurations might excite the boundary layer very significantly, albeit transiently (i.e. over reduced streamwise distances). This transient growth, which originates in the linear operator non-normality, can induce such a large disturbance energy amplification as to render the linear hypothesis not valid. If the disturbance amplitude reaches a very large value, it is argued that nonlinear effects become operational and may lead the boundary layer to transition. Recent works dedicated to this aspect of the receptivity process are e.g Butler & Farrell (1992); Corbett (2000); Andersson *et al.* (1999*a*); Luchini (2000). It is interesting to note that the most dangerous initial disturbances can be obtained through an optimization procedure which employs direct and adjoint systems of linear stability equations. A concept related to that of the receptivity is that of sensitivity. The sensitivity is defined as the gradient of the flow state with respect to a forcing or a control action. Sensitivity functions arise from adjoint equations in a natural manner (see Pralits *et al.* 2000*a*,*b*).

A large body of literature exists on flow control and in aeronautical applications many forms of control can be envisioned. Among the different flow control strategies, the *Hybrid Laminar Flow Control* is being actively pursued in Europe. It consists simply in providing a suction to the boundary layer to affect its growth and to render the flow less susceptible to destabilization. It has been known for a long time that the asymptotic suction boundary layer is much more stable to Tollmien-Schlichting waves than its counterpart without suction. There is now growing experimental evidence (cf. recent work carried out by J. Fransson and P.H. Alfredsson in the Mechanics Department at the Royal Institute of Technology in Stockholm), that the suction boundary layer is also more stable with respect to bypass transition, i.e. longitudinal streaks do not grow as much in this parallel boundary layer. This is encouraging also in practical applications where the boundary layer with suction is not necessarily parallel and the suction distribution is not simply uniform as in the theoretical case.

Theoretical work on flow control through suction at the wall can take different forms. The form we have chosen here is based on optimal control theory and it employs adjoint equations. Other recent works on this form of control have been proposed by Joslin (1998*a*,*b*); Joslin *et al.* (1996, 1995*a*, 1997, 1995*b*) and by Bewley & Liu (1998); Bewley *et al.* (2000). A similar approach based on the boundary layer equations model has been pursued in Cathalifaud & Luchini (2000). In the present work, optimal suction control will be determined on the basis of the PSE system (see Hanifi 1995; Herbert 1997; Airiau & Casalis 1993; Simen 1992).

3.2. *A parabolic model problem*

To explain the role that adjoint equations play in defining the sensitivity or receptivity to forcing terms for a given direct field, it is best to start from a simple model problem and to introduce the relevant definitions and terminology.

3.2.1. *State equations*

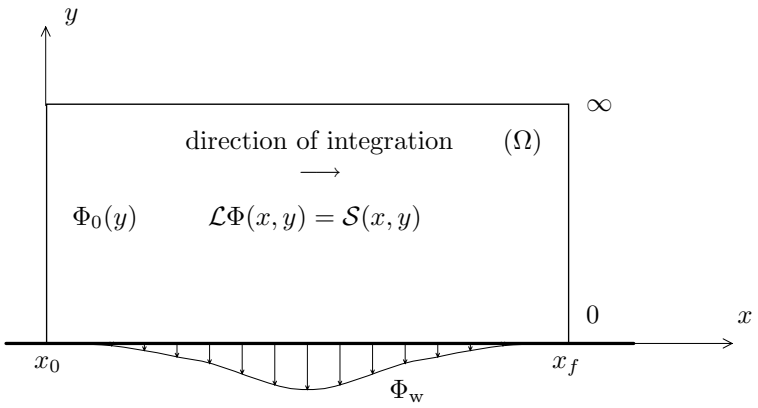

FIGURE 1. Domain of the model equation

We consider a Cartesian domain $\Omega = \{x \in [x_0, x_f], y \in [0, \infty[\}$, x is the streamwise coordinate and y the normal-to-the-wall coordinate. The wall is located at $y = 0$. A physical problem is defined on Ω with a typical complex function $\Phi(x, y)$ representing the state variable. The linear problem can be written by introducing an operator $\mathcal{L}$ and an unknown forcing source term $\mathcal{S}$; the initial condition $\Phi_0(y)$ at x_0 is fixed, whereas at $y = 0$, the control function $\Phi_{\rm w}(x)$ needs to be determined. $\mathcal{S}$ and $\Phi_{\rm w}(x)$ are used to affect some norm of the function Φ, which represents a measure of the state. The state equations can be written as:

$$\begin{array}{rcl} \mathcal{L}\,\Phi(x,y) & = & \mathcal{S}(x,y) \\ \Phi(x_0,y) & = & \Phi_0(y) \\ \lim\limits_{y\to\infty} \Phi(x,y) & = & 0 \\ \Phi(x,0) & = & \Phi_{\rm w}(x) \end{array} \tag{1}$$

3.2.2. *Measures*

The problem is characterized by a measure of a certain quantity. This measure is a norm of the state function Φ. Let us define two possible norms. The first one is based on the local amplitude of the function Φ at the output of the domain:

$$E_f = \frac{1}{2}\int_0^{+\infty} \bar{\Phi}\Phi\Big|_{x=x_f} dy. \tag{2}$$

The second one is a global measure of the function in the whole domain:

$$E_g = \frac{1}{2}\int_{x_0}^{x_f}\int_{0}^{+\infty} \bar{\Phi}\Phi \; dydx. \tag{3}$$

The over-bar stands for the complex conjugate. Both measures are defined over the real range.

3.2.3. *Sensitivity*

The sensitivity function can be defined as the gradient of the state measure with respect to the control; if the control variables are $\mathcal{S}$ and Φ_{w}, variation in E are written as:

$$\delta E = \mathtt{Real}\{\int_{x_0}^{x_f}\int_{0}^{+\infty} \overline{\nabla}_{\mathcal{S}} E \; \delta\mathcal{S} \; dxdy + \int_{x_0}^{x_f} \overline{\nabla}_{\Phi_{\mathrm{w}}} E \; \delta\Phi_{\mathrm{w}} \; dx\}, \tag{4}$$

where

$$\mathtt{Real}\{\overline{\nabla}_{\xi} E \; \delta\xi\} = \mathtt{Real}\{\nabla_{\xi} E\}\delta\xi_r + \mathtt{Im}\{\nabla_{\xi} E\}\delta\xi_i = \lim_{s\to 0}\frac{E(\xi + s\delta\xi) - E(\xi)}{s},$$

with $\delta\xi = \delta\xi_r + i\delta\xi_i$. The gradients $\nabla_{\Phi_{\mathrm{w}}} E$ and $\nabla_{\mathcal{S}} E$ may be obtained from the adjoint equations in two ways. The first one is described in Pralits et al. Pralits *et al.* (2000*b*). The main points are briefly sketched below:

1. The measure (2 or 3) is perturbed (differentiated) and δE_f (or δE_g) becomes a function of $\delta\Phi$.
2. The governing equations (1) are also perturbed. An inner product of these perturbed governing equations with a function Φ^* is defined along the whole domain. After some integrations by parts, the co-state (or adjoint) equation for the variable Φ^* is defined.
3. Finally the boundary and initial conditions are chosen such that the gradient can be identified from the boundary terms.

A similar approach is proposed in this report but it is based on the variation of an augmented (Lagrangian) functional δJ. The approach is later extended for optimal control purposes in chapter 4. Here the derivations are presented based on the first measure (2); later on results will be shown for both local and global measures. The augmented functional is defined by:

$$J = E_f - \mathtt{Real}\{\langle\Phi^*, \mathcal{L}\Phi - \mathcal{S}\rangle\}. \tag{5}$$

The inner product between the co-state Φ^* and the governing equations $\langle\Phi^*, \mathcal{L}\Phi - \mathcal{S}\rangle$ is equal to zero whenever Φ satisfies (1). The gradient of E_f are given by perturbing equation (5). The difference with the first approach is that the gradients are now derived from δJ ($\delta J = \delta E_f$ since $J = E_f$). More details are provided in section 3.2.5.

3.2.4. *Inner product and adjoint operator*

An inner product defining a norm in $\mathbb{R}$ is needed to obtain an adjoint problem:

$$\langle \Phi, \Psi \rangle = \int_{x_0}^{x_f} \int_0^{+\infty} \bar{\Phi}(x,y)\ \Psi(x,y)\ dy\ dx, \tag{6}$$

where $\Phi(x,y)$ and $\Psi(x,y)$ are complex functions. The formal adjoint operator of $\mathcal{L}$ verifies

$$\langle \Phi^*, \mathcal{L}\Phi \rangle = \langle \mathcal{L}^*\Phi^*, \Phi \rangle + \int_{x_0}^{x_f} \int_0^{\infty} \mathrm{div}\mathbf{J}(\bar{\Phi}^*, \Phi)\ dy\ dx. \tag{7}$$

The superscript * refers to the adjoint quantity. This equation is known also as the 'Green-Lagrange Identity', the right hand side is obtained by integration by parts. $\mathbf{J} = (J_x, J_y)$ is the bilinear concomitant vector (see Hill Hill (1995)) and is a function of the boundary and initial conditions of both direct and adjoint problems. The last term of this identity will, in the following, also be referred to as 'BT', for 'Boundary Terms'. Let Φ^* satisfy the adjoint equations:

$$\mathcal{L}^*\ \Phi^* = 0. \tag{8}$$

3.2.5. *Example of adjoint problem*

A simple model equation which includes an evolution term, an advection term, a diffusion term and a forcing term is the linearized, inhomogeneous Burgers equations:

$$\mathcal{L}\Phi = \frac{\partial \Phi}{\partial x} + U(y)\frac{\partial \Phi}{\partial y} - \frac{\partial^2 \Phi}{\partial y^2} = \mathcal{S}(x,y), \qquad U(y) \in \mathbb{R}. \tag{9}$$

The boundary conditions and the initial condition at x_0 are given in equations (1). The variation of the functional J yields:

$$\delta J = \mathtt{Real}\{\int_0^{+\infty} \bar{\Phi}\delta\Phi\big|_{x=x_f}\ dy - \langle \Phi^*, \mathcal{L}\delta\Phi - \delta\mathcal{S}\rangle - \langle \delta\Phi^*, \mathcal{L}\Phi - \mathcal{S}\rangle\}. \tag{10}$$

where Φ^* is a Lagrange multiplier, and also the solution of the adjoint equation. The third term on the right-hand-side of equation (10) is null from equation (9). Using integrations by parts of the inner product, the second term becomes:

$$\langle \Phi^*, \mathcal{L}\delta\Phi - \delta\mathcal{S}\rangle = \int_{x_0}^{x_f} \int_0^{\infty} \left[-\frac{\partial \Phi^*}{\partial x} - \frac{\partial [U(y)\Phi^*]}{\partial y} - \frac{\partial^2 \Phi^*}{\partial y^2}\right] \delta\Phi dx dy +$$
$$\int_{x_0}^{x_f} \left[\bar{\Phi}^*\ U(y)\ \delta\Phi - \bar{\Phi}^*\frac{\partial \delta\Phi}{\partial y} + \frac{\partial \bar{\Phi}^*}{\partial y}\delta\Phi\right]_{y=0}^{y=\infty} dx + \int_0^{\infty} \left[\bar{\Phi}^*\delta\Phi\right]_{x_0}^{x_f} dy - \langle \Phi^*, \delta\mathcal{S}\rangle. \tag{11}$$

Introducing (11) into (10), and setting to zero every term except those in front of $\delta\mathcal{S}$ and $\delta\Phi_{\rm w} = \delta\Phi(x,0)$, we identify the adjoint problem or co-state problem:

$$\begin{aligned} \mathcal{L}^*\Phi^* = -\frac{\partial\Phi^*}{\partial x} - \frac{\partial[U(y)\Phi^*]}{\partial y} - \frac{\partial^2\Phi^*}{\partial y^2} &= 0 \\ \Phi^*(x,0) &= 0 \\ \lim_{y\to\infty}\Phi^*(x,y) &= 0 \\ \Phi^*(x_f,y) &= \Phi(x_f,y) \end{aligned} \tag{12}$$

With the global measure (3), the adjoint system reads:

$$\begin{aligned} \mathcal{L}^*\Phi^* &= \Phi \\ \Phi^*(x,0) &= 0 \\ \lim_{y\to\infty}\Phi^*(x,y) &= 0 \\ \Phi^*(x_f,y) &= 0 \end{aligned} \tag{13}$$

The global norm introduces a source term in the adjoint equation and the terminal condition at x_f vanishes. Note that, in equation (11), $\delta\Phi(x_0,y) = 0$ since the input disturbance $\Phi(x_0,y)$ is fixed. The first equation of system (12) is parabolic in the upstream direction: it must be integrated from x_f to x_0, with a terminal condition provided at x_f. Finally, the variation of the functional δJ is:

$$\delta J = \texttt{Real}\{\int_{x_0}^{x_f}\frac{\partial\bar{\Phi}^*_{\rm w}}{\partial y}\delta\Phi_{\rm w}\,dx + \int_{x_0}^{x_f}\int_0^{+\infty}\bar{\Phi}^*\delta\mathcal{S}\,dxdy\}. \tag{14}$$

From equation (4) and knowing that $J = E_f$, the gradients are identified to be:

$$\nabla_{\mathcal{S}}E_f = \Phi^*, \qquad \nabla_{\Phi_{\rm w}}E_f = \frac{\partial\Phi^*_{\rm w}}{\partial y}. \tag{15}$$

These gradients are the Green's functions associated to a source and a wall perturbation, respectively.

3.2.6. *Receptivity to wall perturbation*

Let us consider the same model equation given in section 3.2.5, but without any source term ($\mathcal{S} = 0$) and assume that for instance, the function Φ is a component of the velocity. We consider the same domain Ω and the initial condition at x_0 is zero. The disturbance Φ will be generated through a wall perturbation (roughness, bump, blowing or suction) in the domain Ω. We can define a receptivity problem in the following terms:

1. What is the amplitude of Φ, defined as $\max_y|\Phi(x,y)|$ at the output, x_f, with a wall roughness of equation $y_{\rm w}(x) = h(x)$ on $\Gamma_{\rm w}$, where $\Gamma_{\rm w} = \{x \in [a,b]\}$?
2. What is the amplitude of Φ at the output if $\Phi_{\rm w}(x)$ is non-zero on $\Gamma_{\rm w}$ and models a suction or bleeding of fluid through the wall ?

Answers can be provided by the adjoint equation approach, with (11) which now reads:

$$\begin{aligned}\langle \Phi^*, \mathcal{L}\Phi \rangle = \int_{x_0}^{x_f} \int_0^{\infty} \left[-\frac{\partial \Phi^*}{\partial x} - \frac{\partial [U(y)\Phi^*]}{\partial y} - \frac{\partial^2 \Phi^*}{\partial y^2} \right] \Phi dx dy + \\ \int_{x_0}^{x_f} \left[\bar{\Phi}^* \, U(y) \, \Phi - \bar{\Phi}^* \frac{\partial \Phi}{\partial y} + \frac{\partial \bar{\Phi}^*}{\partial y} \Phi \right]_{y=0}^{y=\infty} dx + \int_0^{\infty} \left[\bar{\Phi}^* \Phi \right]_{x_0}^{x_f} dy.\end{aligned} \tag{16}$$

With the same adjoint equation as in (12), equation (16) gives:

$$\int_0^{\infty} \bar{\Phi}_f^* \Phi_f dy = \int_0^{\infty} \bar{\Phi}_0^* \Phi_0 dy + \int_{x_0}^{x_f} \left. \frac{\partial \bar{\Phi}^*}{\partial y} \right|_{\mathrm{w}} \Phi_{\mathrm{w}} dy. \tag{17}$$

ϕ_{w} is non-zero in $x \in [a, b]$. Assuming that the initial condition is zero, we have

$$\int_0^{\infty} \bar{\Phi}_0^* \Phi_0 dy = 0. \tag{18}$$

If $\Phi_{\max} = \max_y |\phi(x, y)|$, the function Φ may be normalized as:

$$\Phi(x, y) = \Phi_{\max}(x) \tilde{\Phi}(x, y). \tag{19}$$

Introducing equations (18) and (19) in equation (17) provides the answer to the receptivity problem, *i.e.* the output amplitude of the disturbance generated through a wall perturbation:

$$\Phi_{\max}(x_f) = \frac{\displaystyle\int_a^b \left. \frac{\partial \bar{\Phi}^*}{\partial y} \right|_{\mathrm{w}} \Phi_{\mathrm{w}} dy}{\displaystyle\int_0^{\infty} \bar{\Phi}_f^* \tilde{\Phi}_f dy}. \tag{20}$$

Considering the case of a two-dimensional roughness of small amplitude compared to the boundary layer thickness (see figure 2), to first order the no-slip condition is written as

$$\vec{V}(x, h, t) = \vec{V}(x, 0, t) + h(x) \frac{\partial \vec{V}}{\partial y}(x, 0, t) = \vec{0},$$

where $\vec{U} = (U, V)$ is the total flow velocity. Using the usual decomposition into a mean flow quantity (U) and a disturbance (u), a condition on the streamwise disturbance velocity, modeled here ($\Phi = u$) reads:

$$\Phi_W(x) = -h(x) \frac{\partial U}{\partial y}(x, 0).$$

Considering the case of wall suction, Φ_W models the suction velocity at the wall. It can be shown that the amplitude at $x = b$ is given by:

$$\Phi_{\max}(b) = \frac{\displaystyle\int_a^b \left. \frac{\partial \bar{\Phi}^*}{\partial y} \right|_{\mathrm{w}} \Phi_{\mathrm{w}} dy}{\displaystyle\int_0^{\infty} \bar{\Phi}^*(b, y) \tilde{\Phi}(b, y) dy}.$$

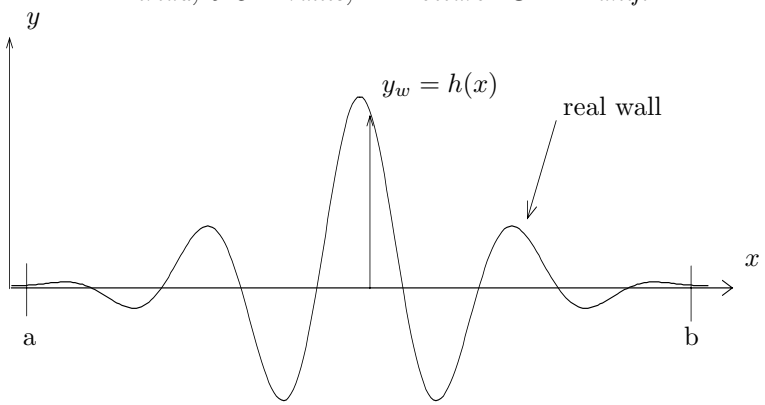

FIGURE 2. Roughness model

All receptivity details using an adjoint approach are given in Airiau (2000); Hill (1995). The receptivity to unsteady wall disturbances is based on the theory sketched here. Acoustic receptivity requires more calculations and theoretical steps as shown in Airiau (2000).

From a practical point of view, we have first to solve the state equations (with non-vanishing initial conditions) and then solve the adjoint equations in order to have Φ^*. Finally, the receptivity functions are given by equation (20) (under the assumption $\Phi_0 = 0$).

3.3. *The PSE and the APSE*

3.3.1. *Introduction*

The sensitivity of two- and three dimensional disturbances in a compressible boundary layer for changes in unsteady wall- and momentum forcing is investigated. This analysis is formulated as an input/output problem and will be discussed below considering the domain Ω given in figure 3. Here, x^1, x^2 and x^3 are the streamwise, spanwise and wall normal coordinates, respectively, and U_e the streamwise freestream velocity. The computational domain Ω is defined such that $x^1 \in [X_0, X_1]$, $x^2 \in [Z_0, Z_1]$ and $x^3 \in [0, \infty[$. An initial disturbance is superimposed to the boundary layer base flow at an upstream position X_0. $Z_1 - Z_0$ corresponds to the spanwise periodicity of the disturbance. It should be noticed that the infinite swept wing assumption leads the metrics to be given by $h_2 = h_3 = 1$ and $h_1 = h_1(x^1, x^3)$. In this chapter, the theory is written keeping all the metrics $h_i(x^1, x^3)$.

3.3.2. *State equations*

The governing equations are the non-local stability equations formulated using the PSE technique for quasi-three dimensional viscous, compressible flow, in primitive variables and general, orthogonal curvilinear coordinates. Here, we consider a general case where the boundary layer is subject to unsteady sources

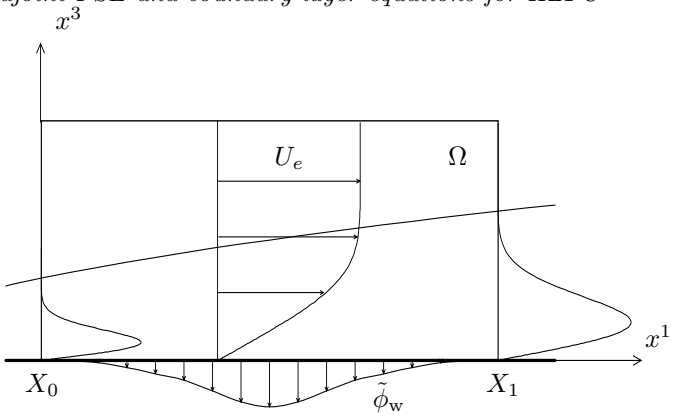

FIGURE 3. Computational domain in the (x^1, x^3) plane.

of mass, momentum and energy $\tilde{\mathcal{S}}$, unsteady inhomogeneous perturbation velocity $\tilde{\mathbf{u}}_{\rm w}$ and perturbation temperature $\tilde{T}_{\rm w}$ at the wall. The notation, the reference quantities, the assumptions and the derivation of the PSE are given in appendix Appendix A. More informations may also be found in Herbert (1997); Simen (1992); Airiau & Casalis (1993); Hanifi (1995).

The equations in symbolic form are written as

$$\begin{aligned}
\hat{\mathcal{L}}\,\hat{\phi} &= \hat{\mathcal{S}} && \text{in} \quad \Omega \\
\hat{\phi} &= \hat{\phi}_0 && \text{at} \quad x^1 = X_0 \\
(\hat{\mathbf{u}}, \hat{T}) &= (\hat{\mathbf{u}}_{\rm w}(x^1), \hat{T}_{\rm w}(x^1)) && \text{at} \quad x^3 = 0 \\
(\hat{\mathbf{u}}, \hat{T}) &\to 0 && \text{as} \quad x^3 \to \infty \\
\int_0^\infty \hat{\phi}^H \frac{\partial \hat{\phi}}{\partial x^1}\, h_2 h_3 dx^3 &= 0 && \text{in} \quad \Omega
\end{aligned} \tag{21}$$

The disturbance vector $\tilde{\phi}$ and the source $\tilde{\mathcal{S}}$ are divided into an amplitude function and a wave function

$$\tilde{\phi}(x^i, t) = \hat{\phi}(x^1, x^3)\Theta, \quad \tilde{\mathcal{S}}(x^i, t) = \hat{\mathcal{S}}(x^1, x^3)\Theta, \tag{22}$$

where

$$\Theta(x^1, x^2) = \exp\, i\,(\int_{X_0}^{x^1} \alpha(x')dx' + \beta x^2 - \omega t). \tag{23}$$

Here, α is the complex streamwise wave number, β the spanwise wave number and ω the frequency of the perturbation. The integral expression in equation (21), the so called auxiliary condition, is used to transfer the major part of the growth into the wave function Θ.

In agreement with the underlying PSE assumptions, the input parameters ($\hat{\mathbf{u}}_{\rm w}$, $\hat{T}_{\rm w}$ and $\hat{\mathcal{S}}$) are assumed to be weak functions of the streamwise coordinate, *i.e.* $\partial/\partial x^1 \sim \mathcal{O}(R^{-1})$.

The system of equations (21), which is nonlinear in $(\alpha, \hat{\phi})$, is integrated in the downstream direction using a marching procedure, with the initial condition at $x^1 = X_0$ given by the local stability theory. At each streamwise position, the value of α is iterated such that the auxiliary condition is satisfied.

3.3.3. *Measures*

In optimal control theory, sensitivity is defined as the derivative of the state variables (output) with respect to the control variables (input). It is related to the gradient of a functional J (called cost or objective functional) which normally includes both a measure of the state E and a measure of the control E_c. These measures are weighted together by a positive factor ϵ, a regularization parameter, such that $J = E + \epsilon E_c$. The regularization parameter serves the purpose of limiting the size of the control. The optimal input can then be obtained via an optimality condition using gradient based optimization techniques, *e.g.* steepest descent or conjugate gradient (cf. Bewley *et al.* 2000; Gunzburger 2000).

Here, the control is represented by the inhomogeneous wall velocity $\tilde{\mathbf{u}}_{\mathrm{w}}$, the temperature $\tilde{T}_{\mathrm{w}}$ on the wall $x^3 = 0$, and the source $\tilde{\mathcal{S}}$ in the equations. The output is a function of the unknown state vector $\tilde{\phi} = (\tilde{\rho}, \tilde{u}, \tilde{v}, \tilde{w}, \tilde{T})$, for instance, expressed as the disturbance energy norm at X_1:

$$E = \frac{1}{2} \int_{Z_0}^{Z_1} \int_0^{\infty} \tilde{\phi}_1^H \mathcal{M} \tilde{\phi}_1 h_2 h_3 \, dx^3 \, dx^2, \tag{24}$$

or, alternatively, as the global disturbance energy norm:

$$E = \frac{1}{2} \int_{X_0}^{X_1} \int_{Z_0}^{Z_1} \int_0^{+\infty} \tilde{\phi}^H \mathcal{M} \tilde{\phi} \, h_1 h_2 h_3 \, dx^1 \, dx^2 \, dx^3, \tag{25}$$

where h_i denote the scale factors and $\tilde{\phi}_1$ the disturbance vector at X_1. The positive diagonal matrix $\mathcal{M}$ defines the measure of the disturbance, and the superscript ^{H} denotes the transpose complex conjugate. In this report $\mathcal{M} = \mathrm{Diag}(0, 1, 1, 1, 0)$ such that disturbances are measured by the modulus of their velocity components. We define the sensitivity as the gradient of E with respect to $\tilde{\mathbf{u}}_{\mathrm{w}}$, $\tilde{T}_{\mathrm{w}}$ and $\tilde{\mathcal{S}}$. Here we consider the case with no penalty, *i.e.* $\epsilon = 0$, so that the output can be written simply $J = E$.

In the present study the amplitude of the control parameters is assumed to be so small that nonlinear interactions with the mean flow can be neglected. However, the procedure presented here is later extended to account for the modification of the mean flow, (see Pralits *et al.* 2000*b*) and chapter 4.

3.3.4. *Inner product*

For a compact notation of the adjoint equations, we will use the *formal adjoint* $\mathcal{L}^*$ of the differential operator $\mathcal{L}$ defined by the relation

$$\langle \mathcal{L}^* \Psi, \Phi \rangle = \langle \Psi, \mathcal{L} \Phi \rangle + \mathrm{B.T.},$$

where the inner product $\langle \cdot, \cdot \rangle$ is defined as

$$\langle \Phi, \Psi \rangle = \int_{X_0}^{X_1} \int_{Z_0}^{Z_1} \int_0^{+\infty} \Phi^H \Psi \; h_1 h_2 h_3 \; dx^3 \; dx^2 \; dx^1, \tag{26}$$

for $\mathbb{C}^n$-valued functions Φ and Ψ. In the following, the superscript * is used to denote adjoint quantities.

3.3.5. *Derivation of the gradient*

Let us define the new Lagrangian functional as

$$J = E - \texttt{Real}\{\langle \hat{\phi}^*, \hat{\mathcal{L}}\, \hat{\phi} - \hat{\mathcal{S}} \rangle + \langle r^* \hat{\phi}, \frac{1}{h_1} \frac{\partial \hat{\phi}}{\partial x^1} \rangle\}. \tag{27}$$

The terms in the inner product come from the governing equations including the auxiliary condition. The functions $\hat{\phi}^*(x^1, x^3)$ and $r^*(x^1)$ define the co-state. The gradient of the output given by (24) or (25), is defined through the directional derivative as

$$\begin{aligned} \delta J = \quad & \texttt{Real} \left\{ \int_{X_0}^{X_1} \int_{Z_0}^{Z_1} \left(\nabla_{\tilde{\mathbf{u}}_\mathrm{w}} J^H \delta \tilde{\mathbf{u}}_\mathrm{w} + \nabla_{\tilde{T}_\mathrm{w}} J^H \delta \tilde{T}_\mathrm{w} \right) h_1 h_2 \; dx^2 \; dx^1 + \right. \\ & \left. \int_{X_0}^{X_1} \int_{Z_0}^{Z_1} \int_0^{\infty} \nabla_{\tilde{\mathcal{S}}} J^H \delta \tilde{\mathcal{S}} \; h_1 h_2 h_3 \; dx^3 \; dx^2 \; dx^1 \right\}, \end{aligned} \tag{28}$$

where $\delta \tilde{\mathbf{u}}_\mathrm{w}, \delta \tilde{T}_\mathrm{w}$ and $\delta \tilde{\mathcal{S}}$ are the variations of the input parameters. The gradient expressions, *i.e.* the sensitivities, are derived in appendix Appendix B, using a perturbation technique of the Lagrangian functional together with integration by parts in space. It is found:

$$\begin{aligned} \nabla_{\tilde{u}_\mathrm{w}} J &= \frac{\mu}{\bar{\Theta} R} D_3(\hat{u}^*) && \text{at} \quad x^3 = 0 \\ \nabla_{\tilde{v}_\mathrm{w}} J &= \frac{\mu}{\bar{\Theta} R} D_3(\hat{v}^*) && \text{at} \quad x^3 = 0 \\ \nabla_{\tilde{w}_\mathrm{w}} J &= \frac{\rho \hat{\rho}^*}{\bar{\Theta}} && \text{at} \quad x^3 = 0 \\ \nabla_{\tilde{T}_\mathrm{w}} J &= -\frac{\kappa}{\bar{\Theta} Pr R} D_3(\hat{T}^*) && \text{at} \quad x^3 = 0 \\ \nabla_{\tilde{\mathcal{S}}} J &= \frac{\hat{\phi}^*}{\bar{\Theta}} && \text{in} \quad \Omega \end{aligned} \tag{29}$$

where μ, κ, R and Pr are the dynamic viscosity, the heat conductivity, the Reynolds and Prandtl numbers, respectively, and

$$D_i = \frac{1}{h_i} \frac{\partial}{\partial x^i}.$$

3.3.6. *Adjoint PSE*

The co-state variables $\hat{\phi}^* = (\hat{\rho}^*, \hat{u}^*, \hat{v}^*, \hat{w}^*, \hat{T}^*)$ and r^* satisfy the adjoint equations

$$\begin{aligned}
\hat{\mathcal{L}}^*\ \hat{\phi}^* &= \mathcal{S}^* && \text{in} \quad \Omega \\
(\hat{\mathbf{u}}^*, \hat{T}^*) &= 0 && \text{at} \quad x^3 = 0 \\
(\hat{\mathbf{u}}^*, \hat{T}^*) &\to 0 && \text{as} \quad x^3 \to \infty \\
(\hat{\phi}^*, r^*) &= (\hat{\phi}_1^*, r_1^*) && \text{at} \quad x^1 = X_1 \\
\frac{\partial}{\partial x^1} \int_0^{+\infty} \hat{\phi}^{*H} \frac{\partial \hat{\mathcal{L}}}{\partial \alpha}\ \hat{\phi}\ h_1 h_2 h_3\ dx^3 &= f^* && \text{in} \quad \Omega
\end{aligned} \tag{30}$$

where

$$\mathcal{S}^* = -\Big[\bar{r}^* D_1(\hat{\phi}) - D_1(r^*\hat{\phi}) - (m_{21} + m_{31}) r^* \hat{\phi}\Big], \tag{31}$$

$$\begin{aligned}
f^* = i \int_0^{+\infty} \hat{\phi}^{*H} \hat{\mathcal{S}}\ h_1 h_2 h_3\ dx^3 + i h_1 h_2 \Big[-\frac{\kappa}{PrR} D_3(\bar{\hat{T}}^*) \hat{T} \\
+ (\rho \bar{\hat{\rho}}^*) \hat{w} + \frac{\mu}{R} D_3(\bar{\hat{u}}^*) \hat{u} + \frac{\mu}{R} D_3(\bar{\hat{v}}^*) \hat{v} \Big] \Big|_{x^3=0}.
\end{aligned} \tag{32}$$

and

$$m_{ij} = \frac{1}{h_i h_j} \frac{\partial h_i}{\partial x^j}.$$

The co-state equations (30) are integrated in the upstream direction with the terminal condition at $x^1 = X_1$ which reads:

$$\hat{\phi}_1^* = |\Theta_1|^2 (\mathcal{D}^H)^{-1} (\mathcal{M} - c_1 \mathcal{I}) \hat{\phi}_1, \qquad r_1^* = |\Theta_1|^2\ c_1 \tag{33}$$

where c_1 is given in the appendix and $\mathcal{I}$ is the identity matrix. Equations (30) are solved iteratively to find r^* such that the integral expression is satisfied.

Now, the gradients of J can be obtained from the following steps. First, the state variable ϕ is calculated by integrating equations (21) along x^1 from X_0 to X_1. Then the co-state equations (30) are integrated backward in the streamwise direction from X_1 to X_0 to obtain the co-state variables $\hat{\phi}^*$. Finally, equations (29) give the gradients with respect to each control parameter.

It is worth mentioning that the expression for $\mathcal{S}^*$ depends on the choice of the auxiliary condition while the adjoint operator $\hat{\mathcal{L}}^*$ remains unchanged for other choices of this condition. If the output is defined as in (25) the adjoint system will be

$$\begin{aligned}
\hat{\mathcal{L}}^*\ \hat{\phi}^* &= \mathcal{S}^* + \mathcal{M}^H \hat{\phi} |\Theta|^2 && \text{in} \quad \Omega \\
(\hat{\mathbf{u}}^*, \hat{T}^*) &= 0 && \text{at} \quad x^3 = 0 \\
(\hat{\mathbf{u}}^*, \hat{T}^*) &\to 0 && \text{as} \quad x^3 \to \infty \\
(\hat{\phi}^*, r^*) &= 0 && \text{at} \quad x^1 = X_1
\end{aligned} \tag{34}$$

$$\frac{\partial}{\partial x^1}\int_0^{+\infty} \hat{\phi}^{*H}\frac{\partial \hat{\mathcal{L}}}{\partial \alpha}\,\hat{\phi}\,h_1h_2h_3dx^3 + i\,|\Theta|^2\int_0^{+\infty}\hat{\phi}^H\mathcal{M}\hat{\phi}\,h_1h_2h_3\,dx^3 = f^* \text{ in } \Omega$$

Note that in this case both $\hat{\phi}^*$ and r^* are subject to homogeneous terminal conditions.

4. The adjoints for Hybrid Laminar Flow Control

4.1. *Review of previous work*

Numerical works on control of boundary layer instabilities do not abound in the literature; some references have been given in section 3.1.

Balakumar & Hall (1999) used the technique of minimization of a functional which was based on the 'N factor'.The advantage is that the control acts on several wave frequencies, which could be amplified. The constraint is given by a fixed amount of energy spent by the suction system. The gradients are given by a differentiation of the state equations. Transition delay is obtained for Blasius and Swept Hiemenz flows, when transition location is based to a given value of the 'N factor'. Mughal (1998) used the compressible linear and non linear PSE with a blowing/suction acting only on the disturbance and linked to the perturbed wall shear stress and wall pressure:

$$\hat{v}_{\rm w} = \lambda\frac{\partial \hat{u}_{\rm w}}{\partial y} + \omega\hat{p}_{\rm w}$$

λ and ω are parameters *a priori* unknown. This control is linked to a single-frequency instability. Calculations were carried out in the $\lambda - \omega$ plane for TS-waves, attachment line instability and Goertler's vortices. Flow stabilization was achieved for a certain range of the parameters.

Recently, Gmelin & Rist (2001) investigate the active control of T.S. waves in the Blasius boundary layer using three-dimensional Direct Numerical Simulations. The spanwise vorticity at the wall and at a given location, is sensed. Multiplied by an amplitude factor and after a time delay, it provides a normal to the wall disturbance velocity. Attenuation of the disturbances in the linear and non-linear stage is obtained. A similar work to the one which is described in this report was first presented by Hill (1997*a*). The incompressible case is found in Pralits *et al.* (2000*b*).

4.2. *The direct problem for an infinite swept wing*

The state governing equations correspond to the Boundary Layer Equations and the Parabolized Stability Equations, including their initial and boundary conditions. They are given with formal operators in this chapter; details can be found in the appendices. The most important point is that only the basic state of the boundary layer is controlled via steady blowing or suction. The mass flux coming from the wall suction leads to a change of the mean normal-to-the wall velocity and also to the mean density (and therefore the mean temperature) at the wall.

The assumption of infinite swept wing is made, the steady quantity are independent with respect to the spanwise direction x^2, and the disturbances depend on x^2 only through a real spanwise wave number. Moreover, the metrics are now given by $h_2 = h_3 = 1$ and $h_1 = h_1(x^1, x^3)$.

4.2.1. *The Boundary Layer Equations (BLE)*

The three-dimensional steady boundary layer equations for compressible flows are written with an inhomogeneous wall velocity $\mathbf{U}_{\rm w}(x^1)$:

$$\begin{array}{rcll} \mathcal{L}_{\rm BL}(\psi)\ \psi(x^1,x^3) & = & 0 & \text{in} \quad \Omega, \\ \psi(x^1,x^3) & = & \psi_0(x^3) & \text{at} \quad x^1 = X_0, \\ (\mathbf{U},\ D_3(T)) & = & (\mathbf{U}_{\rm w}(x^1), 0) & \text{at} \quad x^3 = 0, \\ (U,V,T) & \to & (U_e, V_e, T_e), & \text{as} \quad x^3 \to \infty, \end{array} \tag{35}$$

where the non-dimensional boundary layer state vector is $\psi = (\rho, U, V, W, T)$. Here, the components of the state vector are defined on the real axis. This is the basic boundary layer state. The BLE are nonlinear in ψ and parabolic in the streamwise direction. The equations are detailed in appendix Appendix D. In this report, control via suction at the wall is considered, so that wall boundary conditions verify:

$$U_{\rm w} = V_{\rm w} = 0, \quad W_{\rm w} \neq 0 \qquad \text{and} \qquad D_3(T_{\rm w}) = 0. \tag{36}$$

The wall density is given via the state equation $\rho_{\rm w} T_{\rm w} = \gamma M^2 P_e$. The BLE are solved with $W_{\rm w} = 0$ during the first iteration of the control iterative procedure. The wall suction of the fluid is assumed to keep the adiabatic wall condition $D_3(T(x^1, 0)) = 0$.

4.2.2. *The stability equations*

The stability equations are the PSE given in the section 3.3.2 but with homogeneous boundary conditions and no source term:

$$\begin{array}{rcll} \hat{\mathcal{L}}(\psi)\ \hat{\phi}(x^1,x^3) & = & 0 & \text{in} \quad \Omega, \\ \hat{\phi}(x^1,x^3) & = & \hat{\phi}_0(x^3) & \text{at} \quad x^1 = X_0, \\ (\hat{\mathbf{u}}, \hat{T}) & = & 0 & \text{at} \quad x^3 = 0, \\ (\hat{\mathbf{u}}, \hat{T}) & \to & 0 & \text{as} \quad x^3 \to \infty, \\ \displaystyle\int_0^\infty \hat{\phi}^H \frac{\partial \hat{\phi}}{\partial x^1}\, dx^3 & = & 0 & \text{in} \quad \Omega, \end{array} \tag{37}$$

where $\hat{\phi} = (\hat{\rho}, \hat{u}, \hat{v}, \hat{w}, \hat{T})$. It should be noted that the PSE operator is a function of ψ, the mean flow field. This is important during the differentiation step with respect to ψ.

4.3. *The cost functional*

The cost functional plays an important role in the optimal problem, since it defines the quantities to control (energy, mass flux, velocity), how the control is made, and the relative cost of the control with respect to the objectives to reach. Here, the definition of the cost functional includes a local and a global measure of the disturbance, plus the cost of the control:

$$J_0 = \gamma_1 E_f + \gamma_2 E_g + \epsilon E_c. \tag{38}$$

The local energy E_f and the global energy E_g are given in section 3.3.3 respectively by equations (24) and (25). The cost of the control with the mass flux $\dot{m} = \rho_{\rm w} W_{\rm w}$ is:

$$E_c = \frac{1}{2} \int_{X_0}^{X_1} \int_{Z_0}^{Z_1} \dot{m}^2 \; h_1 dx^2 dx^1. \tag{39}$$

The weight coefficients γ_1, γ_2 and ϵ are constant and real. They allow for a balancing of the different terms in the cost functional J_0. The optimal control velocity and temperature profiles minimize the cost functional J_0 and render stationary the augmented Lagrangian functional

$$\begin{aligned} J &= \gamma_1 E_f + \gamma_2 E_g + \epsilon E_c \\ &- [\langle \psi^*, \mathcal{L}_{\rm BL} \; \psi \rangle + \texttt{Real}\{\langle \hat{\phi}^*, \hat{\mathcal{L}} \; \hat{\phi} \rangle + \langle r^* \hat{\phi}, D_1(\hat{\phi}) \rangle\}] \\ &- \int_{X_0}^{X_1} \int_{Z_0}^{Z_1} \{\mu_0 [\dot{m}(x^1) - \rho(x^1, 0) W(x^1, 0)]\} \; h_1 dx^1 dx^2, \end{aligned} \tag{40}$$

where $\psi^* = (\rho^*, U^*, V^*, W^*, T^*)$ is the real co-state vector associated to the adjoint of the boundary layer equations, $\hat{\phi}^* = (\hat{\rho}^*, \hat{u}^*, \hat{v}^*, \hat{w}^*, \hat{T}^*)$ and r^* are the co-state variables associated to the adjoint of the stability equations and the real coefficients μ_0 and μ_1 provide the optimality conditions.

4.4. *The dual problem*

The calculations of the dual problem are detailed in Appendix Appendix B and Appendix Appendix E. They are similar to those carried out with the sensitivity. The Lagrangian functional is differentiated with respect to small variations of the state quantities. Terms in front of these variations are collected and cancelled in order to have $\delta J = 0$. In particular, this means that the gradient with respect to $\delta W_{\rm w}$, $\delta T_{\rm w}$, $\delta W(x^1, 0)$ and $\delta T(x^1, 0)$ are set to zero. The gradients, as seen in the section 3, are directly given by the adjoint variables.

4.4.1. *Adjoint of the Boundary Layer Equations (ABLE)*

The full equations are in Appendix Appendix E. In a formal way, we can write:

$$\begin{aligned}
\mathcal{L}^*_{\rm BL}(\psi)\ \psi^* &= \mathcal{S}^*_{\rm BL} \quad \text{in} \quad \Omega,\\
\psi^* &= 0 \quad \text{at} \quad x^1 = X_1,\\
(U^*, V^*) &= 0 \quad \text{at} \quad x^3 = 0,\\
\frac{\kappa}{P_r R} D_3(h_1 T^*) + h_1 \rho C_p W T^* &= 0 \quad \text{at} \quad x^3 = 0,\\
(U^*, V^*, W^*, T^*) &\to 0, \quad \text{as} \quad x^3 \to \infty.
\end{aligned} \tag{41}$$

They are parabolic upstream, *i.e.* they must be integrated from X_1 to X_0. The forcing term $\mathcal{S}^*_{\rm BL}$ comes from the dependence of the PSE and its adjoint operator on the base flow variables. It is the link between the adjoint boundary layer equations and the stability equations.

4.4.2. *Adjoint of the Parabolized Stability Equations (APSE)*

The full equations are in Appendix Appendix B. In operator notation they read:

$$\begin{aligned}
\hat{\mathcal{L}}^*\ \hat{\phi}^* &= \mathcal{S}^* + \gamma_2\ |\Theta|^2\ \mathcal{M}^H \hat{\phi} && \text{in} \quad \Omega,\\
(\hat{u}^*, \hat{v}^*, \hat{w}^*, \hat{T}^*, \hat{\rho}^*) &= 0, && \text{at} \quad x^3 = 0,\\
(\hat{u}^*, \hat{v}^*, \hat{T}^*) &\to 0 && \text{as} \quad x^3 \to \infty,\\
(\hat{\phi}^*, r^*) &= \gamma_1\ (\hat{\phi}^*_1, r^*_1) && \text{at} \quad x^1 = X_1,\\
\frac{\partial}{\partial x^1} \int_0^{+\infty} \hat{\phi}^{*H} \frac{\partial \hat{\mathcal{L}}}{\partial \alpha}\ \hat{\phi}\ h_1 dx^3 &+ \gamma_2\ i\ |\Theta|^2 \int_0^{+\infty} \hat{\phi}^H \mathcal{M} \hat{\phi}\ h_1\ dx^3 = 0 && \text{in} \quad \Omega,\\
\mathcal{S}^* &= D_1(r^* \hat{\phi}) - \bar{r}^* D_1(\hat{\phi}).
\end{aligned} \tag{42}$$

It should be noticed that depending of the choice of the measure of the state, one of the two coefficients γ_1 or γ_2 can be set to zero.

4.5. *The optimality conditions and its iterative implementation*

The optimality conditions render stationary the functional J. The optimal wall mass flux is:

$$\dot{m}^{\rm opt} = \rho_{\rm w}^{\rm opt} W_{\rm w}^{\rm opt} = -\frac{W^*_{\rm w}}{\epsilon} \tag{43}$$

The density is a solution of the BLE. From equation (43) we obtain the optimal normal to the wall velocity $W_{\rm w}^{\rm opt}$. The solution of the optimal control problem can be obtained using a simple gradient procedure. Let us call k the iteration number.

The iterative procedure is described on figure 4 and follows the steps:

1. The homogeneous BLE and PSE, *i.e.* equations (35) and (37) respectively are solved, with homogeneous wall velocity.

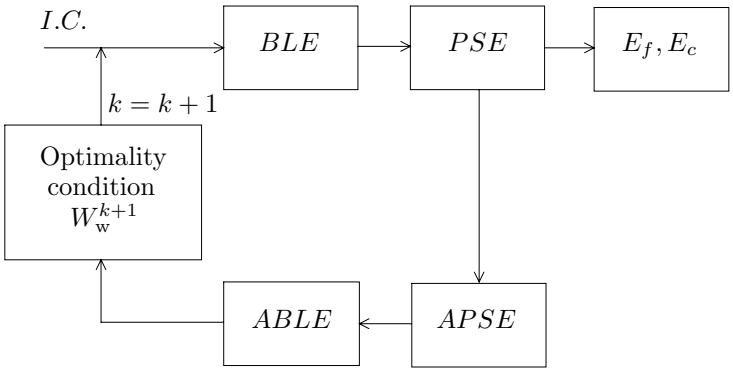

FIGURE 4. Algorithm

2. The adjoint equations APSE and ABLE *i.e.* equations (41) and (42) respectively, are solved.
3. The new wall boundary conditions of the state are calculated employing (43).
4. $k = k + 1$. The non-homogeneous BLE and the PSE, are solved, with the new boundary conditions.
5. The adjoint equations PSE and ABLE are solved with the upgraded source terms.
6. The new boundary conditions are calculated via the relation:
$$W_{\mathrm{w}}^{(k+1)} = W_{\mathrm{w}}^{(k)} + \tau_1 (W_{\mathrm{w}}^{\mathrm{opt}\,(k+1)} - W_{\mathrm{w}}^{(k)}) \tag{44}$$
where τ_1 is a positive relaxation factor which might depend on the iteration number k.
7. The maximum of the relative variation $var = |\dfrac{W_{\mathrm{w}}^{(k+1)}}{W_{\mathrm{w}}^{(k)}} - 1|$ is computed.
8. If $var \geq \varepsilon_0$, a given tolerance, go to step 4, else convergence is reached.

A more sophisticated optimization algorithm can be employed in step 6, *i.e.* conjugate gradient or BFGS. A convergence criterion based on the value of the functional J may also be used. The number of iterations to attain convergence depends on such a criterion.

This work has been partly carried out during several stays (for a total of three months) of the first author in Stockholm, and during a one-month stay of the second author in Toulouse. The former visits were made possible by financial support awarded by ARIEL, in the frame of a French-Swedish cooperative agreement, by the Royal Institute of Technology, Stockholm, and by FOI (formerly FFA).

The second author is funded by the Swedish Foundation for Strategic Research (SSF) through the national research program *Integral Vehicle Structure (IVS)*. The work of the Swedish authors on the coupling between the adjoint

PSE and the adjoint BL equations was initially funded by the IVS program and FOI.

Appendix A. The non-local stability equations

A.1. *Governing equations and assumptions*

A model of convectively unstable waves with weakly curved or divergent wave-rays in a non-uniform flow is described here. The equations are derived from the equations of conservation of mass, momentum and energy and the equation of state governing the flow of a viscous, compressible, ideal gas expressed in primitive variables and curvilinear coordinates. The non-dimensional conservation equations in vector notation are given by

$$\rho\,[\frac{\partial \mathbf{u}}{\partial t} + (\mathbf{u}\cdot\nabla)\mathbf{u}] = -\nabla p + \frac{1}{R}\nabla[\lambda(\nabla\cdot\mathbf{u})] + \frac{1}{R}\nabla\cdot[\mu(\nabla\mathbf{u} + \nabla\mathbf{u}^T)], \tag{45}$$

$$\frac{\partial \rho}{\partial t} + \nabla\cdot(\rho\mathbf{u}) = 0, \tag{46}$$

$$\rho c_p[\frac{\partial T}{\partial t} + (\mathbf{u}\cdot\nabla)T] = \frac{1}{RPr}\nabla\cdot(\kappa\nabla T) + (\gamma-1)M^2[\frac{\partial p}{\partial t} + (\mathbf{u}\cdot\nabla)p + \frac{1}{R}\Phi], \tag{47}$$

$$\gamma M^2 p = \rho T, \tag{48}$$

with viscous dissipation given as

$$\Phi = \lambda(\nabla\cdot\mathbf{u})^2 + \frac{1}{2}\mu[\nabla\mathbf{u} + \nabla\mathbf{u}^T]^2.$$

All flow quantities are non-dimensionalized by the corresponding reference flow quantity at a fixed streamwise position $x_0^\star$, except the pressure which is normalized by twice the corresponding dynamic pressure. The reference length scale is fixed and taken as

$$l_0^\star = \sqrt{\frac{\nu_0^\star x_0^\star}{U_0^\star}}.$$

Here t represents time, ρ, p, T stand for density, pressure and temperature, $\mathbf{u}$ is the velocity vector. The quantities λ, μ are the second and the dynamic viscosity coefficient, γ is the ratio of specific heats, κ the heat conductivity, c_p the specific heat at constant pressure. The Mach number, M, Prandtl number, Pr and Reynolds number, R are defined as

$$M = \frac{U_0^\star}{\sqrt{\Re\gamma T_0^\star}}, \quad Pr = \frac{\mu_0^\star c_{p0}^\star}{\kappa_0^\star}, \quad R = \frac{U_0^\star l_0^\star}{\nu_0^\star},$$

where $\Re$ is the specific heat constant. The flow and material quantities are decomposed into mean flow quantity Q and a disturbance quantity q as $q(x^i,t) = Q(x^i) + \tilde{q}(x^i,t)$ where x^1, x^2 and x^3 are the normal, spanwise and streamwise components respectively. Here $Q \in [U,V,W,p,T,\rho]$ and $\tilde{q} \in [\tilde{u},\tilde{v},\tilde{w},\tilde{p},\tilde{T},\tilde{\rho}]$. The domain considered is defined as $x^1 \in [X_0, X_1]$, $x^2 \in [Z_0, Z_1]$ and $x^3 \in$

$[0, \infty[$. To simplify the analysis the mean flow is considered to be independent of the spanwise coordinate x^2. Two assumptions are made to derive the non-local stability equations. The first is of WKB type where the disturbance $\tilde{q}$ is divided into an amplitude function and a wave function

$$\tilde{q}(x^i, t) = \hat{q}(x^1, x^3)\Theta, \quad \Theta = \exp\ i\,(\int_{X_0}^{x^1} \alpha(x')dx' + \beta x^2 - \omega t).$$

Here α is a complex wave number, β is the spanwise wave number and ω is the wave frequency. The second assumption is a scale separation $1/R$ between the weak variation in the x^1 direction and the rapid variation in the x^3 direction analogous to the multiple scales method. We assume

$$\frac{\partial}{\partial x^1} \sim \mathcal{O}(R^{-1}), \quad V \sim \mathcal{O}(R^{-1}).$$

Furthermore, it is assumed that the metrics are of order $\mathcal{O}(R^{-1})$.

A.2. *The linear non-local stability equations*

The non-local stability equations are derived using the Parabolized Stability Equation (PSE) ansatz. We consider a general case where the boundary layer is subjected to sources of mass, momenta and energy, $\tilde{\mathcal{S}}$, and inhomogeneous boundary conditions on the wall. The linearized disturbance equations are obtained by introducing the variable decomposition into the governing equations (45)-(48), subtracting the equations for the mean flow and removing the products of disturbances. We proceed with the derivation of the stability equations by introducing the scaling relations given in section A.1. Finally, collecting terms up to order $\mathcal{O}(R^{-1})$ gives a set of nearly parabolic partial differential equations. A note on the parabolic nature of PSE can be found in Li & Malik (1996); Andersson *et al.* (1999*b*). The equation can formally be written as:

$$\hat{\mathcal{L}}\ \hat{\phi}(x^1, x^3) = \hat{\mathcal{S}}(x^1, x^3). \tag{49}$$

where the vector of the amplitude functions is $\hat{\phi} = (\hat{\rho}, \hat{u}, \hat{v}, \hat{w}, \hat{T})$. The boundary conditions are

$$\begin{aligned} &\hat{\mathbf{u}}(x^1, 0) = \hat{\mathbf{u}}_{\mathrm{w}}(x^1), \quad \hat{T}(x^1, 0) = \hat{T}_{\mathrm{w}}(x^1), \\ &\lim_{x^3 \to \infty} \hat{\mathbf{u}} = 0 \quad \text{and} \quad \lim_{x^3 \to \infty} \hat{T} = 0. \end{aligned} \tag{50}$$

The operator $\hat{\mathcal{L}}$ is defined as

$$\hat{\mathcal{L}} = \mathcal{A} + \mathcal{B}D_3 + \mathcal{C}D_{33} + \mathcal{D}D_1, \tag{51}$$

where

$$D_i = \frac{1}{h_i}\frac{\partial}{\partial x^i}, \qquad D_{ii} = \frac{1}{h_i^2}\frac{\partial^2}{(\partial x^i)^2}.$$

Here, h_i is the scale factor such that a length element is defined as $ds^2 = (h_1 dx^1)^2 + (h_2 dx^2)^2 + (h_3 dx^3)^2$. The coefficients of the 5×5 matrices $\mathcal{A}$, $\mathcal{B}$, $\mathcal{C}$ and $\mathcal{D}$ can be found in Appendix Appendix C. Furthermore, as both the

amplitude function and the wave function depend on the x^1 coordinate, an auxiliary condition is employed:

$$\int_0^\infty \hat{\phi}^H \frac{\partial \hat{\phi}}{\partial x^1}\, h_2 h_3 dx^3 = 0. \tag{52}$$

This condition also guarantees that the x^1-variation of the disturbance amplitude function remains small, so that second streamwise derivatives are negligible.

Appendix B. Derivation of the adjoint PSE and of the gradients

The gradients are derived using the adjoint PSE. A discrete or a continuous formulation may be used. It was concluded by Högberg & Berggren (2000) that a continuous formulation is a good enough approximation if control is performed on a problem with a dominating instability. This type of analysis can be done with the PSE which is the reason why a continuous approach is used here.

B.1. *Derivation of the adjoint PSE*

The functional to be differentiated is:

$$J = E - \mathtt{Real}\{\langle \hat{\phi}^*, \hat{\mathcal{L}}\ \hat{\phi} - \hat{\mathcal{S}} \rangle + \langle r^* \phi, D_1(\hat{\phi}) \rangle\}, \tag{53}$$

where the complex vector $\hat{\phi}^* = (\hat{\rho}^*, \hat{u}^*, \hat{v}^*, \hat{w}^*, \hat{T}^*)$ and the complex function $r^*(x^1)$ define the co-state. The differentiation with respect to the input variables $\hat{\mathbf{u}}_\mathrm{w}, \hat{T}_\mathrm{w}, \hat{\mathcal{S}}$ and the state variables α and ϕ leads to :

$$\begin{aligned}
\delta J \;=\; & \mathtt{Real}\Bigg\{ \int_{Z_0}^{Z_1} \int_0^\infty |\Theta_1|^2 \hat{\phi}_1^H \mathcal{M} \delta\hat{\phi}_1 h_2 h_3\, dx^3\, dx^2 + \\
& i \int_{X_0}^{X_1} \delta\alpha dx' \int_{Z_0}^{Z_1} \int_0^\infty |\Theta_1|^2 \hat{\phi}_1^H \mathcal{M} \hat{\phi}_1\, h_2 h_3\, dx^3\, dx^2 \\
& - \Bigg[\langle \hat{\phi}^*,\ \hat{\mathcal{L}}\ \delta\hat{\phi} - \delta\hat{\mathcal{S}} + \frac{\partial \hat{\mathcal{L}}}{\partial \alpha} \delta\alpha\ \hat{\phi} \rangle + \langle r^* \delta\hat{\phi}, D_1(\hat{\phi}) \rangle + \langle r^* \hat{\phi}, D_1(\delta\hat{\phi}) \rangle \\
& + \langle \delta\hat{\phi}^*, \hat{\mathcal{L}}\ \hat{\phi} - \hat{\mathcal{S}} \rangle \Bigg] \Bigg\}.
\end{aligned} \tag{54}$$

The last inner product is equal to zero because of the state equation $\hat{\mathcal{L}}\ \hat{\phi} = \hat{\mathcal{S}}$. Note here that the variation of a disturbance $\tilde{\phi}$ results in the variation of both the amplitude function $\hat{\phi}$ and the streamwise wave-number α.

The adjoint equations are derived from the inner product of vector $\hat{\phi}^*$ with the differentiated state equations, and r^* with the differentiated auxiliary condition according to the inner product (26). The derivatives are removed

from the differentiated variables in the inner products of equation (54) using integration by parts, *i.e.*:

$$
\begin{aligned}
&\langle \hat{\phi}^*,\ \hat{\mathcal{L}}\ \delta\hat{\phi} - \delta\hat{\mathcal{S}} + \frac{\partial \hat{\mathcal{L}}}{\partial \alpha}\delta\alpha\ \hat{\phi}\rangle + \langle r^*\delta\hat{\phi}, D_1(\hat{\phi})\rangle + \langle r^*\hat{\phi}, D_1(\delta\hat{\phi})\rangle = \\
&\langle \hat{\mathcal{L}}^*\hat{\phi}^*, \delta\hat{\phi}\rangle - \langle \hat{\phi}^*, \delta\hat{\mathcal{S}}\rangle - \\
&\int_{X_0}^{X_1}\int_{Z_0}^{Z_1}\int_0^{+\infty} \frac{\partial}{\partial x^1}(\hat{\phi}^{*H}\frac{\partial \hat{\mathcal{L}}}{\partial \alpha}\ \hat{\phi}\ h_1h_2h_3)\int_{X_0}^{x^1}\delta\alpha dx'\ dx^3\ dx^2\ dx^1 + \\
&\int_{Z_0}^{Z_1}\int_0^{+\infty}\Big[\hat{\phi}^{*H}\frac{\partial \hat{\mathcal{L}}}{\partial \alpha}\ \hat{\phi}\ h_1h_2h_3\int_{X_0}^{x^1}\delta\alpha dx'\Big]_{X_0}^{X_1} dx^3\ dx^2 + \\
&\int_{Z_0}^{Z_1}\int_0^{+\infty}\Big[\hat{\phi}^{*H}\ \mathcal{D}\ \delta\hat{\phi}\ h_2h_3\Big]_{X_0}^{X_1} dx^3\ dx^2 + \\
&\int_{Z_0}^{Z_1}\int_{X_0}^{X_1}\Big[\Big\{\hat{\phi}^{*H}\Big(\mathcal{B}\ -\ (m_{13}+m_{23}-m_{33})\ \mathcal{C}\ -\ D_3(\mathcal{C})\Big)\ \delta\hat{\phi} + \\
&\qquad -D_3(\hat{\phi}^{*H})\ \mathcal{C}\ \delta\hat{\phi}\ +\ \hat{\phi}^{*H}\ \mathcal{C}\ D_3(\delta\hat{\phi})\Big\}\ h_1h_2\ dx^2\ dx^1\Big]_0^{\infty} + \\
&\int_{X_0}^{X_1}\int_{Z_0}^{Z_1}\int_0^{+\infty}\Big(r^*D_1(\hat{\phi}^H) - D_1(\bar{r}^*\hat{\phi}^H) - \\
&\qquad (m_{21}+m_{31})\bar{r}^*\hat{\phi}^H\Big)\ \delta\hat{\phi}\ h_1h_2h_3dx^3\ dx^2\ dx^1 + \\
&\int_{Z_0}^{Z_1}\int_0^{+\infty}\Big[h_2h_3\bar{r}^*\hat{\phi}^H\delta\hat{\phi}\Big]_{X_0}^{X_1} dx^3\ dx^2 = 0.
\end{aligned}
\tag{55}
$$

where

$$m_{ij} = \frac{1}{h_ih_j}\frac{\partial h_i}{\partial x^j}.$$

Terms of $\delta\alpha$ have also been integrated in equation (55). The inner products equation (55) are now substituted into equation (54). Collecting terms of $\delta\hat{\phi}$ in the integral on Ω leads to the adjoint equations

$$\hat{\mathcal{L}}^*\hat{\phi}^* = -\Big[\bar{r}^*D_1(\hat{\phi}) - D_1(r^*\hat{\phi}) - (m_{21}+m_{31})\ r^*\hat{\phi}\Big]. \tag{56}$$

In order to remove the terms of $\delta\hat{\phi}$ in equation (55) as $x^3 \to \infty$, the following homogeneous boundary conditions are chosen

$$
\begin{array}{rclcrcl}
\hat{\mathbf{u}}^*(x^1,0) & = & 0 & \text{and} & \hat{T}^*(x^1,0) & = & 0, \\
\lim\limits_{x^3\to\infty}\hat{\mathbf{u}}^* & = & 0 & \text{and} & \lim\limits_{x^3\to\infty}\hat{T}^* & = & 0,
\end{array}
\tag{57}
$$

where $\hat{\mathbf{u}}^* = (\hat{u}^*, \hat{v}^*, \hat{w}^*)$. Using the operator matrices of the forward problem, the adjoint operator $\hat{\mathcal{L}}^*$ can be identified

$$\hat{\mathcal{L}}^* \;=\; \tilde{\mathcal{A}} \;+\; \tilde{\mathcal{B}}\, D_3 \;+\; \tilde{\mathcal{C}}\, D_{33} \;+\; \tilde{\mathcal{D}}\, D_1 \tag{58}$$

where $\tilde{\mathcal{A}}, \tilde{\mathcal{B}}, \tilde{\mathcal{C}}$ and $\tilde{\mathcal{D}}$ are

$$\begin{array}{rcl}
\tilde{\mathcal{A}} & = & \mathcal{A}^H \;-\; D_3(\mathcal{B}^H) \;-\; (m_{13}+m_{23})\,\mathcal{B}^H \;+\; D_{33}(\mathcal{C}^H) \\
& + & 2\,(m_{13}+m_{23}-m_{33})\,D_3(\mathcal{C}^H) \\
& - & D_1(\mathcal{D}^H) \;-\; (m_{21}+m_{31})\,\mathcal{D}^H, \\
\tilde{\mathcal{B}} & = & -\mathcal{B}^H \;+\; 2\,D_3(\mathcal{C}^H) \;+\; 2\,(m_{13}+m_{23}-m_{33})\,\mathcal{C}^H, \\
\tilde{\mathcal{C}} & = & \mathcal{C}^H, \\
\tilde{\mathcal{D}} & = & -\mathcal{D}^H.
\end{array}$$

The system of equations (56) with corresponding boundary conditions (57) is parabolic in the streamwise direction and must be integrated upstream, from X_1 to X_0.

B.2. *Terminal condition, auxiliary condition and derivation of gradients*

The terminal conditions $\hat{\phi}^*$ and r^* at X_1 are found by cancelling the terms multiplying $\delta\hat{\phi}(X_1, y)$ and $\displaystyle\int_{X_0}^{X_1} \delta\alpha dx'$ in the functional δJ. They are the solution of the following system of equations :

$$\begin{aligned}
|\Theta_1|^2 \int_0^\infty \hat{\phi}_1^H \mathcal{M} \delta\hat{\phi}_1 h_2 h_3 \; dx^3 &= \int_0^{+\infty} (\hat{\phi}^{*H}\,\mathcal{D} + \bar{r}^*\hat{\phi}^H)\;\delta\hat{\phi}\; h_2 h_3 dx^3\Big|_{X_1} \\
i|\Theta_1|^2 \int_0^\infty \hat{\phi}_1^H \mathcal{M} \hat{\phi}_1 h_2 h_3 \; dx^3 &= \int_0^{+\infty} \hat{\phi}^{*H} \frac{\partial\hat{\mathcal{L}}}{\partial\alpha}\;\hat{\phi}\; h_1 h_2 h_3 \; dx^3\Big|_{X_1}.
\end{aligned} \tag{59}$$

Solving the above equations provides the terminal conditions for the adjoint equations at X_1 given below:

$$\begin{aligned}
\hat{\phi}_1^* = |\Theta_1|^2 \mathcal{D}^+ (\mathcal{M} - c_1\mathcal{I})\hat{\phi}_1, \qquad r_1^* = |\Theta_1|^2\, c_1, \\
\bar{c}_1 = \frac{\displaystyle\int_0^\infty (h_1 \hat{\phi}_1^H \mathcal{M}\; D^{+H} \frac{\partial\hat{\mathcal{L}}}{\partial\alpha}\hat{\phi}_1 - i\hat{\phi}_1^H \mathcal{M}\hat{\phi}_1)\; h_2 h_3 \; dx^3}{\displaystyle\int_0^\infty \hat{\phi}_1^H \mathcal{D}^{+H} \frac{\partial\hat{\mathcal{L}}}{\partial\alpha}\hat{\phi}_1 \; h_1 h_2 h_3 \; dx^3},
\end{aligned} \tag{60}$$

where $\mathcal{D}^+ = (\mathcal{D}^H)^{-1}$. Since by definition $\delta\phi = 0$ at X_0, the remaining terms of equation (55) together with equation (54) can be written

$$\begin{aligned}\delta J = \mathtt{Real}\Bigg\{ & \int_{X_0}^{X_1}\int_{Z_0}^{Z_1}\int_0^{+\infty} \hat{\phi}^{*H}\delta\hat{\mathcal{S}}\; h_1h_2h_3\; dx^3\; dx^2\; dx^1 + \\ & \int_{X_0}^{X_1}\int_{Z_0}^{Z_1}\int_0^{+\infty} \frac{\partial}{\partial x^1}(\hat{\phi}^{*H}\frac{\partial\hat{\mathcal{L}}}{\partial\alpha}\;\hat{\phi}\; h_1h_2h_3)\int_{X_0}^{x^1}\delta\alpha dx'\; dx^3\; dx^2\; dx^1 + \\ & \int_{Z_0}^{Z_1}\int_{X_0}^{X_1}\Big\{\hat{\phi}^{*H}\Big[\mathcal{B} \;-\; (m_{13}+m_{23}-m_{33})\,\mathcal{C} \;-\; D_3(\mathcal{C})\Big]\;\delta\hat{\phi} + \\ & \qquad -D_3(\hat{\phi}^{*H})\,\mathcal{C}\;\delta\hat{\phi} \;+\; \hat{\phi}^{*H}\,\mathcal{C}\;D_3(\delta\hat{\phi})\Big\}\; h_1h_2\; dx^2\; dx^1\Big|_{x^3=0}\Bigg\}.\end{aligned} \tag{61}$$

The gradient is given by

$$\begin{aligned}\delta J = \quad \mathtt{Real}\Bigg\{ & \int_{X_0}^{X_1}\int_{Z_0}^{Z_1}\Big(\nabla_{\tilde{\mathbf{u}}_{\mathrm{w}}}J^H\delta\tilde{\mathbf{u}}_{\mathrm{w}} + \nabla_{\tilde{T}_{\mathrm{w}}}J^H\delta\tilde{T}_{\mathrm{w}}\Big)\; h_1h_2\; dx^2\; dx^1 + \\ & \int_{X_0}^{X_1}\int_{Z_0}^{Z_1}\int_0^{\infty}\nabla_{\tilde{\mathcal{S}}}J^H\delta\tilde{\mathcal{S}}\; h_1h_2h_3\; dx^3\; dx^2\; dx^1\Bigg\}.\end{aligned} \tag{62}$$

The gradient should be identified from the variation of $\tilde{\phi}$ and $\tilde{\mathcal{S}}$. However in equation (61) the variation of the momentum source and wall boundary condition is expressed in terms of $\hat{\phi}$ and $\hat{\mathcal{S}}$. The total variation of $\tilde{\phi}$ and $\tilde{\mathcal{S}}$ is written as:

$$\delta\tilde{\phi} = \delta\hat{\phi}\;\Theta + \tilde{\phi}\;i\int_{X_0}^{x^1}\delta\alpha dx'\;, \qquad \delta\tilde{\mathcal{S}} = \delta\hat{\mathcal{S}}\;\Theta + \tilde{\mathcal{S}}\;i\int_{X_0}^{x^1}\delta\alpha dx'. \tag{63}$$

From equation (63), $\delta\hat{\phi}$ and $\delta\hat{\mathcal{S}}$ are substituted into equation (61). The variation of the functional δJ with respect to the total variation of $\tilde{\phi}$ and $\tilde{\mathcal{S}}$ now reads:

$$\begin{aligned}\delta J = \mathtt{Real}\Bigg\{ & \int_{X_0}^{X_1}\int_{Z_0}^{Z_1}\int_0^{+\infty}\frac{1}{\Theta}\hat{\phi}^{*H}\delta\tilde{\mathcal{S}}\; h_1h_2h_3\; dx^3\; dx^2\; dx^1 + \\ & \int_{X_0}^{X_1}\int_{Z_0}^{Z_1} h_1h_2\Big[-\frac{\kappa}{\Theta PrR}D_3(\bar{\tilde{T}}^*)\delta T + \frac{(\rho\bar{\tilde{\rho}}^*)}{\Theta}\delta\tilde{w} + \\ & \qquad \frac{\mu}{\Theta R}D_3(\bar{\tilde{u}}^*)\delta\tilde{u} + \frac{\mu}{\Theta R}D_3(\bar{\tilde{v}}^*)\delta\tilde{v}\Big]\; dx^2\; dx^1\Big|_{x^3=0} - \\ & \int_{X_0}^{X_1}\int_{Z_0}^{Z_1}\int_0^{+\infty}\frac{\partial}{\partial x^1}(\hat{\phi}^{*H}\frac{\partial\hat{\mathcal{L}}}{\partial\alpha}\;\hat{\phi}\; h_1h_2h_3)\int_{X_0}^{x^1}\delta\alpha dx'\; dx^3\; dx^2\; dx^1 +\end{aligned}$$

$$\int_{X_0}^{X_1}\int_{Z_0}^{Z_1}\int_0^{+\infty}\hat{\phi}^{*H}\hat{\mathcal{S}}\;h_1h_2h_3\;i\;\int_{X_0}^{x^1}\delta\alpha dx'dx^3\;dx^2\;dx^1+$$
$$\int_{X_0}^{X_1}\int_{Z_0}^{Z_1}h_1h_2\Big[-\frac{\kappa}{PrR}D_3(\bar{\hat{T}}^*)\hat{T}+(\rho\bar{\hat{\rho}}^*)\hat{w}+\frac{\mu}{R}D_3(\bar{\hat{u}}^*)\hat{u}+ \tag{64}$$
$$\frac{\mu}{R}D_3(\bar{\hat{v}}^*)\hat{v}\Big]\;i\;\int_{X_0}^{x^1}\delta\alpha dx'\;dx^2\;dx^1\Big|_{x^3=0}\Bigg\}.$$

In equation (64) the expression for the wall boundary terms has been expanded to clarify the dependence between each state variable and the adjoint quantities. In the derivation of the adjoint equations the co-state variable $r^*(x^1)$ has been used in order to incorporate the auxiliary condition. However, equation (56) gives a system with five equations and six co-state variables. Therefore, an additional equation is needed to close the system. Collecting the terms of $\delta\alpha$ in equation (64) provides such an additional equation which must be satisfied for each position in x^1:

$$\int_0^{+\infty}\frac{\partial}{\partial x^1}(\hat{\phi}^{*H}\frac{\partial\hat{\mathcal{L}}}{\partial\alpha}\;\hat{\phi}\;h_1h_2h_3)\;dx^3=i\;\int_0^{+\infty}\hat{\phi}^{*H}\hat{\mathcal{S}}\;h_1h_2h_3\;dx^3+$$
$$i\;h_1h_2\Big[-\frac{\kappa}{PrR}D_3(\bar{\hat{T}}^*)\hat{T}+(\rho\bar{\hat{\rho}}^*)\hat{w}+\frac{\mu}{R}D_3(\bar{\hat{u}}^*)\hat{u}+\frac{\mu}{R}D_3(\bar{\hat{v}}^*)\hat{v}\Big]\Big|_{x^3=0}. \tag{65}$$

This is denoted as the 'adjoint auxiliary condition' and is solved with an iterative process for r^* in a similar manner that equation (52) is solved for the streamwise wavenumber α.

The gradient of the functional ∇J, with respect to the momentum forcing and wall disturbances can now be identified from the remaining terms of equation (64) as

$$\begin{aligned}
\nabla_{\tilde{u}_w}J &= \frac{\mu}{\bar{\Theta}R}D_3(\hat{u}^*) && \text{on} \quad x^3=0,\\
\nabla_{\tilde{v}_w}J &= \frac{\mu}{\bar{\Theta}R}D_3(\hat{v}^*) && \text{on} \quad x^3=0,\\
\nabla_{\tilde{w}_w}J &= \frac{\rho\hat{\rho}^*}{\bar{\Theta}} && \text{on} \quad x^3=0,\\
\nabla_{\tilde{T}_w}J &= -\frac{\kappa}{\bar{\Theta}PrR}D_3(\hat{T}^*) && \text{on} \quad x^3=0,\\
\nabla_{\tilde{\mathcal{S}}}J &= \frac{\hat{\phi}^*}{\bar{\Theta}} && \text{in} \quad \Omega.
\end{aligned} \tag{66}$$

Appendix C. Operator matrices of the PSE

The non-zero components of matrices $\mathcal{A}, \mathcal{B}, \mathcal{C}$ and $\mathcal{D}$ in equation (51) are

$$
\begin{aligned}
a(1,1) &= U(m_{31}+m_{21}) + D_3(W) + D_1(U) + i\xi \\
a(1,2) &= \rho(i\alpha_0 + m_{31} + m_{21}) + D_1(\rho) \\
a(1,3) &= i\beta_0\rho \\
a(1,4) &= \rho(m_{13}+m_{23}) + D_3(\rho) \\
a(2,1) &= \frac{1}{\gamma M^2}(D_1(T) + i\alpha_0 T) + D_1(U)U + D_3(U)W - m_{21}V^2 \\
a(2,2) &= \rho(D_1(U) + i\xi) + \frac{\mu}{R}(\alpha_0^2 l_2 + \beta_0^2) \\
a(2,3) &= -2\rho m_{21}V + \frac{\mu}{R}\alpha_0\beta_0 l_1 \\
a(2,4) &= \rho(m_{13}U + D_3(U)) - \frac{i\alpha_0}{R}\frac{d\mu}{dT}D_3(T) \\
a(2,5) &= \frac{1}{\gamma M^2}(D_1(\rho) + i\rho\alpha_0) + \frac{1}{R}(-\frac{d\mu}{dT}D_{33}(U) - \\
&\quad D_3(U)\frac{d^2\mu}{dT^2}D_3(T)) \\
a(3,1) &= U(m_{21}V + D_1(V)) + D_3(V)W + \frac{i\beta_0}{\gamma M^2}T \\
a(3,2) &= \rho(m_{21}V + D_1(V)) + \frac{\mu}{R}\alpha_0\beta_0 l_1 \\
a(3,3) &= \rho(m_{21}U + i\xi) + \frac{\mu}{R}(\beta_0^2 l_2 + \alpha_0^2) \\
a(3,4) &= \rho(m_{23}V + D_3(V)) - \frac{i\beta_0}{R}\frac{d\mu}{dT}D_3(T) \\
a(3,5) &= \frac{i\beta_0}{\gamma M^2}\rho + \frac{1}{R}(-\frac{d\mu}{dT}D_{33}(V) - D_3(V)\frac{d^2\mu}{dT^2}D_3(T)) \\
a(4,1) &= \frac{1}{\gamma M^2}D_3(T) - m_{13}U^2 - m_{23}V^2 + \frac{i\mu}{R}\frac{l_2}{\rho}(\beta_0 D_3(V) + \\
&\quad \alpha_0 D_3(U)) \\
a(4,2) &= -2\rho m_{13}U - \frac{i\alpha_0}{R}l_0\frac{d\mu}{dT}D_3(T) + \frac{D_3(\rho)}{\rho}\frac{i\alpha_0}{R}\mu l_2 \\
a(4,3) &= -2\rho m_{23}V - \frac{i\beta_0}{R}l_0\frac{d\mu}{dT}D_3(T) + \frac{D_3(\rho)}{\rho}\frac{i\beta_0}{R}\mu l_2 \\
a(4,4) &= \rho(D_3(W) + m_{31}U + i\xi) + \frac{1}{R}\mu(\beta_0^2 + \alpha_0^2) + \\
&\quad \frac{D_{33}(\rho)}{\rho}\frac{\mu}{R}l_2 \\
a(4,5) &= \frac{1}{\gamma M^2}D_3(\rho) + \frac{1}{R}\frac{d\mu}{dT}i(-\beta_0 D_3(V) - D_3(U)\alpha_0)
\end{aligned}
$$

$$
\begin{aligned}
a(5,1) &= \frac{(\gamma-1)}{\gamma}(UD_1(T)+WD_3(T)+iT\xi)+c_p(-WD_3(T)-UD_1(T))\\
a(5,2) &= (\gamma-1)M^2D_1(p)-\rho c_pD_1(T)\\
a(5,4) &= (\gamma-1)M^2\left[\frac{2i\mu}{R}(\beta_0D_3(V)+D_3(U)\alpha_0)\right]-\rho c_pD_3(T)\\
a(5,5) &= \rho\left\{\frac{dc_p}{dT}(-WD_3(T)-UD_1(T))+i\left[\frac{(\gamma-1)}{\gamma}-c_p\right]\xi\right\}+\\
&\quad \frac{(\gamma-1)}{\gamma}(UD_1(\rho)+WD_3(\rho))+\\
&\quad \frac{(\gamma-1)}{R}\frac{d\mu}{dT}M^2\left[(D_3(U))^2+(D_3(V))^2\right]+\\
&\quad \frac{1}{RPr}\left[\frac{d\kappa}{dT}D_{33}(T)+\frac{d^2\kappa}{dT^2}(D_3(T))^2+\kappa(-\beta_0^2-\alpha_0^2)\right]\\
b(1,1) &= W\\
b(1,4) &= \rho\\
b(2,2) &= \rho W-\frac{1}{R}\frac{d\mu}{dT}D_3(T)\\
b(2,4) &= -\frac{i\mu}{R}\alpha_0l_1\\
b(2,5) &= -\frac{1}{R}D_3(U)\frac{d\mu}{dT}\\
b(3,3) &= \rho W-\frac{1}{R}\frac{d\mu}{dT}D_3(T)\\
b(3,4) &= -\frac{i\mu}{R}\beta_0l_1\\
b(3,5) &= -\frac{1}{R}D_3(V)\frac{d\mu}{dT}\\
b(4,1) &= \frac{1}{\gamma M^2}T+\frac{i\mu}{R}\frac{l_2}{\rho}\xi\\
b(4,2) &= \frac{i\mu}{R}\alpha_0\\
b(4,3) &= \frac{i\mu}{R}\beta_0\\
b(4,4) &= \rho W+\frac{l_2}{R}(2\mu\frac{D_3(\rho)}{\rho}-\frac{d\mu}{dT}D_3(T))\\
b(4,5) &= \frac{1}{\gamma M^2}\rho\\
b(5,1) &= \frac{(\gamma-1)}{\gamma}WT\\
b(5,2) &= 2(\gamma-1)M^2\frac{\mu}{R}D_3(U)
\end{aligned}
$$

$$
\begin{aligned}
b(5,3) &= 2(\gamma-1)M^2\frac{\mu}{R}D_3(V)\\
b(5,5) &= \rho W\left[\frac{(\gamma-1)}{\gamma}-c_p\right]+\frac{2}{RPr}\frac{d\kappa}{dT}D_3(T)\\
c(2,2) &= -\frac{\mu}{R}\\
c(3,3) &= -\frac{\mu}{R}\\
c(5,5) &= \frac{\kappa}{RPr}\\
d(1,1) &= U\\
d(1,2) &= \rho\\
d(2,1) &= \frac{T}{\gamma M^2}\\
d(2,2) &= \rho U\\
d(2,5) &= \frac{\rho}{\gamma M^2}\\
d(3,3) &= \rho U\\
d(4,4) &= \rho U\\
d(5,1) &= \frac{(\gamma-1)}{\gamma}UT\\
d(5,5) &= \rho U\left[\frac{(\gamma-1)}{\gamma}-c_p\right]
\end{aligned}
$$

where

$$D_i=\frac{1}{h_i}\frac{\partial}{\partial x^i},\quad D_{ij}=\frac{1}{h_ih_j}\frac{\partial^2}{\partial x^i\partial x^j},\quad \alpha_0=\frac{\alpha}{h_1},\quad \beta_0=\frac{\beta}{h_2},\quad l_j=\frac{\lambda}{\mu}+j,$$

and

$$\xi=(\alpha_0U+\beta_0V-\omega).$$

Infinite swept wing assumption:

$$h_2=h_3=1, h_1=h_1(x_1,x_3)\quad\text{and}\quad m_{ij}=0\quad\text{except}\quad m_{11}\quad\text{and}\quad m_{13}$$

Appendix D. Boundary Layer Equations

The boundary layer equations are derived for a quasi 2D flow of a compressible, thermally perfect gas using the infinite swept wing assumption. The flow and metrics are assumed to depend only on the streamwise and normal coordinates, x^1 and x^3. The spanwise coordinate x^2 is the homogeneous direction. The coordinate system used here is an orthogonal curvilinear system in which a length element is defined as $ds^2 = (h_1dx^1)^2 + (h_2dx^2)^2 + (h_3dx^3)^2$. Here, h_i denotes the scale factors. However, in the case of an infinite swept wing $h_2 = h_3 = 1$.

Assuming the curvature radius of the surface to be large, $r \gg 1$, and keeping terms up to $\mathcal{O}(R^{-1})$, as in the derivation of the nonlocal stability

equations, the following boundary layer equations are obtained

$$\begin{aligned}
D_1(\rho U) + D_3(\rho W) &= 0, && (67)\\
\rho U D_1(U) + \rho W D_3(U) + D_1(P_e) - \frac{1}{R} D_3(\mu D_3(U)) &= 0, && (68)\\
\rho U D_1(V) + \rho W D_3(V) - \frac{1}{R} D_3(\mu D_3(V)) &= 0, && (69)\\
D_3(\rho T) &= 0, && (70)\\
c_p \rho U D_1(T) + c_p \rho W D_3(T) - \frac{1}{RPr} D_3(\kappa D_3(T)) - & \\
(\gamma - 1) M^2 U D_1(P_e) - \frac{(\gamma-1)}{R} M^2 \mu \left[D_3(U)^2 + D_3(V)^2 \right] &= 0. && (71)
\end{aligned}$$

The mean flow field is subject to the following boundary conditions

$$\begin{aligned}
U = V = 0, W = W_{\rm w}, D_3(T) = 0 \qquad & \text{at} \qquad x^3 = 0,\\
(U, V, T) \to (U_e, V_e, T_e) \qquad & \text{as} \qquad x^3 \to \infty.
\end{aligned} \tag{72}$$

Appendix E. Co-state in the Hybrid Laminar Flow Control

The variation of the cost functional and the way to obtain the optimality condition is detailed in this appendix. The augmented Lagrangian functional to minimize is:

$$\begin{aligned}
J &= \gamma_1 E_f + \gamma_2 E_g + \epsilon E_c\\
&- [\langle \psi^*, \mathcal{L}_{\rm BL}\ \psi \rangle + \texttt{Real}\{\langle \hat{\phi}^*, \hat{\mathcal{L}}\ \hat{\phi} \rangle + \langle r^* \hat{\phi}, D_1(\hat{\phi}) \rangle\}]\\
&- \int_{X_0}^{X_1} \int_{Z_0}^{Z_1} \{\mu_0 [\dot{m}(x^1) - \rho(x^1, 0) W(x^1, 0)]\}\ h_1 dx^1 dx^2,
\end{aligned} \tag{73}$$

where $\dot{m} = \rho_{\rm w} W_{\rm w}$. The variation is written:

$$\begin{aligned}
\delta J &= \gamma_1 \delta E_f + \gamma_2 \delta E_g + \epsilon \delta E_c\\
&- [\langle \psi^*, \delta \mathcal{L}_{\rm BL}\ \delta\psi \rangle\\
&+ \texttt{Real}\{\langle \hat{\phi}^*,\ \hat{\mathcal{L}}\ \delta\hat{\phi} + \frac{\partial \hat{\mathcal{L}}}{\partial \alpha} \delta\alpha\ \hat{\phi} + \delta\hat{\mathcal{L}}(\psi)\ \hat{\phi} \rangle\\
&+ \langle r^* \delta\hat{\phi}, D_1(\hat{\phi}) \rangle + \langle r^* \hat{\phi}, D_1(\delta\hat{\phi}) \rangle\}]\\
&- \int_{X_0}^{X_1} \int_{Z_0}^{Z_1} \{\mu_0 [\delta\dot{m} - \delta(\rho W)\big|_{x^3=0}]\ h_1 dx^1 dx^2.
\end{aligned} \tag{74}$$

$\delta\hat{\mathcal{L}}(\psi)$ and $\delta\mathcal{L}_{\rm BL}\ \delta\psi$ are respectively the variation of the PSE operator and of the boundary layer equations with respect to the mean flow quantities ψ. The variation of the adjoint quantity δr^*, $\delta\hat{\phi}^*$ and $\delta\psi^*$ disappear because they are scalarly multiplied by the state equations. Every line of equation (74) is expanded below.

1. First the variation of the terms $\gamma_1\delta E_f + \gamma_2\delta E_g + \epsilon\delta E_c$ is given by:

$$\begin{aligned}\gamma_1\delta E_f \quad + \quad & \gamma_2\delta E_g + \epsilon\delta E_c = \\ & \gamma_1\Big[\mathtt{Real}\Big\{\int_{Z_0}^{Z_1}\int_0^{\infty}|\Theta_1|^2\hat{\phi}_1^H\mathcal{M}\delta\hat{\phi}_1\;dx^3\;dx^2 + \\ & i\int_{X_0}^{X_1}\delta\alpha dx'\int_{Z_0}^{Z_1}\int_0^{\infty}|\Theta_1|^2\hat{\phi}_1^H\mathcal{M}\hat{\phi}_1\;dx^3\;dx^2\Big\}\Big] + \\ & \gamma_2\Big[\mathtt{Real}\Big\{\int_{X_0}^{X_1}\int_{Z_0}^{Z_1}\int_0^{\infty}|\Theta|^2\hat{\phi}^H\mathcal{M}\delta\hat{\phi}h_1\;dx^3\;dx^2\;dx^1 + \\ & i\int_{X_0}^{X_1}\delta\alpha dx'\int_{X_0}^{X_1}\int_{Z_0}^{Z_1}\int_0^{\infty}|\Theta|^2\hat{\phi}^H\mathcal{M}\hat{\phi}h_1\;dx^3\;dx^2\;dx^1\Big\}\Big] + \\ & \epsilon\int_{X_0}^{X_1}\int_{Z_0}^{Z_1}\dot{m}\delta\dot{m}\;h_1dx^1dx^2.\end{aligned} \tag{75}$$

2. The adjoint of the boundary layer equations are obtained by integrations by part of the inner product $\langle\psi^*, \delta\mathcal{L}_{\rm BL}\;\delta\psi\rangle$:

$$\langle\psi^*, \delta\mathcal{L}_{\rm BL}\;\delta\psi\rangle = \langle\mathcal{L}^*_{\rm BL}\psi^*, \delta\psi\rangle + {\rm BT}_{\rm BL}. \tag{76}$$

The boundary conditions of the adjoint problem are imposed such that the boundary terms ($\rm BT_{BL}$) are just a function of $\delta(\rho W)$ at $x^3 = 0$. To obtain this result we also need the following boundary conditions, which come from the state equations:

$$\begin{aligned}\delta U = \delta V = 0 \qquad & \text{at} \quad x^3 = 0, \\ \delta U = \delta V = \delta W = \delta T = 0 \qquad & \text{when} \quad x^3 \to \infty.\end{aligned}$$

The full equations $\mathcal{L}^*_{\rm BL}\psi^*$ are given in Appendix Appendix F. It should be noticed that the equations were derived with the variation of the density $\delta\rho$ given by:

$$\delta\rho = -\frac{\rho}{T}\delta T, \qquad \text{with} \quad \rho = \frac{\gamma M^2 P_e}{T}. \tag{77}$$

The wall suction is assumed to not modify the pressure P_e at the order of the equations. Therefore the boundary term is:

$${\rm BT}_{\rm BL} = -\int_{X_0}^{X_1}\int_{Z_0}^{Z_1}(h_1W^*(\rho\delta W + W\delta\rho)\Big|_{x^3=0}dx^2dx^1. \tag{78}$$

3. The following term

$$\langle\hat{\phi}^*,\ \hat{\mathcal{L}}\;\delta\hat{\phi} + \frac{\partial\hat{\mathcal{L}}}{\partial\alpha}\delta\alpha\;\hat{\phi}\rangle + \langle r^*\delta\hat{\phi}, D_1(\hat{\phi})\rangle + \langle r^*\hat{\phi}, D_1(\delta\hat{\phi})\rangle$$

has been developed in the section 3.3. It constitutes a part of the adjoint PSE. New boundary conditions for the APSE are chosen in order to cancel any new terms coming from the assumption that the mean flow velocity component $W_{\rm w}$ verifies $W_{\rm w} \neq 0$. The boundary term which

comes from the integration by parts is now equal to zero whenever we assume that any adjoint component of the disturbance goes to zero when $x^3 \to \infty$.

4. The term $\texttt{Real}\{\langle \phi^*, \delta\hat{\mathcal{L}}(\psi)\ \hat{\phi}\rangle\}$ of the equation (74) provides source terms in the ABLE because in the PSE (51) we find the mean flow quantities. We have:

$$\texttt{Real}\{\langle \phi^*, \delta\hat{\mathcal{L}}(\psi)\ \hat{\phi}\rangle\} =$$
$$-\int_{X_0}^{X_1}\int_{Z_0}^{Z_1}\int_0^{\infty}[F_U\delta U + F_V\delta V + F_W\delta W + F_T\delta T]h_1 dx^3 dx^2 dx^1 + \mathrm{BT},$$

where F_U, F_V, F_W and F_T are given in Appendix Appendix G and the boundary term BT is equal to zero whenever any adjoint quantity goes to zero when $x^3 \to \infty$.

After substitution of the APSE and ABLE in equation (74), δJ is given by:

$$\delta J = \int_{X_0}^{X_1}\int_{Z_0}^{Z_1}\Big\{[\epsilon\ \dot{m} - \mu_0]\delta\dot{m} + [\mu_0 + W^*]\delta(\rho W)\Big|_{x^3=0}\Big\}h_1 dx^2 dx^1. \qquad (79)$$

Imposing $\delta J = 0$ and collecting the terms in $\delta\dot{m}$ and $\delta(\rho W)\Big|_{x^3=0}$ yields:

$$\begin{array}{llcl} \text{from} & \delta\dot{m}: & \mu_0 & = \epsilon\ \dot{m} \\ \text{from} & \delta(\rho W)\Big|_{x^3=0}: & \mu_0 & = -W^*_{\mathrm{w}} \end{array}$$

We obtain the optimality condition written for the wall mass flux:

$$\dot{m}^{\mathrm{opt}} = \rho^{\mathrm{opt}}_{\mathrm{w}} W^{\mathrm{opt}}_{\mathrm{w}} = -\frac{W^*_{\mathrm{w}}}{\epsilon}$$

Appendix F. Adjoint Boundary Layer Equations

The same procedure as in the derivation of the adjoint stability equations is followed. The left hand side term of the adjoint boundary layer equations is found by integration, on the domain Ω, of the variation of the BLE weighted by the adjoint quantities with the relation : W^* δ(eq.67) + U^* δ(eq.68)+ V^* δ(eq.69) + ρ^* δ(eq.70) + T^* δ(eq.71). Collecting δU terms, we have:

$$\begin{array}{c} -h_1 D_1(\rho U U^*) - D_3(h_1\rho W U^*) + \\ h_1\rho\left(D_1(V)V^* + D_1(U)U^* - D_1(W^*) + c_p D_1(T)T^*\right) - \\ h_1(\gamma-1)M^2 D_1(P_e)T^* + \dfrac{2(\gamma-1)}{R}M^2 D_3(h_1\mu D_3(U)T^*) - \\ \dfrac{1}{R}D_3(\mu D_3(h_1 U^*)) = h_1 F_U, \end{array} \qquad (80)$$

Collecting δV terms, we have:

$$\begin{array}{c} -h_1 D_1(\rho U V^*) - D_3(h_1\rho W V^*) + \dfrac{2(\gamma-1)}{R}M^2 D_3(h_1\mu D_3(V)T^*) \\ -\dfrac{1}{R}D_3(\mu D_3(h_1 V^*)) = h_1 F_V, \end{array} \qquad (81)$$

Collecting δW terms, we have:

$$-\rho D_3(h_1 W^*) + h_1\rho(D_3(U)U^* + D_3(V)V^* + c_p D_3(T)T^*) = h_1 F_W, \qquad (82)$$

Finally, from collection of the $\delta T - \dfrac{\rho}{T}\delta\rho$ terms, we obtain:

$$\begin{gathered} -h_1 c_p D_1(\rho U T^*) - c_p D_3(h_1\rho W T^*) - \\ \frac{\rho U h_1}{T}\left(D_1(U)U^* + D_1(V)V^* - D_1(W^*) + c_p D_1(T)T^*\right) - \\ \frac{(\gamma-1)}{R}M^2 h_1 \frac{d\mu}{dT}\left[D_3(U)^2 + D_3(V)^2\right]T^* + \\ \frac{1}{R}\frac{d\mu}{dT}\left[D_3(U)D_3(h_1U^*) + D_3(V)D_3(h_1V^*)\right] \\ -\frac{\kappa}{RPr}D_{33}(h_1 T^*) = h_1\left(F_T + \frac{W}{T}F_W\right). \end{gathered} \qquad (83)$$

Since the pressure gradient $D_3(p)$ is equal to zero in the boundary layer we have $\rho\delta T + T\delta\rho = 0$, and from integration by parts we obtain

$$D_3(h_1\rho^*) = 0 < \qquad (84)$$

This equation is useless because it is fully decoupled from the others. The five equations ((80) to (84)) may be written under the form :

$$\mathcal{L}^*_{BL}(\psi)\ \psi^* = \mathcal{S}^*_{BL}, \qquad \mathcal{S}^*_{BL} = \left(F_U, F_V, F_W, F_T + \frac{W}{T}F_W, 0\right)$$

The adjoint field is subjected to the following boundary and terminal conditions:

$$\begin{aligned} U^* = V^* = 0 \quad &\text{at} \quad x^3 = 0, \\ \frac{\kappa}{P_r R}D_3(h_1 T^*) + h_1\rho C_p W = 0 \quad &\text{at} \quad x^3 = 0, \\ U^*,\ V^*,\ W^*,\ T^* \to 0 \quad &\text{as} \quad x^3 \to \infty, \\ U^* = V^* = W^* = T^* = 0 \quad &\text{at} \quad x^1 = x_1, \end{aligned} \qquad (85)$$

Appendix G. Forcing terms of the ABLE

The forcing terms S^*_{BL} of the adjoint boundary layer equations are derived from the vector $\mathbf{f}$ defined as

$$\begin{aligned} \mathbf{f} &= \text{real}\left\{A_F\ \bar{\phi}^* + B_F\ D_3(\bar{\phi}^*) + C_F\ D_{33}(\bar{\phi}^*) + D_F\ D_1(\bar{\phi}^*)\right\} \\ &= \text{real}\left\{(F_W,\ F_U,\ F_V,\ F_T)^T\right\}, \end{aligned}$$

where

$$\phi^* = (\hat{\rho}^*,\ \hat{u}^*,\ \hat{v}^*,\ \hat{w}^*,\ \hat{T}^*)^T$$

and

$$D_i = \frac{1}{h_i}\frac{\partial}{\partial x^i}.$$

A_F, B_F, C_F and D_F are 4×5 matrices with non-zero elements as

$$
\begin{aligned}
A_F(1,1) &= -m_{13}\hat{\rho} \\
A_F(1,2) &= \rho D_3(\hat{u}) + \hat{\rho} D_3(U) \\
A_F(1,3) &= \rho D_3(\hat{v}) + \hat{\rho} D_3(V) \\
A_F(1,4) &= \hat{w}(-D_3(\rho) - m_{13}\rho) \\
A_F(1,5) &= D_3(\rho)\hat{T} + D_3(\hat{\rho})T + \rho D_3(\hat{T})(1-c_p) \\
&+ D_3(T)(-\rho\frac{dc_p}{dT}\hat{T} + \hat{\rho}(1-c_p)) \\
&+ \frac{1}{\gamma}(-D_3(\hat{\rho})T - \rho D_3(\hat{T}) - D_3(\rho)\hat{T} - \hat{\rho} D_3(T)) \\
A_F(2,1) &= i\,\hat{\rho}\alpha_0 \\
A_F(2,2) &= -D_1(\hat{\rho})U - D_1(\rho)\hat{u} - D_3(\rho)\hat{w} - D_3(\hat{\rho})W \\
&- \hat{\rho} D_3(W) + \rho(-D_3(\hat{w}) + i\,\hat{u}\alpha_0) \\
&+ m_{13}(-\hat{\rho}W + \frac{1}{R}(-\frac{d^2\mu}{dT^2}D_3(T)\hat{T} - \frac{d\mu}{dT}D_3(\hat{T}))) \\
A_F(2,3) &= \hat{\rho} D_1(V) + \rho(i\,\hat{v}\alpha_0 + D_1(\hat{v})) \\
A_F(2,4) &= -2\hat{\rho}m_{13}U + \frac{1}{R} i\,\alpha_0(\frac{d\mu}{dT}D_3(\hat{T}) + \frac{d^2\mu}{dT^2}D_3(T)\hat{T}) \\
&+ \rho(-2m_{13}\hat{u} + D_1(\hat{w}) + i\,\hat{w}\alpha_0) + \frac{1}{\rho^2}\hat{\rho}\mu\frac{1}{R} i\, D_3(\rho) \\
&\quad \alpha_0(\frac{\lambda}{\mu} + 2) + \frac{\hat{\rho}}{\rho}\frac{1}{R}D_3(T)\frac{d\mu}{dT} i\,\alpha_0(-2 - \frac{\lambda}{\mu}) \\
A_F(2,5) &= D_1(\rho)\hat{T} + D_1(\hat{\rho})T + \frac{1}{\gamma}(-D_1(\hat{\rho})T - D_1(\rho)\hat{T}) \\
&+ \hat{\rho}(D_1(T)(1-c_p) + \ i\,T\alpha_0(1-\frac{1}{\gamma})) \\
&+ \rho(D_1(\hat{T})(1-c_p-\frac{1}{\gamma}) + \hat{T}(-\frac{dc_p}{dT}D_1(T) + i\,\alpha_0(1-c_p-\frac{1}{\gamma}))) \\
&+ M^2\frac{1}{R}(2\frac{d^2\mu}{dT^2}D_3(T)\hat{T}D_3(U) + \mu(2i\, D_3(\hat{w})\alpha_0 \\
&+ 2m_{13}D_3(\hat{u}) + 2D_{33}(\hat{u})) + \frac{d\mu}{dT}(2\hat{T}D_{33}(U) + 2D_3(\hat{T})D_3(U) \\
&+ D_3(T)(2D_3(\hat{u}) + 2i\,\hat{w}\alpha_0)) + \gamma(-2i\,\frac{d\mu}{dT}D_3(T)\hat{w}\alpha_0 \\
&+ \hat{T}(-2\frac{d\mu}{dT}D_{33}(U) + D_3(U)(-2m_{13}\frac{d\mu}{dT} - 2\frac{d^2\mu}{dT^2}D_3(T))) \\
&+ \mu(-2m_{13}D_3(\hat{u}) - 2D_{33}(\hat{u}) - 2i\, D_3(\hat{w})\alpha_0))) \\
&+ 2m_{13}M^2\frac{1}{R}\frac{d\mu}{dT}\hat{T}D_3(U) \\
&+ \gamma M^2\frac{1}{R}\frac{d\mu}{dT}(-2D_3(\hat{T})D_3(U) - 2D_3(T)D_3(\hat{u})) - \frac{1}{\gamma}\hat{\rho}D_1(T)
\end{aligned}
$$

$$
\begin{aligned}
A_F(3,1) &= i\,\hat{\rho}\beta_0 \\
A_F(3,2) &= i\,\rho\hat{u}\beta_0 \\
A_F(3,3) &= -D_1(\rho)\hat{u} - D_3(\rho)\hat{w} - D_3(\hat{\rho})W - D_1(\hat{\rho})U \\
&+ \frac{1}{R}m_{13}(-\frac{d^2\mu}{dT^2}D_3(T)\hat{T} - \frac{d\mu}{dT}D_3(\hat{T})) + \hat{\rho}(-D_3(W) - m_{13}W) \\
&- \hat{\rho}D_1(U) + \rho(-m_{13}\hat{w} - D_1(\hat{u}) + i\,\hat{v}\beta_0 - D_3(\hat{w})) \\
A_F(3,4) &= i\,\beta_0(\rho\hat{w} + \frac{1}{R}(\frac{d\mu}{dT}D_3(\hat{T}) + \hat{T}(\frac{d^2\mu}{dT^2}D_3(T) + m_{13}\frac{d\mu}{dT}) \\
&+ \hat{\rho}(\frac{1}{\rho^2}\mu D_3(\rho)(2 + \frac{\lambda}{\mu}) \\
&+ \frac{1}{\rho}(-2\frac{d\mu}{dT}D_3(T) - 2m_{13}\mu + \frac{\lambda}{\mu}(-\frac{d\mu}{dT}D_3(T) - m_{13}\mu))))) \\
A_F(3,5) &= i\,\beta_0\hat{T}\rho(-c_p - \frac{1}{\gamma} + 1) + M^2\frac{1}{R}(2\frac{d^2\mu}{dT^2}D_3(T)\hat{T}D_3(V) \\
&+ \mu(2m_{13}D_3(\hat{v}) + 2D_{33}(\hat{v}) + i\,\beta_0(2D_3(\hat{w}) + 2m_{13}\hat{w})) \\
&+ \frac{d\mu}{dT}(2D_3(\hat{T})D_3(V) + D_3(T)(2i\,\hat{w}\beta_0 + 2D_3(\hat{v})) \\
&+ \hat{T}(2D_{33}(V) + 2m_{13}D_3(V))) + \gamma(-2\frac{d^2\mu}{dT^2}D_3(T)\hat{T}D_3(V) \\
&+ \mu(-2D_{33}(\hat{v}) - 2m_{13}D_3(\hat{v}) + i\,\beta_0(-2m_{13}\hat{w} - 2D_3(\hat{w}))) \\
&+ \frac{d\mu}{dT}(-2D_3(\hat{T})D_3(V) + D_3(T)(-2i\,\hat{w}\beta_0 - 2D_3(\hat{v})) \\
&+ \hat{T}(-2m_{13}D_3(V) - 2D_{33}(V))))) + i\,\beta_0\hat{\rho}T(1 - \frac{1}{\gamma}) \\
A_F(4,1) &= \frac{T}{\rho}\,i\,(-\hat{u}\alpha_0 - \hat{v}\beta_0) \\
A_F(4,2) &= \frac{i\,\alpha_0}{\gamma M^2}\hat{\rho} + \frac{1}{R}(m_{13}D_3(U)\frac{d^2\mu}{dT^2}\hat{T} + \frac{d\mu}{dT}(m_{13}D_3(\hat{u}) \\
&+ \hat{u}\beta_0^2 + \alpha_0^2\hat{u}(2 + \frac{\lambda}{\mu}) + \alpha_0(\hat{v}\beta_0 + \frac{\lambda}{\mu}(\hat{v}\beta_0 - i\,D_3(\hat{w}))))) \\
&+ \frac{1}{T}\rho(-D_1(U)\hat{u} - D_3(\hat{u})W - D_1(\hat{u})U + \hat{w}(-m_{13}U - D_3(U)) \\
&+ i\,(-\frac{\alpha_0}{\gamma M^2}\hat{T} + \hat{u}(-\alpha_0 U - \beta_0 V + \omega))) \\
A_F(4,3) &= \frac{i\,\beta_0}{\gamma M^2}\hat{\rho} + \frac{1}{T}\rho(-D_1(V)\hat{u} - D_3(V)\hat{w} - D_3(\hat{v})W \\
&- D_1(V)wU + i\,(-\frac{1}{\gamma M^2}\beta_0\hat{T} + \hat{v}(-\alpha_0 U - \beta_0 V + \omega))) \\
&+ \frac{1}{R}(m_{13}D_3(V)\frac{d^2\mu}{dT^2}\hat{T} + \frac{d\mu}{dT}(m_{13}D_3(\hat{v}) + \hat{v}\alpha_0^2 \\
&+ \beta_0^2\hat{v}(2 + \frac{\lambda}{\mu}) + \beta_0(i\,m_{13}\hat{w} + \hat{u}\alpha_0 + \frac{\lambda}{\mu}(\hat{u}\alpha_0 - i\,D_3(\hat{w})))))
\end{aligned}
$$

$$
\begin{aligned}
A_F(4,4) &= \frac{1}{T}\rho(-D_1(\hat{w})U - D_3(W)\hat{w}) + \frac{1}{R}(\frac{d\mu}{dT}\hat{w}\alpha_0^2 \\
&+ \frac{\lambda}{\mu}(\frac{d\mu}{dT}(m_{13}D_3(\hat{w}) + D_{33}(\hat{w})) + \frac{\hat{w}}{T\rho}(2\frac{d\mu}{dT}D_3(T)D_3(\rho) \\
&+ \mu(2m_{13}D_3(\rho) + 2D_{33}(\rho)))) + i\ (\frac{d\mu}{dT}D_3(\hat{u})\alpha_0 + \frac{\lambda}{\mu}(m_{13}\frac{d\mu}{dT}\hat{v}\beta_0 \\
&+ \frac{1}{T}(m_{13}\mu\hat{v}\beta_0 + D_3(T)\frac{d\mu}{dT}(\hat{v}\beta_0 + \hat{u}\alpha_0))) \\
&+ \frac{1}{\rho}(\frac{d\mu}{dT}\alpha_0(2D_3(\hat{\rho})U + 2\hat{\rho}D_3(U)) + \frac{\mu}{T}(D_3(\hat{\rho})(2\beta_0 V + 2\alpha_0 U) \\
&+ \hat{\rho}(2\beta_0 D_3(V) + 2\alpha_0 D_3(U))) + \frac{\lambda}{\mu}(\frac{\mu}{T}(\hat{\rho}(\alpha_0 D_3(U) + \beta_0 D_3(V)) \\
&+ D_3(\hat{\rho})(\alpha_0 U + \beta_0 V - \omega)) + \frac{d\mu}{dT}(\beta_0(\hat{\rho}D_3(V) \\
&+ D_3(\hat{\rho})V + \hat{v}D_3(\rho)) + \alpha_0(D_3(\rho)\hat{u} + \hat{\rho}D_3(U) + D_3(\hat{\rho})U)))))) \\
&- m_{13}\frac{1}{\gamma M^2}\hat{\rho} + \frac{1}{T}\rho(i\ \hat{w}\omega + 2m_{13}U\hat{u} - D_3(\hat{w})W) \\
&+ \frac{1}{R}(\frac{1}{T}(-2\frac{d^2\mu}{dT^2}D_3(T)^2\hat{w} + \mu(2D_{33}(\hat{w}) + 2i\ m_{13}\hat{v}\beta_0 \\
&+ \frac{1}{\rho}(4\hat{w}m_{13}D_3(\rho) - 2i\ D_3(\hat{\rho})\omega) + \frac{\lambda}{\mu}(D_{33}(\hat{w}) + i\ (D_3(\hat{u})\alpha_0 \\
&+ D_3(\hat{v})\beta_0) - \frac{2}{\rho^2}\hat{w}D_3(\rho)^2 + \frac{2}{\rho^2}D_3(\rho)D_3(\hat{w})))) + \frac{d\mu}{dT}(2m_{13}D_3(\hat{w}) \\
&+ i\ D_3(\hat{v})\beta_0 + 2D_{33}(\hat{w}) + \hat{w}\beta_0^2 + \frac{1}{T}(-2D_{33}(T)\hat{w} + D_3(T)(\\
&- 2m_{13}\frac{\lambda}{\mu}\hat{w} + i\ (2\hat{v}\beta_0 + 2\hat{u}\alpha_0))) + \frac{1}{\rho}(4D_3(\rho)D_3(\hat{w}) \\
&+ \hat{w}(\frac{4}{T}D_3(T)D_3(\rho) + 2D_{33}(\rho)) + i\ (-\frac{\lambda}{\mu}D_3(\hat{\rho})\omega + 2\alpha_0 D_3(\rho)\hat{u} \\
&+ \beta_0(2\hat{\rho}D_3(V) + 2D_3(\hat{\rho})V + 2\hat{v}D_3(\rho)))))) + \frac{1}{T}\rho(m_{13}\frac{1}{\gamma M^2}\hat{T} \\
&+ \hat{w}i\ (-\alpha_0 U - \beta_0 V)) + \frac{1}{R}(\hat{T}\frac{d^2\mu}{dT^2}i\ (-\beta_0 D_3(V) - \alpha_0 D_3(U)) \\
&+ \frac{d\mu}{dT}(-2i\ \frac{1}{\rho}D_3(\hat{\rho})\omega + \frac{\lambda}{\mu}(i\ (D_3(\hat{u})\alpha_0 + D_3(\hat{v})\beta_0) \\
&+ \frac{1}{\rho}(2D_3(\rho)D_3(\hat{w}) + D_{33}(\rho)\hat{w}))) + \frac{1}{T}(\hat{w}(-4m_{13}\frac{d\mu}{dT}D_3(T) \\
&+ \frac{\lambda}{\mu}(-\frac{d^2\mu}{dT^2}D_3(T)^2 - \frac{d\mu}{dT}D_{33}(T))) + \mu(i\ (2D_3(\hat{v})\beta_0 + 2D_3(\hat{u})\alpha_0) \\
&- \frac{4}{\rho^2}\hat{w}D_3(\rho)^2 + \frac{1}{\rho}(4D_3(\rho)D_3(\hat{w}) + 4D_{33}(\rho)\hat{w}))))
\end{aligned}
$$

$$
\begin{aligned}
A_F(4,5) &= \frac{1}{R}(\hat{T}\frac{d\kappa}{dT}\frac{1}{Pr}(-\beta_0^2-\alpha_0^2)+M^2(\hat{T}\frac{d^2\mu}{dT^2}(-D_3(U)^2-D_3(V)^2)\\
&+ \hat{w}\frac{d\mu}{dT}i\ (-2\beta_0 D_3(V)+D_3(U)\alpha_0(-2+2\gamma))))+\hat{\rho}(-D_3(W)\\
&- D_1(U)+Wm_{13}(\frac{1}{\gamma}+c_p-1)+i\ (\alpha_0 U+\beta_0 V+\frac{1}{\gamma}(-\alpha_0 U\\
&- \beta_0 V)))+\rho(m_{13}c_p\hat{w}+i\ \frac{dc_p}{dT}\hat{T}\omega+\frac{1}{T}(c_p(\hat{w}D_3(T)+\hat{u}D_1(T)\\
&+ WD_3(\hat{T})+UD_1(\hat{T}))+\hat{T}(m_{13}W+D_1(U)+D_3(W)(1-\frac{1}{\gamma})\\
&+ i\ (c_p(\alpha_0 U+\beta_0 V)+\frac{1}{\gamma}(\alpha_0 U+\beta_0 V)))))+\frac{i}{\gamma}\omega\hat{\rho}\\
&+ M^2\frac{1}{R}\frac{d\mu}{dT}(-2D_3(U)D_3(\hat{u})-2D_3(V)D_3(\hat{v})+\gamma(2D_3(U)D_3(\hat{u})\\
&+ D_3(V)(2i\ \hat{w}\beta_0+2D_3(\hat{v}))))\\
&+ c_p(D_3(\hat{\rho})W+D_3(\rho)\hat{w}+D_1(\rho)\hat{u}+\hat{\rho}D_3(W)+\rho(D_3(\hat{w})\\
&+ D_1(\hat{u})))+\hat{T}(\frac{dc_p}{dT}(D_1(\rho)U+D_3(\rho)W)+\gamma M^2\frac{1}{R}\frac{d^2\mu}{dT^2}(D_3(V)^2\\
&+ D_3(U)^2)+\rho(\frac{dc_p}{dT}(m_{13}W+D_1(U)+D_3(W)+i\ (-\alpha_0 U-\beta_0 V))\\
&+ \frac{1}{T}(\frac{dc_p}{dT}(UD_1(T)+WD_3(T))\\
&+ \frac{1}{\gamma}(-D_1(U)-m_{13}W)+i\ (-\alpha_0 U-\beta_0 V+\omega(1-c_p-\frac{1}{\gamma})))))\\
&+ D_1(\hat{\rho})c_p U+\hat{\rho}(c_p D_1(U)-i\ \omega+\frac{1}{\gamma}(D_3(W)+D_1(U)))\\
B_F(1,1) &= -\hat{\rho}\\
B_F(1,4) &= -\rho\hat{w}\\
B_F(2,2) &= -\rho\hat{w}-\hat{\rho}W+\frac{1}{R}(-\frac{d\mu}{dT}D_3(\hat{T})\\
&+ \hat{T}(-\frac{d^2\mu}{dT^2}D_3(T)-2m_{13}\frac{d\mu}{dT}))\\
B_F(2,4) &= \frac{1}{R}i\ \alpha_0(\frac{d\mu}{dT}\hat{T}+\hat{\rho}\frac{\mu}{\rho}(-2-\frac{\lambda}{\mu}))\\
B_F(2,5) &= M^2\frac{1}{R}(\hat{T}D_3(U)\frac{d\mu}{dT}(-2\gamma+2)\\
&+ \mu(2D_3(\hat{u})+2i\ \hat{w}\alpha_0+\gamma(-2D_3(\hat{u})-2i\ \hat{w}\alpha_0)))\\
B_F(3,3) &= -\rho\hat{w}-\hat{\rho}W+\frac{1}{R}(-\frac{d\mu}{dT}D_3(\hat{T})+\hat{T}(-\frac{d^2\mu}{dT^2}D_3(T)-2m_{13}\frac{d\mu}{dT}))\\
B_F(3,4) &= \frac{1}{R}i\ \beta_0(\frac{d\mu}{dT}\hat{T}+\hat{\rho}\frac{\mu}{\rho}(-2-\frac{\lambda}{\mu}))
\end{aligned}
$$

$$
\begin{aligned}
B_F(3,5) &= M^2\frac{1}{R}(\hat{T}D_3(V)\frac{d\mu}{dT}(2-2\gamma)\\
&+ \mu(2i\ \hat{w}\beta_0 + 2D_3(\hat{v}) + \gamma(-2i\ \hat{w}\beta_0 - 2D_3(\hat{v}))))\\
B_F(4,1) &= \hat{w}\frac{\rho}{T}\\
B_F(4,2) &= \frac{1}{R}(D_3(U)\frac{d^2\mu}{dT^2}\hat{T} + \frac{d\mu}{dT}(i\ \hat{w}\alpha_0 + D_3(\hat{u})))\\
B_F(4,3) &= \frac{1}{R}(D_3(V)\frac{d^2\mu}{dT^2}\hat{T} + \frac{d\mu}{dT}(i\ \hat{w}\beta_0 + D_3(\hat{v})))\\
B_F(4,4) &= \frac{1}{\gamma M^2}(\hat{T}\frac{\rho}{T} - \hat{\rho}) + \frac{1}{R}(\frac{d\mu}{dT}(2D_3(\hat{w}) + \frac{\lambda}{\mu}(D_3(\hat{w}) + i\ (\hat{v}\beta_0 + \hat{u}\alpha_0)))\\
&+ \frac{1}{T}(\hat{w}D_3(T)\frac{d\mu}{dT}(-2\frac{\lambda}{\mu} - 4) + \mu(i\ (2\hat{v}\beta_0 + 2\hat{u}\alpha_0) + \hat{w}(\frac{4}{\rho}D_3(\rho)\\
&- 4m_{13}) + \frac{\lambda}{\mu}(i\ (\hat{v}\beta_0 + \hat{u}\alpha_0) + \hat{w}(-2m_{13} + \frac{2}{\rho}D_3(\rho))))))\\
B_F(4,5) &= c_p\ \rho\hat{w} + 2m_{13}\frac{1}{R}\frac{1}{Pr}\frac{d\kappa}{dT}\hat{T}\\
&+ W(\hat{T}\rho(\frac{dc_p}{dT} + \frac{1}{T}(1-\frac{1}{\gamma})) + \hat{\rho}(\frac{1}{\gamma} + c_p - 1))\\
C_F(2,2) &= -\frac{1}{R}\frac{d\mu}{dT}\hat{T}\\
C_F(3,3) &= -\frac{1}{R}\frac{d\mu}{dT}\hat{T}\\
C_F(4,4) &= \frac{\mu\hat{w}}{T}\frac{1}{R}(-2-\frac{\lambda}{\mu})\\
C_F(4,5) &= \frac{1}{R}\frac{1}{Pr}\frac{d\kappa}{dT}\hat{T}\\
D_F(2,1) &= -\hat{\rho}\\
D_F(2,2) &= -\rho\hat{u} - \hat{\rho}U\\
D_F(3,3) &= -\rho\hat{u} - \hat{\rho}U\\
D_F(4,1) &= \frac{\hat{u}\rho}{T}\\
D_F(4,2) &= \frac{1}{\gamma M^2}(\hat{T}\frac{\rho}{T} - \hat{\rho})\\
D_F(4,5) &= c_p\ \rho\hat{u} + U(\hat{T}\rho(\frac{dc_p}{dT} + \frac{1}{T}(1-\frac{1}{\gamma})) + \hat{\rho}(\frac{1}{\gamma} + c_p - 1))
\end{aligned}
$$

References

Airiau, C. 2000 Non-parallel acoustic receptivity of a Blasius boundary layer using an adjoint approach. *to appea in Flow, Turbulence and Combustion* .

Airiau, C. & Casalis, G. 1993 Boundary layer linear stability using a system of parabolic equations. *Rech. Aérosp.* **5**, 57–68.

Airiau, C., Walther, S. & Bottaro, A. 2000 Non-parallel receptivity and the adjoint PSE. In *IUTAM Symposium on Laminar-Turbulent Transition (September 1999, Sedona, AZ)* (ed. H. Fasel & W. Saric). Springer.

Andersson, P., Berggren, M. & Henningson, D. 1999*a* Optimal disturbances and bypass transition in boundary layers. *Phys. Fluids* **11** (1), 134–150.

Andersson, P., Berggren, M. & Henningson, D. 1999*b* Optimal disturbances in boundary layers. In *A.F.S.O.R. Workshop on Optimal Design and Control, 3 october 1997*. Birkhauser's Progress in Systems and Control Theory series.

Balakumar, P. & Hall, P. 1999 Optimum suction distribution for transition prediction. *Theoret. Comput. Fluid Dyn.* **13**, 1–19.

Bewley, T. & Liu, S. 1998 Optimal and robust control and estimation of linear paths to transition. *J. Fluid Mech.* **365**, 305–349.

Bewley, T., Temam, R. & Ziane, M. 2000 A general framework for robust control in fluid mechanics. *Physica D* **138**, 360–392.

Butler, K. & Farrell, B. 1992 Three-dimensional optimal perturbation in viscous shear flow. *Phys. Fluids* **A** (4), 1637.

Cathalifaud, P. & Luchini, P. 2000 Algebraic growth in a boundary layer: optimal control by blowing and suction at the wall. *Eur. J. Mech. B/Fluids* **19**.

Choudhari, M. & Street, C. 1992 A finite Reynolds-number approach for the prediction of boundary-layer receptivity in localized regions. *Physics of Fluids* **A 4** (11).

Collis, S. & Dobrinsky, A. 2000 Evaluation of adjoint based methods for the prediction of the receptivity. In *IUTAM Symposium on Laminar-Turbulent Transition (September 1999, Sedona, AZ)* (ed. H. Fasel & W. Saric). Springer.

Corbett, P. 2000 Non-modal growth in boundary layers, and its optimal control. PhD thesis, Ecole Polytechnique Fédérale de Lausanne, Switzerland.

Crouch, J. 1992 Localized receptivity of boundary layers. *Physics of Fluids* **A 4** (7).

Crouch, J. 1995 Non-localized receptivity of boundary layers. *J. Fluid Mech.* **244**, 567–581.

Crouch, J. & Spalart, P. 1995 A study of non-parallel and non-linear effects on the localized receptivity of boundary layers. *J. Fluid Mech.* **290**, 29–37.

Dobrinsky, A. & Collis, S. 2000 Adjoint parabolized stability equations for receptivity prediction. *AIAA-2000-2651* .

Gmelin, C. & Rist, U. 2001 Active control of laminar-turbulent transition using instantaneous vorticity signals at the wall. *to appear Phys. Fluids* .

Goldstein, M. 1983 The evolution of Tollmien-Schlichting waves near the leading edge. *J. Fluid Mech.* **127**, 59–81.

Goldstein, M. 1985 Scattering of acoustic waves into Tollmien-Schlichting waves by small streamwise variations in surface geometry. *J. Fluid Mech.* **154**, 509–529.

Goldstein, M. & Hultgren, L. 1987 A note on the generation of the T.S. waves by sudden surface-curvature change. *J. Fluid Mech.* **181**, 519–525.

Gunzburger, M. 2000 Adjoint equation-based methods for control problems in incompressible, viscous flows. *In press in Flow, Turbulence and Combustion* .

Hanifi, A. 1995 Local and non-local stability analysis and transition prediction of

compressible boundary layer flows. Ph.D. thesis and TRITA-MEK Technical Report 1995-12. Royal Institute of Technology, Stockholm, Sweden.

Hanifi, A., Henningson, D., Hein, S., Bertolotti, F. & Simen, M. 1994 Linear non-local instability analysis - the linear nolot code. Technical Report FFA TN 1994-54. The Aeronautical Research Institute of Sweden, Stockholm, Sweden.

Hein, S., Bertolotti, F., Simen, M., Hanifi, A. & Henningson, D. 1994 Linear non-local instability analysis - the linear nolot code. Technical Report DLR-IB 223-94 A 43. DLR, Goettingen, Germany.

Herbert, T. 1997 Parabolized stability equations. *Ann. Rev. Fluid Mech.* **29**, 245–283.

Hill, D. 1995 Adjoint system and their role in the receptivity problem for boundary layer. *J. Fluid Mech.* **292**, 183–204.

Hill, D. 1997*a* Inverse design for three-dimensional boundary layers. *Bull. A. Phys. Soc.* **42**, 2120.

Hill, D. 1997*b* Receptivity in non-parallel boundary layers. FEDSM97-3108 , ASME Fluids Engineering Division Summer Meeting.

Högberg, M. & Berggren, M. 2000 Numerical approaches for optimal control of a model equation for shear flow intabilities. *Submitted to Flow, Turbulence and Combustion* .

Joslin, R. 1998*a* Aircraft laminar flow control. *Annu. Rev. Fluid Mech.* **30**, 1–29.

Joslin, R. 1998*b* Overview of laminar flow control. *Tech. Rep.* NASA/TP-1998-208705. NASA.

Joslin, R., Erlebacher, F. & Hussaini, M. 1996 Active control of instabilities in laminar boundary layer flow. Overview and concept validation. *J. Fluids Eng.* **118** (3), 494–497.

Joslin, R., Gunzburger, M., Nicolaides, R., Erlebacher, F. & Hussaini, M. 1995*a* A self-contained, automated methodology for optimal flow control validated for transition delay. Report 95-64. ICASE.

Joslin, R., Gunzburger, M., Nicolaides, R., Erlebacher, F. & Hussaini, M. 1997 A methodology for the automated optimal control of flows including transitional flows. *AIAA J.* **35**, 816–824.

Joslin, R., Nicolaides, R., Erlebacher, F., Hussaini, M. & Gunzburger, M. 1995*b* Active control of instabilities in laminar boundary layer flow. part ii: Use of sensors and spectral controller. *AIAA J.* **33** (8), 1521–1523.

Li, F. & Malik, M. 1996 On the nature of the PSE approximation. *Theoret. Comput. Fluid Dyn.* (8), 253–273.

Luchini, P. 2000 Reynolds-number-independent instability of the boundary layer over a flat surface. Optimal perturbations. *J. Fluid Mech.* **404**, 289–309.

Luchini, P. & Bottaro, A. 1998 Görtler vortices: a backward-in-time approach to the receptivity problem. *J. Fluid Mech.* **363**, 1–23.

Mughal, M. 1998 Active control of wave instabilities in three-dimensional compressible flows. *Theoret. Comput. Fluid dynamics* (12), 195–217.

Pralits, J., Airiau, C., Hanifi, A. & Henningson, D. S. 2000*a* Sensitivity analysis using adjoint parabolized stability equations for compressible flows. *to appear in Flow, Turbulence and Combustion* .

Pralits, J., Hanifi, A. & Henningson, D. 2000*b* Adjoint-based suction optimization for 3D boundary layer flows. FFA TN 2000-58. The Aeronautical Research Institute of Sweden, Stockholm, Sweden.

Simen, M. 1992 Local and nonlocal stability theory of spatially varying flow. In *Instability, Transition and Turbulence* (ed. A. K. M. Y. Hussaini & C. S. (eds)), pp. 181–201. Springer-Verlag.

Tumin, A. 1996 Receptivity of pipe Poiseuille flow. *J. Fluid Mech.* **315**, 119–137.

Tumin, A. & Fedorov, A. 1984 Instability wave excitation by a localized vibrator in the boundary layer. *J. Appl. Mech. Tech. Phys.* **25**, 867–873, (from Russian).